June 2019

Rare Earth Geochemistry of Apatitic Fossils from the Middle-Upper Ordovician Southern Margin of Laurentia

Rafael Adrian Villanueva
Louisiana State University and Agricultural and Mechanical College

RARE EARTH GEOCHEMISTRY OF APATITIC FOSSILS FROM THE MIDDLE-UPPER ORDOVICIAN SOUTHERN MARGIN OF LAURENTIA

A Thesis

Submitted to the Graduate Faculty of the
Louisiana State University and
Agricultural and Mechanical College
in partial fulfillment of the
requirements for the degree of
Master of Science

in

The Department of Geology and Geophysics

by
Rafael Villanueva
B.S., Clemson University, 2016
August 2019

Table of Contents

Abstract

Widespread deposition of phosphate and a transition from tropical to cool water carbonates is seen throughout Middle-Upper Ordovician Nashville Dome area spanning the M4/M5 sequence boundary. Hypotheses explaining the onset of these lithologic changes have included the onset of glaciation, drawdown of CO_2 related to the Guttenburg Isotope Carbon Excursion (GICE), and siliciclastic weathering, yet none of these studies have provided definitive evidence that shows any of these are the sole factor driving paleoenvironmental changes across the M4/M5 boundary. In order to test whether rapid subsidence along the southeastern margin of Laurentia may have caused an influx of phosphate and shift in carbonate facies, a multi-pronged approach was applied using REE and minor and trace elemental geochemistry to apatitic fossils or "steinkerns" and petrographic analysis on samples collected from a Middle-Upper Ordovician limestone outcrop located in Tidwell Hollow, Alabama. Elemental concentrations collected using LA-ICP-MS were normalized to the upper continental crust (UCC). Although the REE's were found to be diagenetically overprinted, minor elements U and Th, as well as Y, were used to aid in interpreting paleo redox conditions. Based on geochemical and petrographic evidence, various stages of carbonate ramp development have been interpreted including a transition from peritidal to deep ramp environment before reverting to proximal shelf facies. These findings highlight the susceptibility of REE's to diagenesis and the value of U and Th as paleo redox proxies. Also, the findings of this study carry implications for local paleoenvironmental changes and future placement of this area into a regional sequence stratigraphic framework.

Introduction

Southeastern Laurentia experienced greenhouse conditions and widespread carbonate deposition during Middle-Upper Ordovician (Sandbian-Katian or North American Mohawkian) time during and after the Blountian and Taconic phases of the Taconic Orogeny (Holland & Patzkowsky, 1997; Sell et al., 2015; Shanmugam & Walker, 1980). Coinciding with the Taconic Orogeny, an abrupt environmental change occurred across the M4/M5 sequence boundary of the Nashville Dome area of South East Laurentia (Holland & Patzkowsky, 1998; Holland & Patzkowsky, 1997; Holland, Patzkowsky, 1996). This change is recognized regionally as a dramatic shift from warm to temperate water carbonate deposition despite Laurentia's position in equatorial latitudes and presence of greenhouse conditions (Ettensohn, 2010; Holland & Patzkowsky, 1997; Holland et al., 1996; Quinton et al., 2016). Sedimentological and geochemical evidence of processes associated with cooling includes increased deposition of phosphate, chert, and a positive carbon isotope excursion referred to as the Guttenberg Isotope Carbon Excursion (GICE) (Holland & Patzkowsky, 1997; Pope & Steffen, 2003; Quinton et al., 2017).

Phosphate in the form of apatitic fossils (steinkerns) first appears along the M4/M5 sequence boundary in carbonates throughout the Nashville Dome area of Southern Laurentia (Holland & Patzkowsky, 1998) with apatitic fossils referred to as apatite for the remainder of this paper. Apatites that occur as internal molds of mollusks are common, however, in addition to apatites, phosphate is present in several other modes such as replacement of bryozoan and crinoid fossils as well as disseminated in packstone and grainstone facies (Holland & Patzkowsky, 1998). The occurrence of phosphatic carbonate sediments and apatite preserved in formations such as the Miocene Monterey formation and modern upwelling zones such as the

Peru and coastal California margins, typically indicates an incursion of cool waters rich in phosphorus (Glenn et al., 1994; Holland & Patzkowsky, 1998; Holland & Patzkowsky, 1997; Vincent & Berger, 1985). This incursion of nutrients, phosphate-rich sediments, and precipitation of apatites are commonly associated with significant climatic changes and relative sea level rise (Föllmi, 1996). However, the exact origin and mechanism that led to deposition of Middle-Upper Ordovician phosphatic sediments and apatites along Laurentia's eastern margin are still unclear. Earlier authors have suggested the occurrence of phosphate originating from various sources including the Sebree Trough which was an opening that may have allowed cool waters to infiltrate from the Iapetus Ocean to the interior of Laurentia, deepening of the Taconic Foreland basin, increased weathering of silicates, and paleoceanographic effects attributed to glaciation (Ettensohn, 2010; Holland & Patzkowsky, 1998; Holland & Patzkowsky, 1997; Kump et al., 1999; Pope & Steffen, 2003)

The GICE occurred during the Middle-Upper Ordovician of Laurentia and is recognized as a positive carbon excursion that occurred at the base of the Katian (Sell et al., 2015) that is associated with an increase in carbon burial prior to Upper Ordovician Hirnantian glaciation that may have led to increased drawdown of CO_2 or transition to icehouse conditions (Quinton et al., 2016; Sell et al., 2015). However, previous studies of southeastern Laurentia carbonates investigating the GICE and its ties to glaciation and climate change found no clear correlation between conodont $\delta^{18}O$ and $\delta^{12}C$ suggesting a change in water temperature was not the driving force for the lithologic changes seen across the M4/M5 boundary (Quinton et al., 2016; Quinton et al., 2017). Further, the buildup of glaciers typically leads to eustatic sea-level fall and reduced productivity, however, $\delta^{13}C$ values of conodonts from southeastern Laurentia as well as numerical modeling of Upper Ordovician ocean-climate systems suggest otherwise (Baker &

Burns, 1985; Brenchley et al., 1994; Fanton & Holmden, 2007; Herrmann et al., 2010; Quinton et al., 2016).

Independent of climatic influences, Laurentia was under the influence of multiple collisions with a series of island arcs to the east at this time. By the Middle-Upper Ordovician (470-453 Ma) approximately at the time of the onset of the M5 sequence, rapid subsidence was occurring across southeast Laurentia due to the onset of the Taconic Orogeny similar to modern processes occurring between the island of Timor and northern Australia (Holland & Patzkowsky, 1997; Shanmugam & Walker, 1980). Earlier workers have argued that southeastern Laurentia's close proximity to the Iapetus Ocean to the south would have made it possible for cool waters to upwell along the margins of Laurentia spurring a chain reaction beginning with an increase in nutrients followed by an increase in primary productivity, phosphate deposition, and potentially resulting in lithologic changes via nutrient poisoning (Hallock & Schlager, 1986; Holland & Patzkowsky, 1997). Further, the presence of cool water (Herrmann et al., 2010) as well as photo-independent organisms such as bryozoans, brachiopods and echinoderms in post Taconic platform facies suggest an increase in turbidity and decrease in available light penetration caused by increased nutrients, siliciclastics, or basin deepening occurring simultaneously (Flügel, 2004; Holland & Patzkowsky, 1997; Kump et al., 1999; Pomar, 2001).

Associated with abundant phosphatic sediments found in southeastern Laurentia is the presence of dolomite and authigenic pyrite framboids in mud-shale rich limestones. The mechanics of dolomitization are still poorly understood with numerous models and environmental factors invoked to explain this economically important mineral's occurrence in nature (Burns et al., 2000; Gregg et al., 2015; Machel, 2004). Multiple studies have been conducted on the origin of dolomites in organic-rich sediments such as those found in the

Miocene age Hawthorn Group of Florida and the Miocene age Monterey formation of the Santa Maria Basin area (Compton, 1988; Compton et al., 1994; Compton & Siever, 1986). By examining the relationship between dolomite in thin section and environmental conditions inferred from geochemical data, it may be possible to uncover conditions promoting dolomitization in these sediments.

The lanthanides or Rare Earth Elements (REE's) consist of a unique series of elements that have proved reliable tracers of multiple natural processes including phosphogenesis as well as paleoenvironmental reconstructions (Alibo & Nozaki, 1999; German, et al., 1995; Piepgras & Wasserburg, 1982; Piper et al., 2007). Marine and authigenic carbonates such as apatites incorporate REE's from the seawater and pore water in which they precipitate lending them useful in interpreting paleo redox conditions (Auer et al., 2017). The value of these elements lies in their chemical behavior whereby changes across the series from the light rare earth's (LREE's) to heavy rare earth's (HREE's) as well as redox sensitive Ce and Eu, allow for interpretation of the aforementioned processes by using normalized REE concentration patterns (Byrne & Sholkovitz, 1996; Elderfield, 1988; Haley et al., 2004). When normalized to a standard such as shale or the upper continental crust, it is possible to use these elements as source signatures that provide information on paleoceanographic conditions present during burial and diagenesis (Byrne & Sholkovitz, 1996; Taylor & McLennan, 1985).

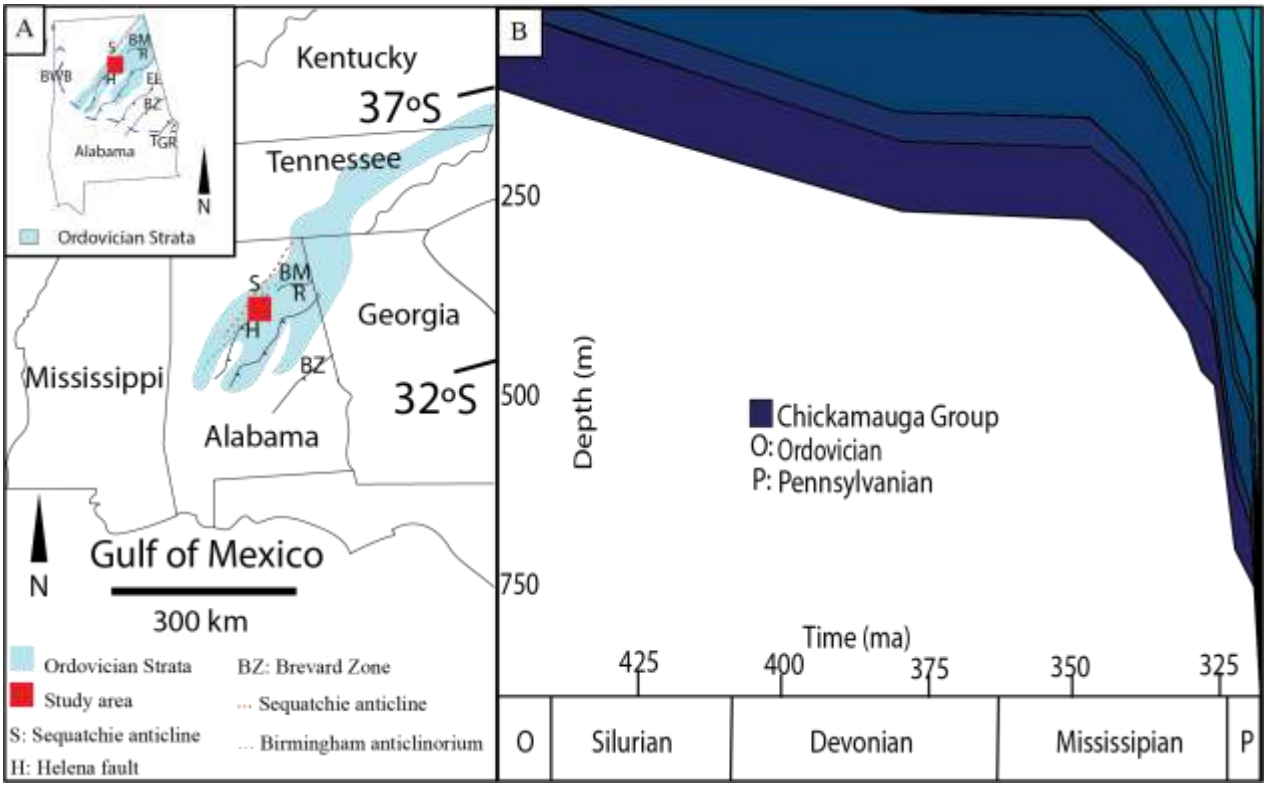

Figure 1. A. Alabama, USA showing approximate location of Tidwell Hollow and Ordovician outcrops of the Valley and Ridge. Location of faults and state outlines modified from (Thomas & Bayona, 2002). B. Diagram showing burial history of the Chickamauga limestone at Tidwell Hollow, Alabama. Redrawn from (Tobin et al., 1997).

The objective of this study is to address the origin of phosphate by analyzing apatitic fossils and by extension, what may have led to a dramatic environmental change and an incursion of nutrient rich waters onto the carbonate platform. A secondary goal will be interpreting the factors influencing the presence of organogenic dolomite found deposited across southern Laurentia. Both of these goals will be accomplished by examining the Middle-Upper Ordovician deposits of the Chickamauga Group at Tidwell Hollow, Alabama (Figure1). This location has been selected due to its position on the southeastern margin of the Laurentia carbonate platform and previous placement of this section into a biostratigraphic framework that

along with presence of the Millbrig and Deicke K bentonite beds and earlier chemostratigraphic interpretations, allows for regional correlation (Quinton et al., 2016; Sell et al., 2015).

By utilizing the unique properties of REE's discussed above, this study will use this set of elements to aid in interpretation of paleoceanographic conditions preserved in Middle-Upper Ordovician apatites during burial and early diagenesis. If basinal deepening or subsidence occurred, then REE patterns preserved in apatites will gradually progress from terrestrial "flat" patterns at the base of the studied section to basinal or more open oceans that exhibit seawater like REE signatures such as low ∑REE, LREE depletion, and a negative Ce anomaly close to the top of the interval (Nothdurft et al., 2004; Piper et al., 2007; Webb & Kamber, 2000). In conjunction with geochemical data, by observing fossil assemblages and occurrence of phosphate in thin sections, paleoenvironmental conditions at this location can be inferred (Flügel, 2004). Finally, signals from mud-shale dolomitized intervals may elude to pore water conditions present during diagenesis such as an anoxic methanogenic or sulfate reducing environment shown by a flat or HREE enriched pattern respectively (Kim et al., 2012).

Background

Regional Paleogeography

The southeastern margin of Laurentia on which the Middle-Upper Ordovician (470-443 Ma) peritidal-deep subtidal limestone deposits of the Chickamauga were deposited was rotated approximately 90˚ from its present location and varied in latitude during the Ordovician from 35° to 15° S with prevailing winds blowing to the west-northwest across a shallow epeiric sea (Ettensohn, 2008; Holland & Patzkowsky, 1997; Pope & Steffen, 2003; Scotese, 2003). A lack of evaporites suggest that this region exhibited relatively humid conditions; however, there are also rare examples of paleokarst which suggests little to no rain or short periods of subaerial exposure (S. Holland & Patzkowsky, 1998). The basin, due to numerous similarities such as basin geometries and subtropical latitude has been compared to the Persian Gulf which serves as a modern analog and allows for a range of depths to be inferred ranging from 0-2m for peritidal - shallow subtidal to 700m in the sediment-starved basin (Holland & Patzkowsky, 1998; Purser & Evans, 1973; Shanmugam & Walker, 1980; Wagner & Van der Togt, 1973). Deposition of these limestones occurred before and during the Blountian and Taconic phases of the Taconic Orogeny and lie unconformably over the regional Knox Unconformity (Benson & Mink, 1983). This unconformity marks the end of the North American Sauk sequence and transgression of the Tippecanoe sequence (Ettensohn, 2010; Holland & Patzkowsky, 1997; Pope & Read, 1998; Sloss, 1963; Thomas, 1985).

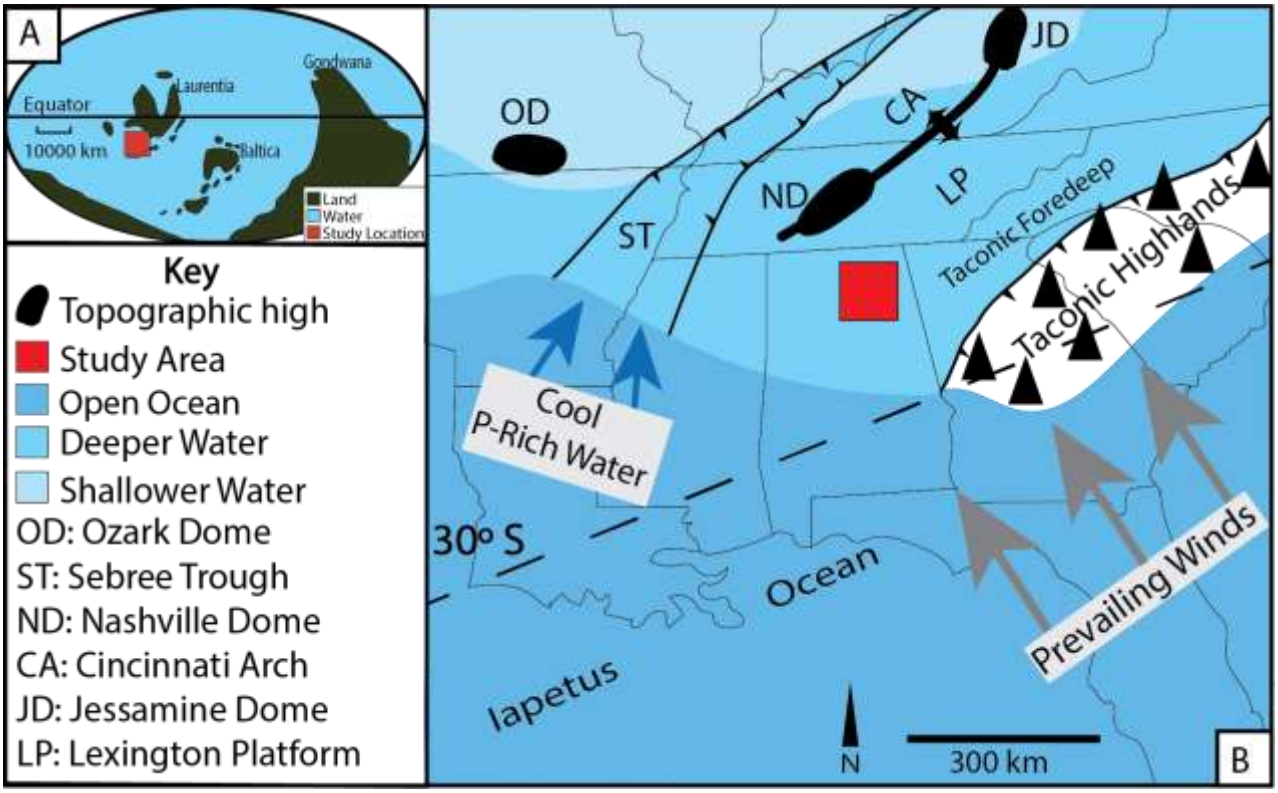

Figure 2. A. Rendition of Tidwell Hollow and Laurentia during the Middle-Late Ordovician from (Pope & Steffen, 2003). B. Paleogeographic location of Tidwell Hollow within the Southeastern United States during the Middle-Late Ordovician from Water depths inferred from $\delta^{13}C‰$ gradients found in Fanton & Holmdon (2007) and depth estimates from (Holland & Patzkowsky, 1998).

Subsidence caused by crustal thickening and uplift during the creation of the Taconic Foreland Basin resulted in development of a forebulge in the distal portion of the basin represented by the Nashville and Jessamine Domes that were connected by the Cincinnati Arch North West of the Chickamauga Group which were the locations of higher energy tidal sedimentation (Castle, 2001; Pope et al., 2009). Using a back stripping algorithm (Holland & Patzkowsky, 1997) suggested that sea level steadily rose due to subsidence occurring at a constant 10.3m/m.y from the M1-M6 sequences with an abrupt increase 3 Ma after the onset of the Taconic Orogeny (453 Ma).This collision produced a series of widespread ash beds in particular the Millbrig and Deicke K-bentonites. These Upper Ordovician K-bentonites contain

unique apatite trace element trends that provides implications for correlations and insights for sequence stratigraphic schemes for early Upper Ordovician North America (Sell et al., 2015). The Sebree Trough, a shale filled depression on the western flank of the carbonate platform, acted as a passage for cool waters from the Iapetus Ocean into Laurentia's interior (Kolata et al., 2001; Pope & Steffen, 2003).

Regional Stratigraphy

Middle-Upper Ordovician strata in Alabama consists of two outcrop belts trending northeast-southwest separated by the Helena Fault (Figure 1A) (Benson & Mink, 1983). West of the Helena Fault in Blount County, the Chickamauga overlies the Knox Group and is interpreted as deposited in peritidal and subtidal environments (Benson 1986a) while east of the Helena, deep water carbonates of the Lenoir and Little Oak persist (Benson, 1986a; Carter & Chowns, 1986). Carbonate facies of the Chickamauga range from peritidal to shallow ramp with thin-thick bedded wackestones, packstones, grainstones, and shale (Benson, 1986a). Biota is diverse including bryozoans, brachiopods, gastropods, trilobites, and oncoids among others (Benson, 1986a). The upper portion of the Chickamauga which includes the Stones River and Nashville formations is composed of peritidal lithologies. These peritidal facies are composed of predominantly mudstones, peloidal wackestones, and packstones grading into subtidal and deep ramp lithologies (Benson & Mink, 1983). Also in the upper section lie the Millbrig and Deicke

K- bentonites which are commonly used for correlation (Benson & Mink, 1983; Chowns & McKinney, 1980; Drahovzal & Neathery, 1971).

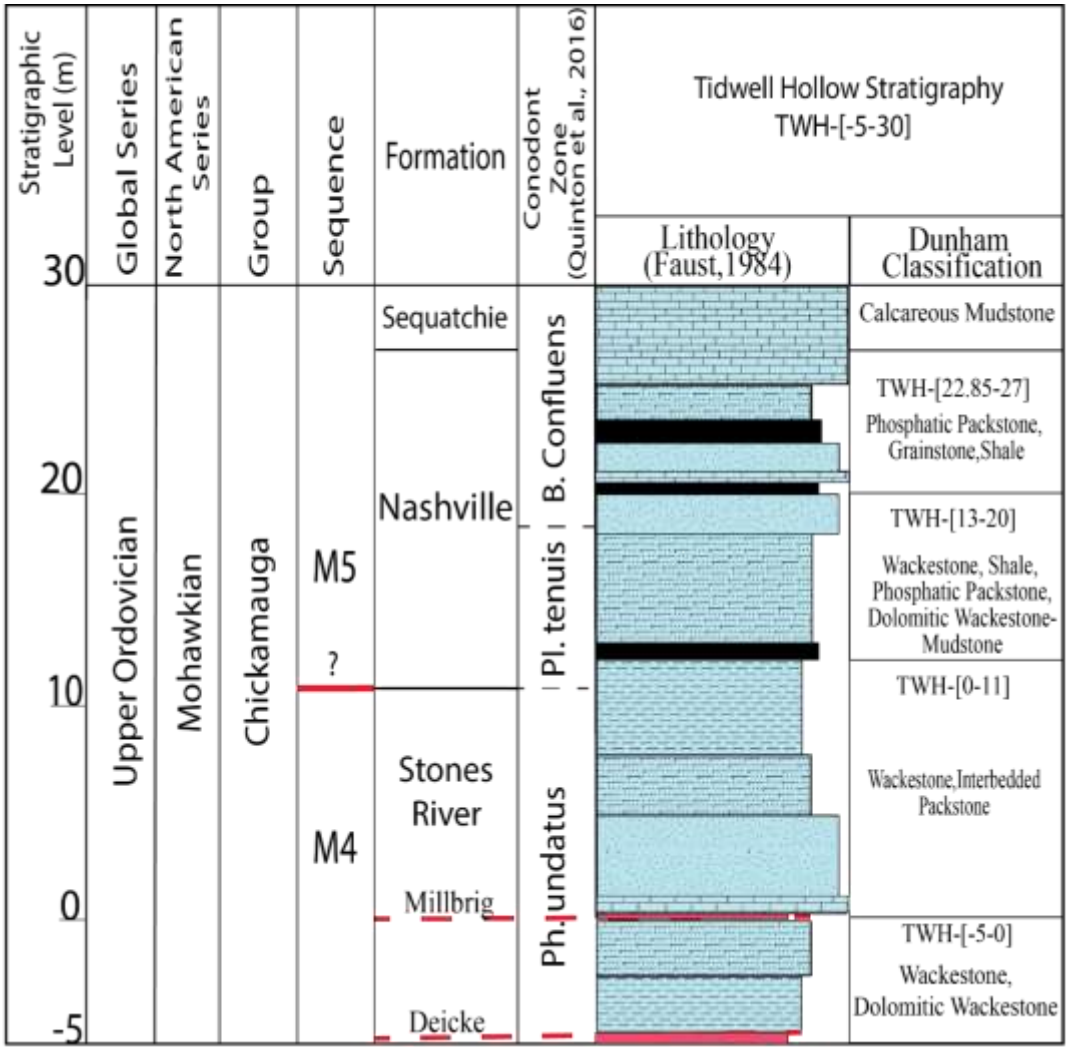

Figure 3. Stratigraphic column of the upper 35m of the Tidwell Hollow Ordovician outcrop that range from peritidal to subtidal ramp depositional environments. Lithologies are those documented by Faust (1984).

Tidwell Hollow Stratigraphy

The stratigraphic units present in this study are the upper portion of the Stones River and Nashville formation of the Chickamauga Group (Figure 3). Grain size and bed thickness of the Tidwell Hollow outcrop was methodically described at centimeter scale by (Faust, 1984) while

depositional setting for the Chickamauga has been interpreted as ranging from peritidal to subtidal-deep ramp depositional environments (Benson, 1986a, 1986b; Benson & Mink, 1983; Carter & Chowns, 1986; Quinton et al., 2016). The upper portion of the Stones River formation forms the bottom 5m of the studied interval and is composed of a peritidal sequence with limited fauna consisting of ostracods and gastropods (Benson, 1986b). This interval includes two K-Bentonite layers, the Deicke, and Millbrig which form two distinct volcanic ash horizons at this location indicating active volcanism during this time (Carter & Chowns, 1986; Drahovzal & Neathery, 1971; Herrmann & Haynes, 2015). Above the Millbrig, the peritidal sequence is overlain by approximately 10.5m of interbedded packstones and wackestones at the uppermost section of the Stones River (Benson, 1986b; Quinton et al., 2016). At this point, approximately 10.5m above the Millbrig, earlier work conducted on the Tidwell Hollow outcrop by (Quinton et al., 2016) argued for the presence of an unconformity based on a lithologic break and a 2‰ decrease in $\delta^{13}C$. In addition, biostratigraphic data collected at Tidwell Hollow marks a shift from the *Ph. undatus* to the lower *Pl. tenuis Zone* which is mostly missing (Hall et al., 1986; Quinton et al., 2016). A transition from medium-fine bedded mudstone-wackestone and packstones to nodular limestone with interbedded shale marks the lithologic transition from the Stones River to the Nashville formation above the unconformity (Benson, 1986b; Quinton et al., 2016). The Nashville comprises the final 16.5m of the studied interval and possesses a much more diverse faunal assemblage consisting of bryozoans, echinoderms, trilobites, and brachiopods as well as a transition to predominantly wackestones and packstones that are

interbedded with shale (Benson, 1986b; Herrmann & Haynes, 2015). Capping the Nashville formation is an 6-8cm layer of iron rich calacareous shale (Herrmann & Haynes, 2015).

Carbon Isotope Stratigraphy

$\delta^{13}C$ data of the Tidwell Hollow outcrop was collected by (Quinton et al., 2016). The intention of this study was to better understand if the GICE occurred on what was the southeastern margin of Laurentia. The values collected at Tidwell Hollow were taken over a 127m interval with results ranging from -3.7‰-2.2‰, however in general, $\delta^{13}C$ values from the upper 40m show stable values ranging from .7‰ at the base and -.7‰ at the top of the section while a 2‰ $\delta^{13}C$ depletion was observed 10.5m above the Millbrig K-Bentonite at the location of the unconformity (Quinton et al., 2016). While the GICE is not seen due to missing time at Tidwell Hollow (Quinton et al., 2016), the gradual increase of $\delta^{13}C$ seen occurring up section culminating with a 2‰ $\delta^{13}C$ depletion at 10.5m was interpreted by (Quinton et al., 2016) as the result of increased carbon burial prior to the GICE that correlates with interpretations made in several earlier studies (Ainsaar et al., 2010; Bergström et al., 2014; Quinton et al., 2016; Saltzman & Young, 2005).

Application of REE and Trace Element Analysis To Apatitic Fossils

REE's have been used in several earlier studies on apatites partly due to the fact that the occurrence of phosphate and the deposition of authigenic phosphate is complex with several authors attempting to explain the occurrence of this vital element as it is a limiting factor of biological activity, an indicator of sea level and climatic change, and because an understanding of these depositional facies are essential in the exploration for hydrocarbons (Auer et al., 2017; Föllmi, 1996; von Huene et al., 1987). Organic phosphorous is the most important supply of phosphorous to marine sediments where it is incorporated in the presence of microbes in

suboxic-anoxic conditions (Auer et al., 2017; Faul et al., 2005; Filippelli, 2008; Föllmi, 1996). This process occurs in areas with high productivity, oxygen-poor bottom waters, and low rates of sedimentation which are typical of environments where upwelling is commonly occurring (Burnett et al., 1982; Fonseca, 2000; Glenn et al., 1994; G. Shields & Stille, 2001).

The REE's occur in similar environments due to their trivalent nature except for Ce^{3+} and Eu^{2+} which are redox sensitive (Haley et al., 2004; Kim et al., 2012). Due to slight differences in ionic radii across the series that lead to fractionation, the lanthanides are grouped into light (LREE; La to Nd), medium (MREE; Sm to Dy), and heavy (HREE; Ho to Lu) rare earth elements (Tostevin et al., 2016). Concentrations of REE's in seawater are low, however REE's are preferentially incorporated into apatites with REE concentrations of authigenic apatites believed to mirror the ocean or pore water chemistry in which they form (Auer et al., 2017; Lécuyer, et al., 2004; Shields & Stille, 2001). However, as several authors have suggested, diagenesis and alteration of REE patterns may occur at or below the sediment-water interface in response to dynamic pore water conditions (Auer et al., 2017; Bright et al., 2009; Föllmi, 1996; Haley et al., 2004). Before interpretation, normalization of REE concentrations to a standard such as a shale or the upper continental crust is common in REE studies and serves two roles. The first is to correct for the odd-even variation in elemental abundance while the second role is to interpret elemental fractionation as REE patterns by comparing REE abundance distribution to the standard (Byrne & Sholkovitz, 1996; Elderfield, 1988).

Earlier authors have shown that natural processes such as paleoceanographic redox conditions can be observed by interpretation of normalized REE patterns (Auer et al., 2017; Haley et al., 2004; Kim et al., 2012; Shields & Stille, 2001). For example, the HREE enriched, LREE depleted seawater pattern, "flat", and middle rare earth enriched or "MREE bulge"

patterns are often observed in paleoceanographic studies and resemble the various processes occurring during burial and diagenesis (German et al., 1990; Haley et al., 2004). The HREE enriched pattern is widely recognized as the typical seawater pattern that possesses a distinct depletion in Ce which is referred to as a cerium anomaly signifying oxic marine conditions (Haley et al., 2004; Tostevin et al., 2016). The "flat" REE pattern has been interpreted as representative of riverine sediments, proximal carbonates, and clay contamination (Frimmel, 2009; Nothdurft et al., 2004). Also, this pattern has been observed in organic-rich sediments and is interpreted as representing an anoxic, sulfidic zone of marine sedimets (Kim et al., 2012). The "MREE" bulge pattern is less understood however, Haley et al. (2004) suggested a dissolved Fe source of these REE's that preferentially scavenge MREE's from the water column which is then released in marine porewaters while Auer et al. (2017) suggested MREE enrichment is due to preferential scavenging of the MREE and prolonged exposure to seawater. Finally, (Bright et al., 2009; Lécuyer et al., 2004) reported that the MREE pattern signifies extensive diagenetic alteration of primary REE patterns.

The two elements within the lanthanide series (Ce and Eu) that exhibit unique behavior can be used to infer paleoceanogrpahic redox conditions (Michael Bau & Dulski, 1996; German et al., 1990; G. Shields & Stille, 2001). Oxidation of Ce^{3+} to insoluble Ce^{4+} occurs in oxic conditions such as shallow water environments leading to removal of Ce^{4+} from solution and development of a negative cerium anomaly or ($Ce/Ce^* < 1$) quantified as $Ce/Ce^* = Ce_N /(0.5La_N+0.5Pr_N)$ (Bau &Dulski, 1996; Haley et al., 2004; Kim et al., 2012). Europium anomalies $Eu/Eu^*=Eu_N/(.67Eu_N+.33Tb_N)$, occur where Eu abundances are increased relative to

Sm and Gd in high temperature (>200°C) alkaline, anoxic conditions resulting in a positive europium anomaly (Eu/Eu* >1) (Kim et al., 2012; MacRae et al.,1992).

Application of Trace Elements

Trace elements have become standard tools in the interpretation of paleoceanographic conditions, in particular, the elements Mn, Th,Y, and U are commonly used to provide information related to redox conditions (Brennecka et al., 2011; Burdige, 1993; Swart, 2015; Wignall & Twitchett, 1996). U is concentrated in organic matter under reducing conditions and precipitates in anoxic conditions while Mn in higher concentrations may reflect oxic conditions but makes a less attractive proxy since it may be released in reducing sediments (Calvert & Pedersen, 1993; Tribovillard et al., 2006). The mass ratio of Y/Ho can be used to aid in interpreting open or restricted marine settings (Tostevin et al., 2016). An analysis of Th in REE studies is essential since this element acts as an indicator of the amount of clay contamination which, due to finer grain size, are enriched in total REE which may cause overprinting of carbonate REE signatures with terrestrial signatures (Taylor & McLennan, 1995; W. Zhang et al., 2014). Further, Th and U have been used to interpret changes in carbonate facies during periods of dynamic sedimentation (Bábek et al., 2013).

Methods

Petrographic Preparation and Analysis

Samples were collected from the Tidwell Hollow exposure of the Chickamauga Limestone located in Blount County, Alabama along State Highway 15 (33.87806 N 86.57555W). The petrographic analysis was performed using a Leica DM750P and Olympus BX50 petrographic microscope. The Dunham classification scheme (Dunham,1962) was used for carbonate classification. The suffixes –rudite, -arenite, -siltite , and –lutite refer to grain size of limestones at Tidwell Hollow documented by (Faust, 1984). Special attention was paid to the intervals that coincide with the appearance of phosphate, pyrite, and dolomite. Marine biota and microfacies of carbonate ramps described in (Flügel, 2004) was used in order to interpret changes in paleoenvironment.

Apatitic Fossil Extraction

Limestone samples collected at Tidwell Hollow were digested in 10% acetic acid. Following digestion, the samples were separated into coarse and fine-grained fractions using 125 µm and 63 µm sieves. After drying, the 125 µm grain size fraction was density separated using sodium poly-tungstate (SPT) diluted to approximately 2.8 g/cm^3. After separation, apatitic fossils, mostly gastropod steinkerns, were picked under a Leica M125 microscope. Three hundred ninety-six apatitic fossils were collected from 20 intervals. After picking, samples were mounted on thin-section slides using thermoplastic adhesive in preparation for laser ablation.

LA-ICP-MS Analysis

In order to measure the elemental composition of apatitic fossils, a Thermo iCap Qc ICP-MS was connected to a Cetac G2-213 Nd: YAG laser system for analysis. Helium was used as the carrier gas because helium enhances the transport efficiency of ablated material (Zhang et al.,

2014). Elements that were analyzed include ^{24}Mg, ^{55}Mn, ^{89}Y, ^{232}Th, ^{139} La, ^{140} Ce, ^{141}Pr, ^{146}Nd, ^{147} Sm, ^{153} Eu, ^{157}Gd, ^{159} Tb, ^{163}Dy, ^{165}Ho, ^{166}Er,^{169}Tm,^{172}Yb,^{175}Lu,^{232} Th, and ^{238}U. Spot analysis was performed using a spot diameter of 100 µm. Three hundred thirty-six apatitic fossils were ablated from twenty intervals TWH- [9.5] to TWH- [27] in order to track lithologic and geochemical changes across the studied interval. Three shots per apatitic fossil were conducted with approximately 100 µm spacing. The LA-ICP-MS settings are compiled in Tables 1 and 2.

Table 1. Cetac G2-213 Laser System Settings

Parameter	Run 1	Run 2	Run 3	Run 4	Run 5	Run 6
Laser Energy (%)	20	20	20	20	20	29
Shot Frequency (Hz)	5	5	5	5	5	5
Shutter Delay (s)	10	10	10	10	10	10
Ablation Time (s)	70	70	70	70	70	70
Washout Time	10	10	10	10	10	10
Spot Size (µm)	100	100	100	100	100	100

Table 2. Operating Parameters for Thermo iCap Qc ICP-MS

Parameter	Run 1	Run 2	Run 3	Run 4	Run 5	Run 6
RF Power (W)	1550	1550	1550	1550	1550	1550
Cool Gas Flow Rate(1/min)	14	14	14	14	14	14
Carrier Gas Flow Rate (mL/min)	723	723	723	723	723	723

Glass standard NIST 612 for LA-ICPMS calibration was based on those produced by the National Institute of Standards and Technology (NIST), while the Madagascar Fractionation Reference Apatite (MAD Apatite) (Thomson, Gehrels, Ruiz, & Buchwaldt, 2012), Durango Apatite (Chew et al., 2011; McDowell et al., 2005; Soares et al., 2015; Yang et al., 2014), and Blue Brazil apatite served as secondary standards to assess precision and drift between sampling runs. Values of Durango apatite found in this study were compared to those in the literature in order to determine the accuracy of the techniques used in this study. BlueBrazil was used to assess precision by comparing the variation in values between the multiple sampling sessions in this study and was sourced from the Minas Gerais state of Brazil. MAD apatite was sourced from the Madagascan 1st Mine Discovery (Thomson et al., 2012) and was only used in Run 1 of this study. The Durango apatite formed in association with intrusions along the southern margin of the Chupaderos caldera complex outside Durango City, Mexico and is typically used in fission track analysis (Chew et al., 2011; McDowell et al., 2005). The glass standard used in this study was NIST SRM 612 as the external standard and ^{43}Ca as the internal standard to monitor for non-phosphatic material. Standards were measured three times each in the beginning, after twenty

measurements Durango and NIST612 three times were measured and three times each once more at the end of the analyses run.

Data reduction was performed using Iolite v2.5 (Hellstrom, Paton, Woodhead, & Hergt, 2008) application extension for IGOR PRO 6.3.7.2. Reduction scheme and DRS settings that were used in this study for the trace element data are those found in (Paton et al., 2011). This data reduction allows for the transformation of data collected from the laser ablation system in counts per second (CPS) to elemental concentrations and analyzed. During data reduction, data was analyzed for anomalously high Mn, U, and Th content that likely formed coatings on the outside of the steinkerns. These elements must be screened for because Mn oxides and siliciclastics contain anomalously high REE concentrations that can alter the true value of the sample (Nothdurft et al., 2004). Further, screening for non phosphatic components during data reduction was completed by setting a cut off limit of 38% ^{43}Ca which is the approximate percent Ca of Ca_3PO_4.

REE data was normalized to the Upper Continental Crust (UCC) from McLennan (1989) and Rudnick and Gao (2003) compiled in Piper & Bau (2013). Because REE concentrations are extremely low (ppm/ppb) in seawater, modern seawater values are magnified by $x10^6$. Modern seawater values used in this study are found in (Alibo & Nozaki, 1999). Eu, Ce, and Pr anomalies were calculated using the following formulas: $Pr/Pr^*=Pr_N/(0.5Ce_N + 0.5Nd_N)$, $Ce/Ce^*=Ce_N/(0.5La_N + 0.5Pr_N)$, $Eu/Eu^* =Eu_N/(.67Eu_N + .33Tb_N)$ (Bau & Dulski, 1996; Zhang et al., 2014). Sm, and Yb were used as proxies for LREE, MREE, and HREE respectively in order to calculate enrichment ratios and infer depositional environment (Garnit et al., 2012; Kowal-Linka et al., 2014; Zhao et al., 2013). Y, U, and Th were used in addition to the REE to quantify the presence of siliciclastic material and paleo redox conditions (Zhao et al., 2013).

Results

Thin Section Description

The distribution of phosphate, transition to more skeletally supported rocks, and increase in abundance of open ocean fauna at the Tidwell Hollow outcrop appears in increasing amounts moving up section. Characterization of rock matrix, biota, and diagenetic features was conducted and are compiled in (Appendix 1). The description that follows is concerned with the presence of phosphate and constituent minerals that may lead to a better understanding of the origin and preservation of the phosphate and organogenic dolomite. In addition, by observing changes in microfacies and fossil assemblages found in thin sections at Tidwell Hollow, changes in paleoenvironmental conditions through time were inferred (Flügel, 2004). This section is divided into three intervals, those rocks occurring below TWH-[10.5] with little to no phosphate, restricted fossil assemblage, and abundant peloids similar to the Pre-Taconic facies (Holland & Patzkowsky, 1998; Holland & Patzkowsky, 1997) and those occurring above TWH-[11] enriched in phosphate and possessing an abundance of suspension feeders such as gastropods and echinoderms similar to the Post-Taconic facies (Holland & Patzkowsky, 1998; Holland & Patzkowsky, 1997). The interval TWH-[10.5-11] is markedly different from both the previous sections as it marks a lithologic break from the underlying interval and contains abundant siliciclastic grains whose origin cannot be fully understood with petrographic analysis alone.

Table 3. Summary of petrographic analysis by interval conducted on intervals TWH- [5-27]

Interval (TWH-[x])	Dunham Classification	Biota
27	Phosphatic Grainstone	Bryozoans, Echinoderms
26.35	Phosphatic Grainstone	Gastropods, Echinoderms
26	Phosphatic Packstone	Gastropods, Echinoderms
24.5	Phosphatic Packstone	Gastropods
23.5	Phosphatic Packstone	Trilobites, Echinoderms, Bryozoans
23	Phosphatic Packstone	Echinoderms
21	Phosphatic Packstone	Gastropods
20.5	Phosphatic Packstone	Bryozoans, Echinoderms, Trilobites
20	Phosphatic Packstone	Brachiopods, Echinoderms
19	Phosphatic Packstone	Brachiopods, Gastropods
18.5	Phosphatic Packstone	Bryozoans, Bivalves
18	Grainstone	Bryozoans
17.5	Dolomitic-Grain-Packstone	Echinoderms
17	Wackestone	Gastropods
16.5	Nodular Packstone	Gastropods, Trilobites, Echinoderms
15.5	Wackestone	Gastropods, Echinoderms
15	Wackestone	NA
14.55	Wackestone	Echinoderms, Bryozoans, Gastropods
14	Dolomitic Wackestone	Echinoderms
13.5	Dolomitic Packstone	Echinoderms, Gastropods
12.5	Phosphatic Packstone	Echinoderms, Gastropods
11	Siliceous Wackestone	NA
10.5	Wackestone	NA
10	Wackestone	Gastropods
9.75	Wackestone	Echinoderms, Gastropods
9	Packstone	Bivalves
8.5	Packstone	Gastropods, Bivalves
8	Wackestone	Gastropods
5	Wackestone	Coral
4.75	Wackestone	Echinoderms
3	Packstone	Gastropods, Brachiopods
1.5	Packstone	Echinoderms
1	Packstone	Gastropods
0	Millbrig	NA
-0.5	Mud-Wackestone	NA
-1	Mud-Wackestone	NA
-1.5	Dolomitic- Mud-Wackestone	NA
-3	Dolomitic- Mud-Wackestone	NA
-3.5	Mud-Wackestone	NA
-4	Mud-Wackestone	NA
-4.5	Dolomitic-Mud-Wackestone	NA
-5	Dolomitic-Mud-Wackestone	NA

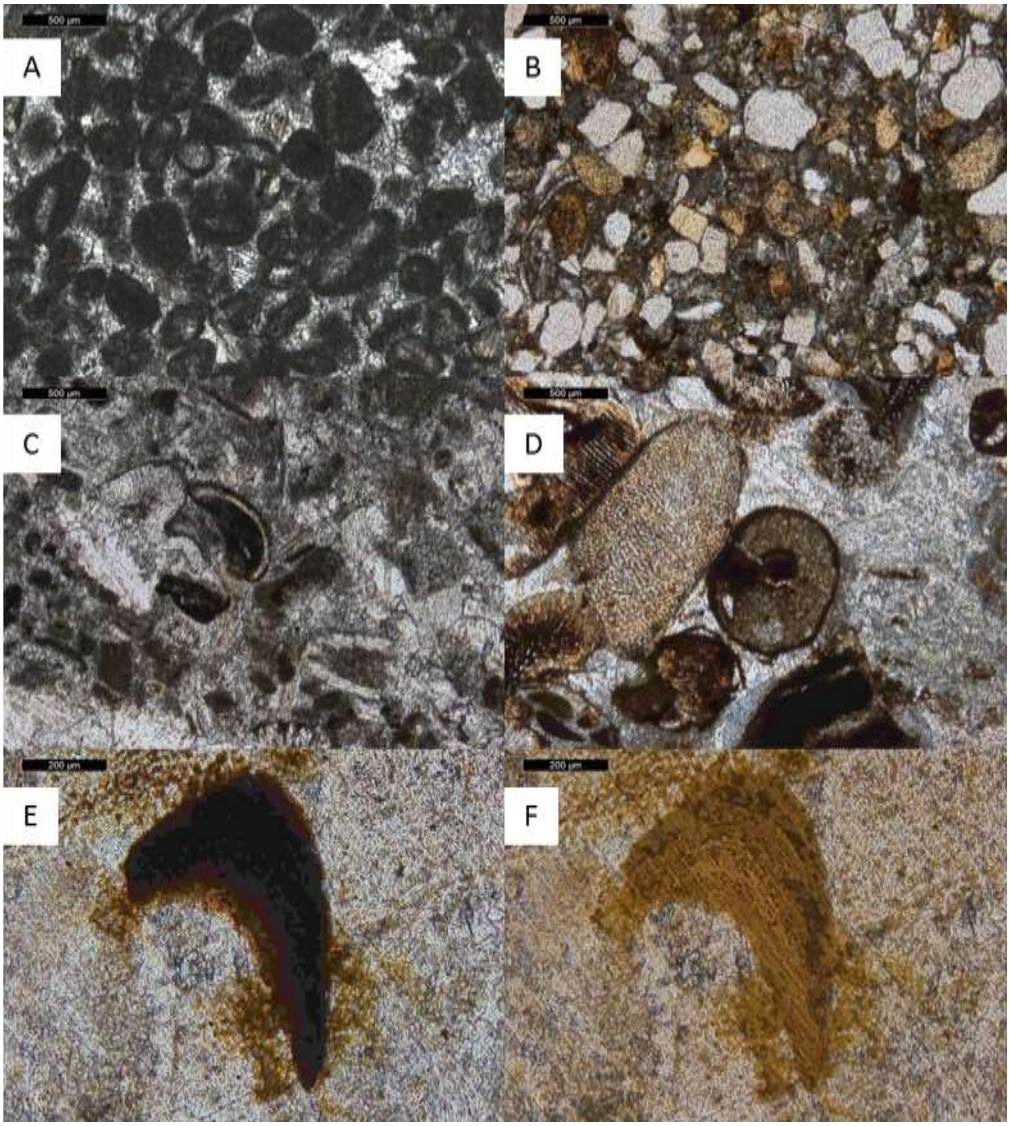

Figure 4. A**.** Sample TWH- [0] is representative of the shale-wackestone peritidal facies found at Tidwell Hollow. This sample contains no fossils, abundant peloids, and calcite cement that may be meteoric in origin. B: Sample TWH-[11]. This sample depicts siliciclastics from the proposed unconformity at Tidwell Hollow. C: Sample TWH-[12.5] marks the first appearance of phosphate and packstones above the siliciclastic interval D: Sample TWH- [26] is a packstone that possesses partially phosphatized echinoderm and gastropod fossils. This image represents the increased presence of echinoderms and gastropods that signify a shift to a more open marine environment. E: Sample TWH-[14.5] shows a echinoderm fragment that has been replaced by phosphate observed under plain polarized light. F: Sample TWH-[14.5]: Same echinoderm fragment under reflected light showing the partial replacement of phosphate by pyrite grains.

The lower interval is composed of samples occurring from TWH-[-5-10.5] and displays similar facies to the Pre-Taconic platform (M1-M4) facies of the Nashville Dome (Holland & Patzkowsky, 1998; Holland & Patzkowsky, 1997). The samples seen in this lower interval are, in general, peloidal-mud-wackestones and have a calcisiltite texture with no phosphate, and no bioturbation or organic material present. The matrix is sucrosic and gray-tan in color. Dolomite grains in this interval tend to occasionally share crystal boundaries and are distributed evenly throughout the section. Those rocks occurring from TWH- [-5 – 3] have been interpreted as being deposited in a peritidal environment (Quinton et al., 2016). Unlike these rocks, the lithologies TWH-[1-10]) transition into interbedded wackestones and packstones and show a slight increase in fossil abundance (i.e., gastropods, bivalves, and coral) (Table 3). It should also be noted that within .5m of the top of this sequence (i.e., TWH-[10.5)], these samples contain minor evidence of subaerial exposure such as meteoric cement that traditionally cap carbonate peritidal sequences (Esteban & Klappa, 1983).

Sample TWH- [11] differs from the rest of the studied section in that this sample contains no phosphate or organic matter and a high amount of siliciclastic sediment. These quartz grains were identified in cross-polarized light by their yellow-grey appearance (Figure 4b). The quartz grains in this sample are sub-angular and poorly sorted with grain size ranging from silt to sand. This lithologic break marks an unconformity previously interpreted by (Quinton et al., 2016).

The final interval includes samples TWH- [12.5-27]. This interval is similar to the post-Taconic subtidal platform facies (M5-C5) sequences of the Nashville Dome (Holland & Patzkowsky, 1998; Holland & Patzkowsky, 1997). TWH- [12.5] marks the first appearance of phosphatic limestone within the studied interval. Phosphatic material is recognized by its brown to black amorphous appearance that shows no cleavage and is partially pyritized in some samples

under plain polarized and reflected light (Figure 4E, F). Phosphate occurs as part of the rock matrix, phosphatized skeletal fragments of echinoderms, gastropods, bryozoans, and trilobites as well as apatitic fossils or steinkerns (Figure 4C, D). In addition to the marked abundance of phosphate, this interval also represents a transition from dominant peloidal-mud-wackestone deposition to primarily packstone-grainstone deposition (Figure 4A, C). Limestone that is organic-rich partially pyritized mud-shale that possess organogenic dolomite is present in multiple intervals interbedded with limestone deposits but is concentrated in intervals TWH-[13.5-17.5]. In contrast with the peritidal sequence, these packstones-grainstones contain a diverse fossil assemblage similar to cool water fauna that are primarily composed of suspension feeders such as echinoderms and gastropods marking an abrupt change in environment from the underlying restricted fossil assemblage of primarily gastropods. Trilobite, bivalve, and bryozoan fossils are also seen throughout the interval. The section is capped by an iron and clay-rich grainstone interval that contains numerous bryozoan and echinoderm fossils.

Standards and Geochemical Data

Durango Apatite

Values for Durango Apatite were collected and are compiled in Table 4. Values collected in runs 2-7 were compared to those found in (Yang et al., 2014) and (Soares et al., 2015). Statistical analysis including calculation of standard deviation (SD), standard error, and % relative standard deviation was conducted on average elemental concentrations to assess variability among the different elements compared to values in previous studies. This comparison was used to infer the degree of accuracy of this experiment to other studies using Durango apatite. Greatest variability in standard error and standard deviation are associated with

the LREE's, Nd, and Y while variability decreases in the HREE and U samples. % relative standard deviation is highest in Th and U.

Table 4.LA-ICP-MS from this study compared to those compiled in (Yang et al., 2014) and (Soares et al., 2015) using LA-ICP-MS and EPMA analysis.

	Measured (This Study)				Reference Values (All Elements)			
Element	**Average (n=151)**	**± SD**	**Standard Error**	**% Relative Standard Deviation**	**Durango Chew**	**Durango Fisher**	**Durango Hou**	**Durango Soares**
^{24}Mg	264.71	17.80	1.44	6.72	241	120.65	181	228
^{89}Y	620.22	24.91	2.02	4.02	911	427	762	NA
^{139}La	2884.86	144.88	11.75	5.02	4285	3176	2772	2941
^{140}Ce	5312.28	282.11	22.88	5.31	5405	3635	6832	4326.5
^{141}Pr	458.25	19.99	1.62	4.36	488	307	832	NA
^{146}Nd	1331.11	55.49	4.50	4.17	1677	1009	1290	NA
^{147}Sm	175.40	6.13	0.50	3.50	237	127	207	NA
^{153}Eu	17.55	0.60	0.05	3.43	21	15	20	NA
^{157}Gd	184.37	16.09	1.31	8.73	204	105	174	NA
^{159}Tb	19.23	0.79	0.06	4.09	28	13	23	NA
^{163}Dy	102.18	3.71	0.30	3.63	154	68	123	NA
^{165}Ho	20.26	0.76	0.06	3.76	32	14	25	NA
^{166}Er	57.33	2.28	0.18	3.98	83	34	64	NA
^{169}Tm	7.00	0.29	0.02	4.19	10	4	8	NA
^{171}Yb	38.80	1.65	0.13	4.26	59	27	47	NA
^{175}Lu	5.24	0.23	0.02	4.36	6	4	6	NA
^{232}Th	148.61	16.34	1.33	10.99	320	151	231	NA
^{238}U	6.50	0.71	0.06	10.98	20	7	11	7.5

BlueBrazil Apatite

BlueBrazil apatite was used to measure the level of precision between individual runs of this study. In order to measure the level of precision, statistics including standard error, % relative standard deviation, and standard deviation were calculated from the average concentration of each element collected during each run that BlueBrazil was used. As with the Durango apatite, standard deviation varied greatest with LREE and Mg while decreasing variability in the HREE values. The % relative standard deviation was calculated as the standard deviation of the element average by the average concentration of the element to assess precision. Greater variation in % relative standard deviation correlates with less precision. As with the standard deviation, % relative standard deviation decreases across the lanthanide series to a minimum at Yb. U has anomalously low concentrations in Run 4 which may be responsible for the higher % relative standard deviation seen for this element.

Table 5. Concentrations of REE, trace, and minor elements reported in ppm collected in this study for BlueBrazil.

Element	Measured (This Study) Average (n=72)	± SD	Standard Error	% Relative Standard Deviation	Run 2 Average (n=6)	Run 3 Average (n=11)	Run 4 Average (n=6)	Run 5 Average (n=12)	Run 6 Average (n=11)	Run 7 Average (n=25)
^{24}Mg	156.20	19.37	2.27	12.40	117.03	119.34	173.80	136.60	161.03	165.67
^{5}Mn	247.20	20.11	2.35	8.13	239.58	258.19	287.00	232.00	244.68	243.31
^{89}Y	119.26	6.20	0.73	5.20	143.23	147.44	117.60	121.63	119.20	119.07
^{139}La	229.41	19.73	2.31	8.60	249.37	241.28	245.85	245.88	219.67	212.88
^{140}Ce	697.81	59.92	7.01	8.59	728.33	736.45	772.50	727.75	665.00	658.50
^{141}Pr	72.83	4.11	0.48	5.64	75.80	76.10	76.42	75.44	70.23	69.94
^{146}Nd	234.70	10.92	1.28	4.65	243.90	241.54	241.83	241.77	230.97	226.51
^{147}Sm	38.68	1.65	0.19	4.27	38.57	39.36	39.38	39.96	38.37	37.82
^{153}Eu	6.74	0.36	0.04	5.35	6.82	6.91	7.10	7.04	6.59	6.50
^{157}Gd	35.05	3.11	0.36	8.86	36.28	35.55	43.63	35.30	33.79	33.05
^{159}Tb	4.18	0.18	0.02	4.34	4.21	4.26	4.34	4.30	4.12	4.08
^{163}Dy	22.85	0.95	0.11	4.17	22.77	23.22	23.16	23.34	22.59	22.52
^{165}Ho	4.31	0.20	0.02	4.54	4.29	4.36	4.35	4.42	4.25	4.27
^{166}Er	11.89	0.52	0.06	4.39	11.78	12.10	11.93	12.08	11.74	11.80
^{169}Tm	1.49	0.06	0.01	4.33	1.47	1.50	1.50	1.51	1.47	1.49
^{171}Yb	8.18	0.32	0.04	3.96	8.08	8.22	8.13	8.26	8.17	8.16
^{175}Lu	8.18	0.04	0.01	4.11	1.08	1.10	1.09	1.10	1.08	1.09
^{232}Th	1.09	33.81	3.96	4.42	760.83	774.64	775.00	768.42	746.00	764.73
^{238}U	47.14	3.85	0.45	8.16	50.15	50.00	40.97	49.71	46.41	45.81

Apatite Geochemical Data

REE data for the apatites capable of being sampled are compiled in (Appendix 2). All of the samples were found to be MREE enriched (Figure 5 a,b).∑REE concentrations collected from TWH-[9.5-27] range from 286.34-4585 ppm. REE patterns were subdivided into three intervals based on ∑REE and petrographic observations. Various plots were made in order to analyze anomalously high values of Th as a proxy for siliciclastic contamination. Crossplots illustrating relative REE enrichment and $(La/Yb)_N$ ratios versus $(La/Sm)_N$ were plotted to assess diagenetic alteration. In general, assessment of diagenesis and siliciclastic enrichment reveals that all of the apatites in this study have been modified due to various processes.

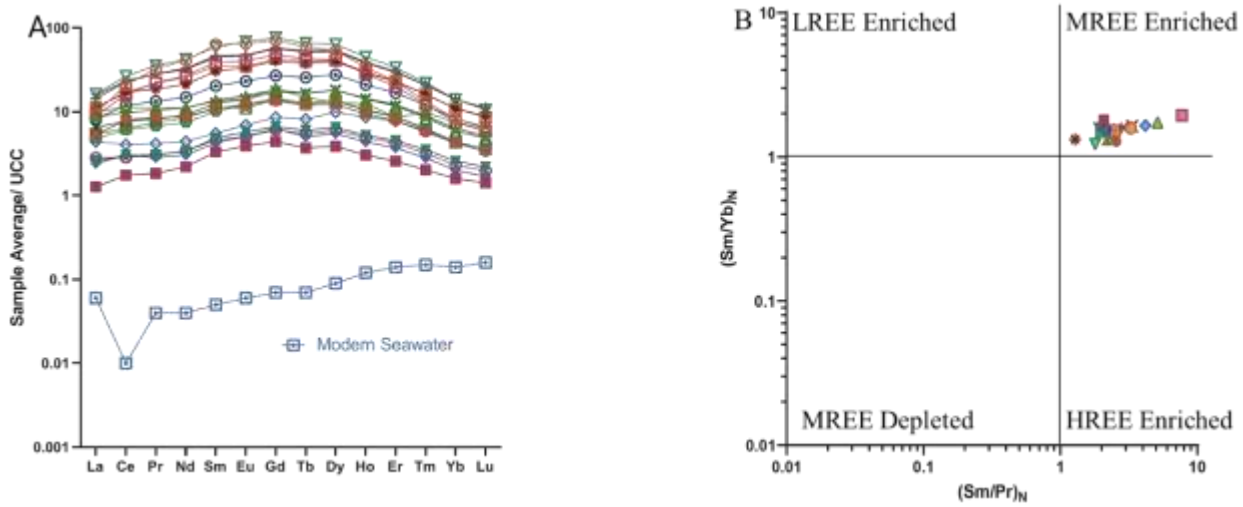

Figure 5. A: Average normalized values of all samples compared to modern seawater from Alibo and Nozaki (1999). B: $(Sm/Yb)_N$ vs $(Sm/Pr)_N$ used to determine REE enrichment after (Garnit et al., 2012).

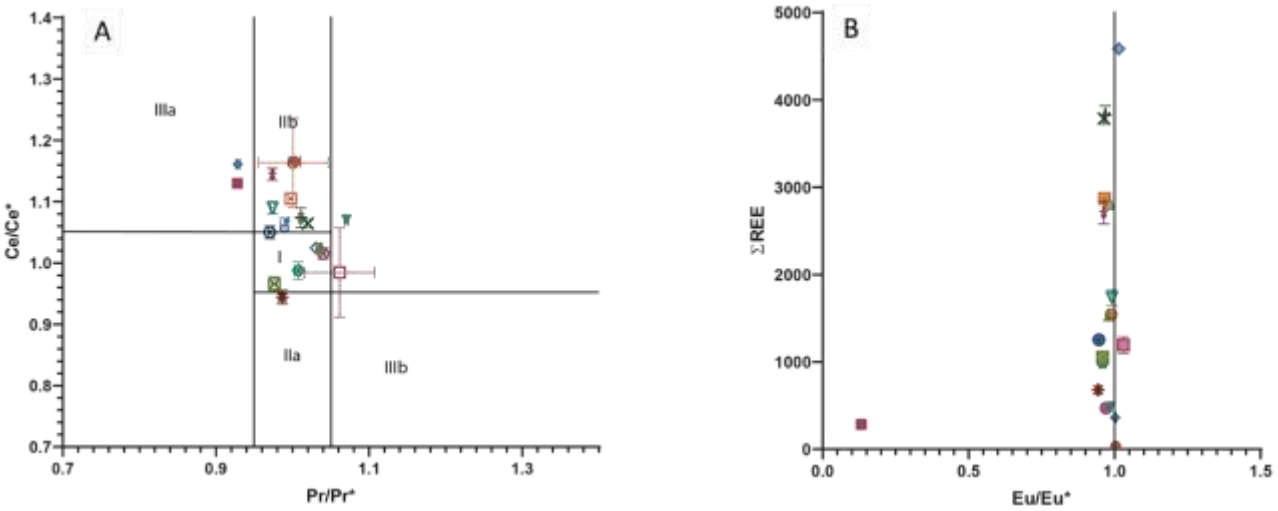

Figure 6. A: Ce/Ce* vs Pr/Pr* plot after (Michael Bau & Dulski, 1996). Field I: neither Ce or La anomaly, field IIa positive La anomaly, no Ce anomaly, field IIb negative La anomaly no Ce anomaly field IIIa positive Ce anomaly, field IIIb negative Ce anomaly. B: Eu/Eu* plot to assess cerium and europium anomalies.

Peritidal and Siliciclastic Interval REE Data

The peritidal and siliciclastic interval is composed of three samples from TWH-[9.5-11] that lie at or below the unconformity at Tidwell Hollow interpreted by Quinton et al., (2016). All three of the are enriched in ∑REE with the ∑REE values for this interval ranging from 471.61-1054 ppm. Ce/Ce* values range from .96-1.06. Eu/Eu* values range from .96-.97 and Pr/Pr* values .97-1. Based on the Ce/Ce* vs. Pr/Pr* plot, the samples exhibit variable anomalies (Figure 6a). TWH-[9.5] and TWH-[10] exhibit neither Ce or La anomalies while TWH-[9.5] exhibits a positive La anomaly with no Ce anomaly. U concentrations range from 10.04-16.14 ppm while Th ranges from 9.36 to 23.56 ppm and Mn ranges from 177.91-221.66 ppm. Y/Ho ratios range from 31 to 35 and Th/U ratios 0.74-1.46.

Wackestone-Packstone Interval REE Data

Wackestone-packstone facies of Tidwell Hollow consists of nine samples from TWH-[13-20]. This interval possesses the highest average ∑REE of the studied section that ranges from 1735.09- 4585.24 ppm. However, Th concentrations in this interval are the highest of the

entire studied section ranging from 9.47-95.05 ppm and therefore these values likely overprint the original REE pattern of the apatites. This interval contains U concentrations ranging from 11.87-22.83 ppm and Mn values range from 143.82-484.09 ppm.Ce/Ce* ranges from .94-1.14 and Eu/Eu* from .96-1.01 while Pr/Pr* ranges from .97-.103. When plotted on the Ce/Ce* vs Pr/Pr* plot, samples TWH-[13,16,16.5] exhibit no anomaly while samples TWH-[13.5,14,14.5,15, 15.5 and 17.5] display negative La anomalies and no Ce anomaly (Figure 6a).Y/Ho ratios range from 27-32 and the highest Th/U ratios of the entire studied section are found between intervals 14.5 and 15 with both intervals reporting ratios of 5.7 while the entire interval ranges from .7-5.7.

Packstone-Grainstone Interval REE Data

The packstone-grainstone interval is made up of eight samples from TWH-[18-27] collected from the upper section of the Tidwell Hollow outcrop that contains primarily phosphatic packstone-grainstone deposition. The REE patterns for this section possess lower ∑REE enrichment than the underlying interval ranging from 286.34-2814.08 ppm. Ce and Eu anomaly values range as follows Ce/Ce* .65-.1.16, Eu/Eu* .13-1.03, and Pr/Pr* from .92-1.07. TWH-[18.5,23,23.5] do not plot within any of the zones. TWH-[22.85] and TWH-[26.35] shows a positive Ce anomaly. Samples TWH-[20] and TWH-[27] possess a negative La anomaly and no Ce anomaly. U concentrations are found in their highest concentrations in this study in sample TWH-[20] with a concentration of 26.42ppm. The range in U concentrations for the interval is 5-26.42 ppm and the range for Mn is 113.62-312.52 ppm. The highest Y/Ho ratios of the studied section are in this interval ranging from 26-56. Th/U ratios range from .44-3.46.

REE and Trace Element Profile

The REE profile (Figure 7) of the studied section was generated in order to observe general trends in REE, trace element concentrations, and elemental ratios, as well as their relationship with $\delta^{13}C$ values, collected at this location by (Quinton et al., 2016). Average ∑REE of the section is greatest in the wackestone-packstone interval (2594 ppm) and lowest in the peritidal and siliciclastic interval (838 ppm) and the packstone-grainstone is in between (126 ppm).

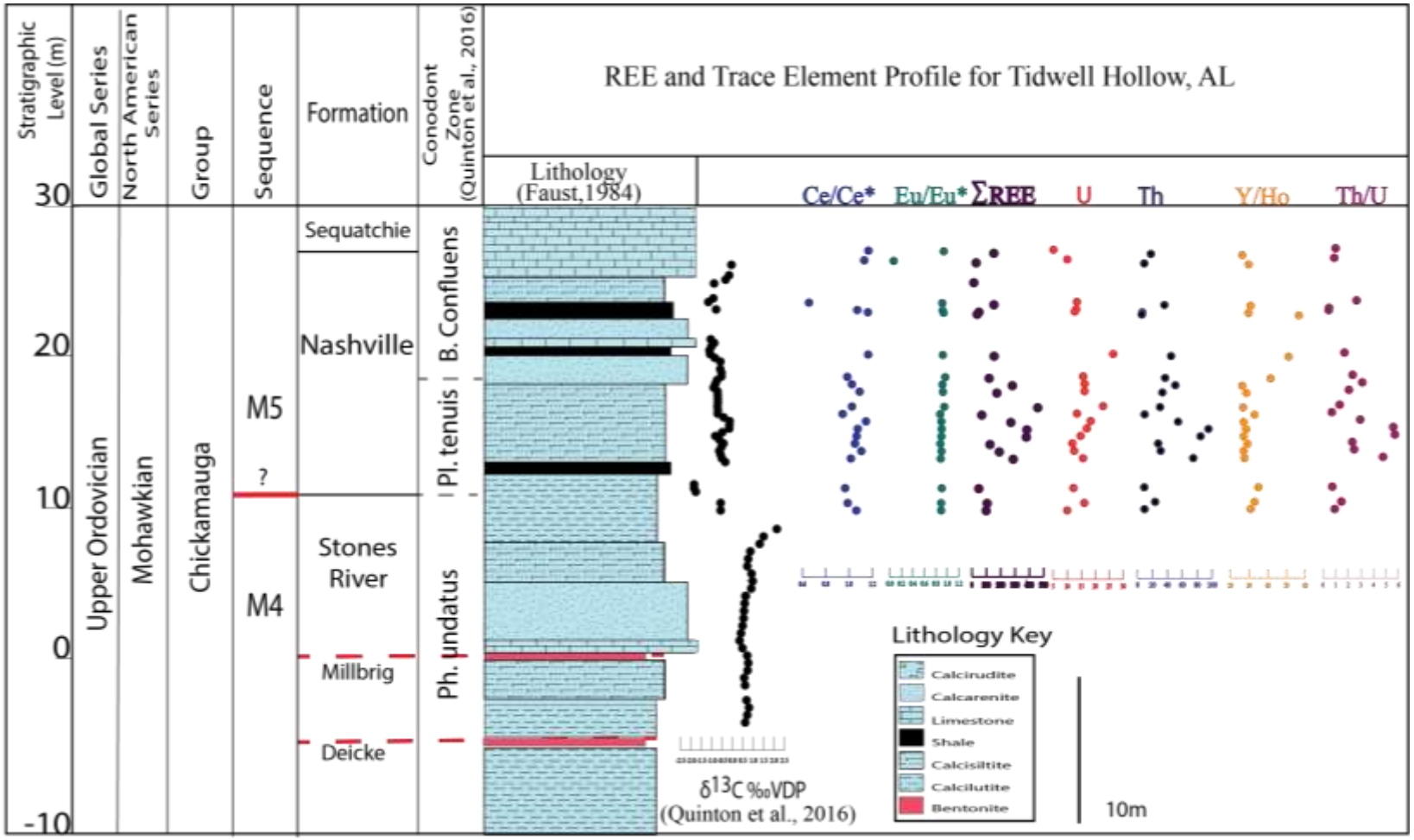

Figure 7. Chemostratigraphic profile of Tidwell Hollow, Alabama. $\delta^{13}C$ values are from (Quinton et al., 2016) and range from TWH-[-5-27]. The element concentrations are in ppm. Element concentrations and elemental ratios range from TWH-[9.5-27].

Th concentrations average 48.91 ppm compared to 14 ppm in the underlying peritidal-siliciclastic interval (14 ppm) and the overlying packstone-grainstone interval (26 ppm).

The Ce/Ce* values show little variation throughout the interval with values ranging from .66 to 1.16. As was discussed earlier, the Ce anomaly is highly variable with none of the samples showing a strong depletion of Ce relative to the other REE's. Eu/Eu* values range from .13 to 1.03 with an average of .93 with the anomalously low value occurring at the top of the section collected from sample TWH-[26.35]. However, immediately above this sample, Eu/Eu* values return to 1.16 in sample TWH-[27].

The Y to Ho ratio is fairly consistent in the bottom half of the section ranging from 26-34 from samples TWH-[9.5-18] while an interval of much higher Y/Ho ratios occurs between TWH-[18.5-22.85] with values ranging from 41-56. Following this dramatic increase in Y/Ho values, a return to lower values similar to the bottom half (26-29) occurs at the top of the section.

U concentrations occur at their lowest at the top of the interval in sample TWH-[27] with a concentration of 5 ppm. The second lowest concntrations occur at the bottom of the interval in sample TWH-[9.5] and below the top of the section in sample TWH-[27]. The remainder of the section ranges from 12-26 ppm with the highest concentration of U in sample TWH-[20] with a concentration of 26 ppm.

Th/U ratios can be divided into three intervals within the studied section that closely mirror the divisions made for REE data. The peritidal-siliciclastic interval has Th/U values that range from .93-1.46. Moving upsection, the wackestone-packstone interval contains the highest Th/U values with a maximum of 5.7 and an average of 3.09. Overlying the wackestone-packstone interval, the Th/U ratios decrease slightly to an average of 1.89.

Interpretation and Discussion

Durango and BlueBrazil Apatites

Elemental concentrations of Durango apatite from this study (Table 4 &5) were compared to values in earlier studies (Soares et al., 2015; Yang et al., 2014) to measure accuracy. The standard deviation of the average concentration was collected to represent standard error collected from the Durango apatite in this study to better compare elemental averages to the published values. LREEs show the greatest variability but variation is also high in Nd, Mg, Th. The values in the literature compiled in (Soares et al., 2015) and (Yang et al., 2014) vary greatly between studies as well. The large discrepancy in values from run to run could be related to the fact that Durango apatite formed in association with intrusions which may have resulted in zonation of the apatite crystals and LREE fractionation from sample to sample used in different studies. However, after conducting analysis on Durango as a suitable reference material using LA-ICP-MS and EPMA measurements in order to assess U homogeneity (Soares et al., 2015) found very low variation of U (%RSD=1) concluding that Durango serves as a suitable reference material. Nevertheless, other studies such as Fisher et al. (2011) concluded that Durango was not a homogenous reference material suggesting the presence of inclusions in Durango apatite. Regardless, the variability in this study decreases across the lanthanide series to a minimum for Lu. When compared to values compiled in (Yang et al., 2014) and (Soares et al., 2015), elemental concentrations of the LREE's fall into the range of published data. This can be said for the remainder of the elements with the exception of U which measured at 6.5ppm in this study and is closest to the values documented in (Fisher et al., 2011).

In this study, BlueBrazil was used to measure the precision of data collection from run to run. Average concentrations of the elements collected for BlueBrazil (Table 5) show a similar

trend in variability as the Durango apatite in that the greatest variability lies in LREE concentrations. However, the %RSD which is a common expression of variability is relatively low for most of the elements including the MREE's and REE's that are calculated at a % RSD ≤5 which is within the range of variability acceptable for standardization (Liang & Grégoire, 2000).

Evaluation of REE In Apatites and Comparison to Modern Seawater

Authigenic and biogenic apatites have been considered as useful paleoenvironmental and paleoceanographic indicators (Garnit et al., 2012; Jarvis, 1995), however, as eluded to earlier, REE signatures are capable of being altered due to diagenesis due to a multitude of diagenetic processes (Bright et al., 2012; Shields & Stille, 2001) and therefore a closer look at these effects before further interpretation is necessary. In addition to diagenesis, incorporation of silclastic material where Th is commonly used as a proxy, may affect REE signatures in carbonates (Bolhar & Van Kranendonk, 2007; Nothdurft et al., 2004). Finally, Lécuyer et al., (2004) suggested that a different scavenging mechanism existed in pre-Cretaceous seawater that could be responsible for different REE patterns in all ancient phosphates. However, given the evidence discussed below supporting other hypotheses, this explanation will not be pursued further in this study.

Uptake of REE's into the crystal lattice of apatites occurs at the sediment-water interface and should record concentrations similar to the seawater they are precipitated from (Elderfield & Pagett, 1986; Garnit et al., 2012; Lécuyer et al., 2004; Reynard et al., 1999). However, enrichment of REE's can occur due to several mechanisms including substitution and adsorption during early and late diagenesis as well as enrichment via iron reduction in the sediments which can overprint original REE signatures (Auer et al., 2017; Föllmi, 1996; Garnit et al., 2012; Haley

et al., 2004; Lécuyer et al., 2004; Reynard et al., 1999). Therefore, in order to assess the validity of the apatatites in this study as records of paleo seawater conditions, diagenetic effects were assessed using the methods of (Reynard et al., 1999) and (Garnit et al., 2012). $(La/Sm)_N$ ratios in this study range from .33-.79 while $(La/Yb)_N$ ratios range from .79-1.38. Modern seawaters from (Reynard et al., 1999) compiled in Garnit et al., (2012) ranges from 0.2–0.5 for (La/Yb) and 0.6–1.6 for (La/Sm). A comparison to modern seawater (Figure 8) after (Reynard et al., 1999) and (Garnit et al., 2012) shows that while these apatites are not dramatically altered, they have undergone diagenetic affects associated with substiution and early diagenesis. Modern seawater possesses $(La/Nd)_N$ ratios that range from .8-2 as suggested in earlier studies (Garnit et al., 2012; Shields & Stille, 2001). The broad range in $(La/Nd)_N$ ratios in this study (.23-.89) suggest that while some apatites display similar values to seawater, there is a significant deviation from seawater in a number of the samples in this study (Shields & Stille, 2001)

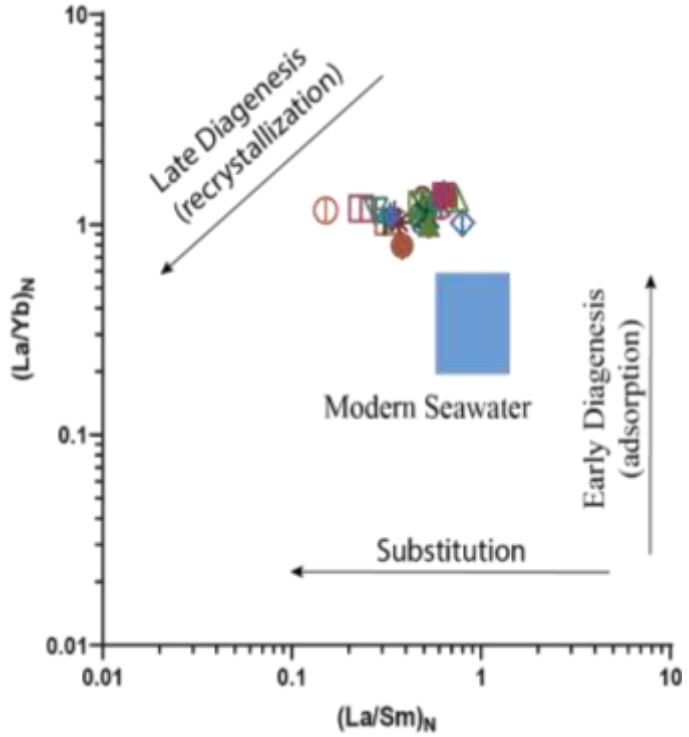

Figure 8. $(La/Yb)_N$ vs $(La/Sm)_N$ plot after (Reynard et al., 1999) and (Garnit et al., 2012) used to assess extent and mode of diagenetic alteration.

Contamination of even small amounts (2% of UCC) can cause alteration of REE patterns (Nothdurft et al., 2004). Th has been used in earlier studies as a proxy for contamination due to a greater concentration in shales and clays than carbonates (Nothdurft et al., 2004; Webb & Kamber, 2000). Two crossplots (Y/Ho vs.∑REE and Y vs.La) after (Zhao et al., 2013) were used to assess contamination due to siliciclastic input. In order to determine silclastic influence, Y/Ho ratios vs. ∑REE were compared (Figure 9a). The Y/La plot was used in addition to the Y/Ho plot to assess similiarites of the sampless with upper contintental crust and modern seawater (Figure 9b). Based on these crossplots, a majority of the samples in this study have been contaminated by siliciclastics and any further interpretations using REE's needs to be done with caution.

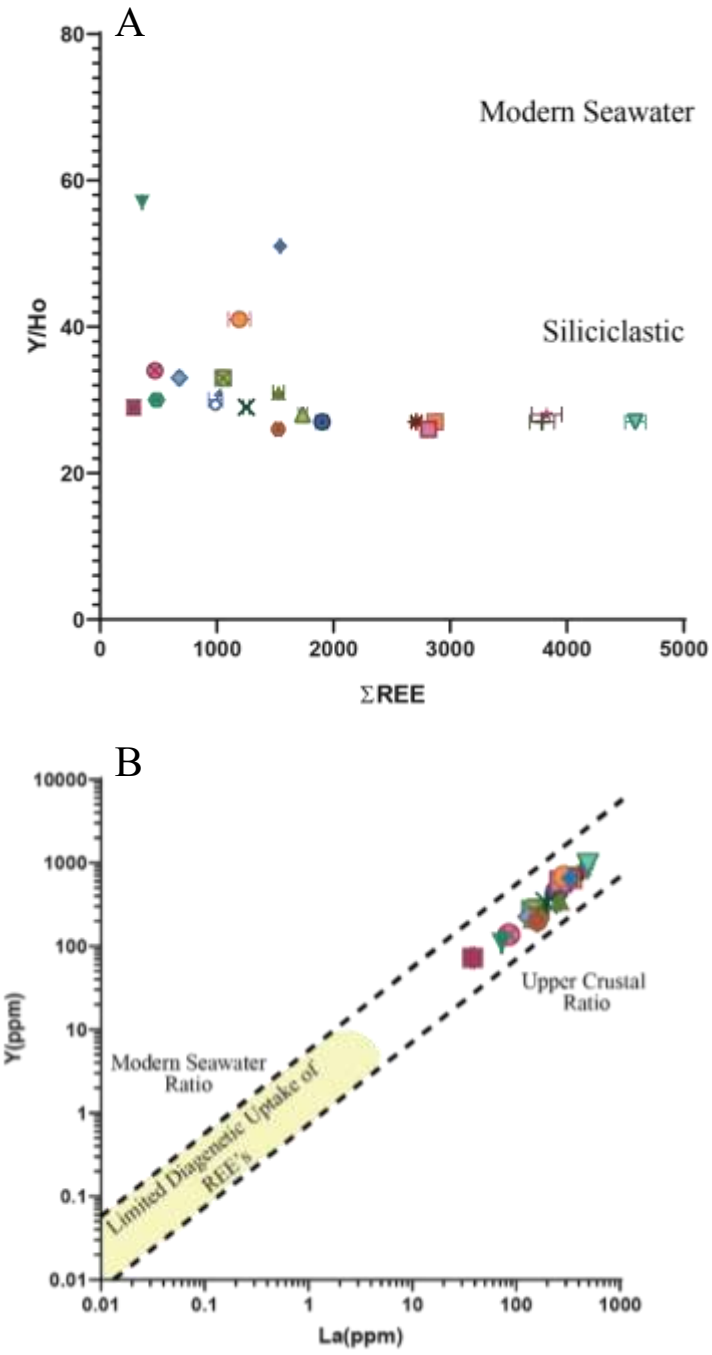

Figure 9. A: Y/Ho vs. ∑REE and B: Y vs. La used to identify siliciclastic overprint of apatites. Dotted lines represent weighted ratio of Y/Ho after (Zhao et al., 2013).

The MREE enrichment of the apatites in this study coupled with an analysis of diagenesis and contamination discussed above agrees with studies that have concluded MREE enrichment in authigenic apatites likely reflects diagenetic alteration of REE's from original seawater values

(Bright et al., 2009; Shields & Stille, 2001; Shields & Webb, 2004). Although the REE concentrations in these apatites are poor proxies for paleo redox conditions of Ordovician seawater, they may shed light on the complex processes of REE mobility during diagenesis and concentrations in pore waters (Bright et al., 2009). MREE enrichment is also linked to anoxic pore waters and Fe cycling supported by Haley et al. (2004) who found MREE patterns in cores from the California margin contained significant concentrations of dissolved Fe. The MREE enrichment was explained by Haley et al. (2004) as a result of preferential scavenging of MREE's onto Fe-oxides (German et al., 1990) and after reduction, the release of the MREE's into the pore water.

Ce and Eu Anomalies as Redox Indicators

Previously, it was noted that cerium and europium provide valuable insight as to the character of redox conditions. The Ce anomaly (Ce/Ce*) is commonly used as an indicator of oxic environments due to it's oxidation from Ce^{3+} to insoluble Ce^{4+} that leads to removal of $Ce^{4+}$from the water column and characteristic Ce anomaly widely seen in modern seawaters (Byrne & Sholkovitz, 1996; Elderfield & Greaves, 1982; Elderfield & Sholkovitz, 1987; German et al., 1995; Haley et al., 2004). However, in contrast to negative Ce anomalies, dissolution of Ce occurs under anoxic conditions which may lead to Ce enrichment (Bright et al., 2009; Elderfield & Sholkovitz, 1987; Haley et al., 2004).

There were no negative cerium anomalies in any of the samples that were tested in this study (Figure 5a). Since it has been established that these apatites likely underwent extensive diagenesis, the absence of a negative Ce anomaly suggests that these samples do not reflect the redox conditions of the overlying water column but instead perhaps the bottom waters near the sediment-water interface (Bright et al., 2009). However, two samples, TWH-[22.85,26.35]

exhibit positive Ce anomalies. Positive Ce anomalies as suggested earlier are believed to interpret anoxic water conditions (Bright et al., 2009; Henry Elderfield & Sholkovitz, 1987; Haley et al., 2004), however this observation should be considered with caution due to ambiguous interpretations of the positive Ce anomaly (Bright et al., 2009; Haley et al., 2004; Sholkovitz et al., 1992).

Europium anomalies occur where Eu abundances are increased relative to Sm and Gd in high temperature (>200ºC), alkaline, anoxic conditions resulting in a positive europium anomaly (Eu/Eu* >1) (Bau & Dulski, 1996; Kim et al., 2012; MacRae et al., 1992). The Eu/Eu* of the apatites in this study are relatively neutral with values ranging from .96-1.01(Figure 5b) which means there is no evidence of a Eu anomaly. The lack of a positive Eu anomaly suggests that these limestones did not experience any alteration or elemental enrichment due to the presence of high-temperature fluids (Bau & Dulski, 1996). However, dolomitizing fluids upwards of 100º C may have been present due to the burial of the Chickamuauga up to 1000m during the Alleghanian Orogeny (Tobin et al., 1997) (Figure 1b). An anomalously low Eu/Eu* value of .13 occurs at sample TWH-[26.35]. Negative Eu anomalies have been described in ironstone deposits (Lottermoser & Ashley, 1996) and the anomaly seen here may be associated with increased dissolved Fe in anoxic sediments (Haley et al., 2004) or mixing from the overlying iron-rich Sequatchie formation present at the top of the outcrop (Herrmann & Haynes, 2015).

U and Th as a Proxy for Carbonate Facies and Redox Conditions

Because the REE signatures of these apatites have been tested and found to be contaminated and diagenetically altered, it is difficult to apply the method of shifting REE patterns to increased subsidence without adding a high level of ambiguity. However, application of additional elements to this study such as U, and Th may serve as reliable indicators of

seawater oxidation and aid in the interpretation of carbonate facies (Bábek et al., 2013; Brennecka et al., 2011; Calvert & Pedersen, 1993; McManus et al., 2006; Wignall & Twitchett, 1996). U exists in two oxidation states U^{+4} and U^{+6} and behaves similarly between ocean basins with depth (Calvert & Pedersen, 1993) where it is stored as insoluble U^{+4} within organic matter in anoxic conditions thereby reducing it's concentration in seawater (Brennecka et al., 2011; Calvert & Pedersen, 1993). Thorium exists in one oxidation state (Th^{+4}) which means it does not participate in redox reactions and is transported in association with clays and commonly used to assess sedimentation rates (Brennecka et al., 2011; Pollack et al., 2009).

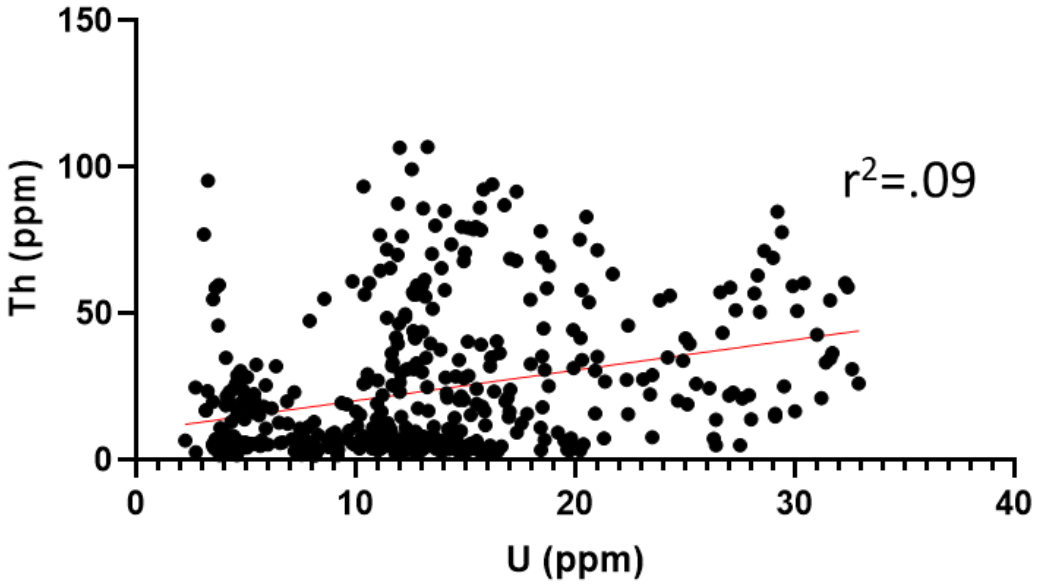

Figure 10. Th vs U plot showing no correlation between the two elements suggesting U is sequestered in organic sediments and not siliciclastic sediments.

Previous studies have interpreted increasing U concentrations as a signal for subtidal lithologies that occur at the base of shallowing upward carbonate depositional cycles (Bábek et al., 2013; Saller et al.,1994). In an earlier study Brennecka et al., (2011) employed the Th/U ratio as a signal of anoxic conditions where increased Th/U ratios represent periods of uranium

sequestration in organic sediments. One drawback to the use of this method at Tidwell Hollow is the large ratio of thorium to uranium present at this location, especially in the wackestone-packstone interval which may indicate proximity to the source instead of anoxic conditions (Baranov et al., 1956; Marenco, et al., 2016). Riverine transport is the dominant input of U into the oceans and therefore concentrated in siliciclastic sediments, however the low covariance between Th and U in (Figure 10) shows no covariance (r^2=.09) between the two elements following the assumption the U is concentrated in the organic and phosphatic material rather than the siliciclastic sediments (Bábek et al., 2007; Brennecka et al., 2011; McManus et al., 2006). Nevertheless, Th/U ratios closely mirror petrographic interpretations made for this section. Average Th/U ratios for the peritidal-siliciclastic facies are 1.04 but dramatically increase to 3.09 in the overlying wackestone-packstone interval before decreasing to 1.9 in the packstone-grainstone interval.

Other than an indicator of anoxia, the relationship between Th and U can be employed as a method to aid in distinguishing between inner ramp and distal ramp lithologies (Bábek et al., 2013). Carbonate production in ramp settings generally decreases down dip grading into siliciclastic rich distal ramp facies (Burchette & Wright, 1992). When sea level change occurs due to rapid sea level rise such as during the Middle-Upper Ordovician (Holland & Patzkowsky, 1998; Holland & Patzkowsky , 1996) facies shift from clean inner carbonate ramp deposits to dominantly fine grained siliciclastic rich deposits represented by higher Th concentrations (Bábek et al., 2013; Saller et al., 1994). Similar patterns are seen at Tidwell Hollow (Figure 11) where fine grained subtidal dolomitic wackestones exhibit high Th and low U/Th ratio while the grainstone-packstone interval decreases in Th. This cycle beginning with initial high Th

concentrations followed by a shallowing upward trend is seen in other rapidly subsiding basins such as the Permian during the late Pennsylvanian and Permian (Saller et al., 1994).

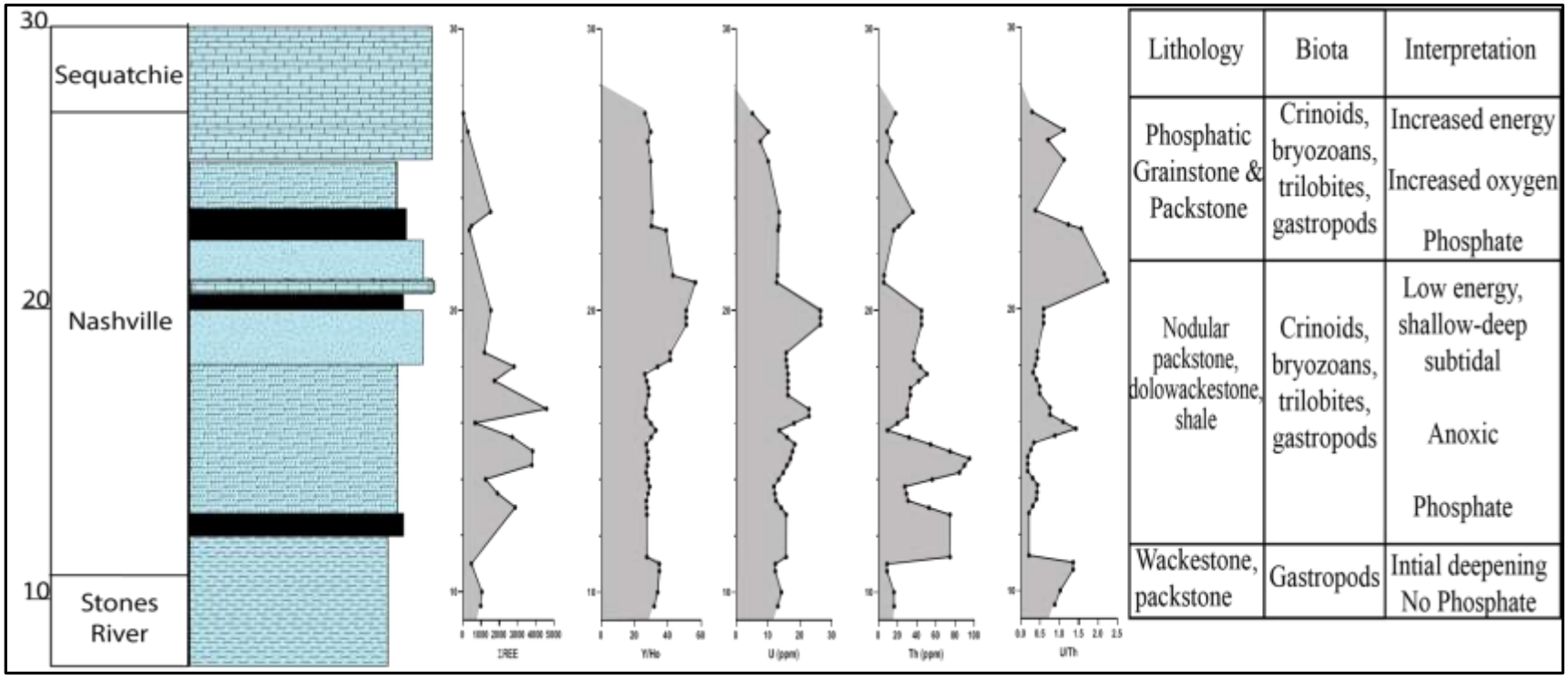

Lithology	Biota	Interpretation
Phosphatic Grainstone & Packstone	Crinoids, bryozoans, trilobites, gastropods	Increased energy Increased oxygen Phosphate
Nodular packstone, dolowackestone, shale	Crinoids, bryozoans, trilobites, gastropods	Low energy, shallow-deep subtidal Anoxic Phosphate
Wackestone, packstone	Gastropods	Intial deepening No Phosphate

Figure 11. Stratigraphic relationships between U, Th, and U/Th. U, Th, and U/Th profiles generated using a three-point moving average

Petrographic and Geochemical Interpretation by Interval

Peritidal and Siliciclastic interval

Phosphatic material in this interval is absent in thin section and this observation is supported by the low (.73-.93) Th/U ratios and U concentrations (9.3,12.28 ppm) in samples TWH-[9.5] and TWH-[11].The ∑REE in this interval are lower than the overlying samples and exhibits an MREE enriched pattern. Further, in this section, before the Millbrig, $\delta^{13}C$ remains steady around +.7‰ suggesting no significant influx of C into the sediments occurred during this period (Quinton et al., 2016). The appearance of dolomitic peloidal-mud-wackestones with a restricted faunal assemblage agrees with earlier interpretations by (Quinton et al., 2016) and (Benson, 1986a) that this interval, at least up to the Millbrig K-Bentonite likely formed in a peritidal shallow ramp environment similar to the pre-Taconic platform facies described in (Holland & Patzkowsky, 1998; Holland & Patzkowsky, 1997). The absence of Ce and Eu anomalies in any of the samples that were analyzed make it challenging to assess redox conditions in this interval however, a positive seawater like La anomaly in sample TWH-[9.5] and a range of Y/Ho ratios of 30-34 from samples in this interval are consistant with nearshore, restricted environments (Bau & Dulski, 1994; Tostevin et al., 2016).

Following the Millbrig, a gradual transition to shallow subtidal facies occurs. These skeletally supported lithologies, wackestones interbedded nodular packstones and shale, and the absence of peloids may be the first indication of a shift away from peritidal, tropicaly associated carbonate deposition at Tidwell Hollow (Holland & Patzkowsky, 1997). Further, a gradual enrichment in $\delta^{13}C$ occurs in this period prior to the silclastic rich interval at TWH-[11] which may reflect an increase in primary productivity prior to the onset of the GICE which is not present at Tidwell Hollow due to the possibility of an unconformity by (Quinton et al., 2016).

This transition to more skeletally supported lithologies and enrichment in $\delta^{13}C$ following deposition of the Millbrig K-Bentonite, may be related to the onset of subsidence, upwelling, and delivery of P-rich waters to the shelf following the collision of Laurentia with a series of volcanic island arcs (Herrmann et al., 2010; Holland & Patzkowsky, 1997). However, the lack of phosphate occuring immediately after the deposition of the K-bentonite beds is puzzling but could be explained by the approximately 3 m.y lag before the onset of crustal relaxation occurred following the onset of the Taconic Orogeny (Holland & Patzkowsky, 1997) or by delayed onset of P cycling back to the photic zone causing further primary productivity discussed below.

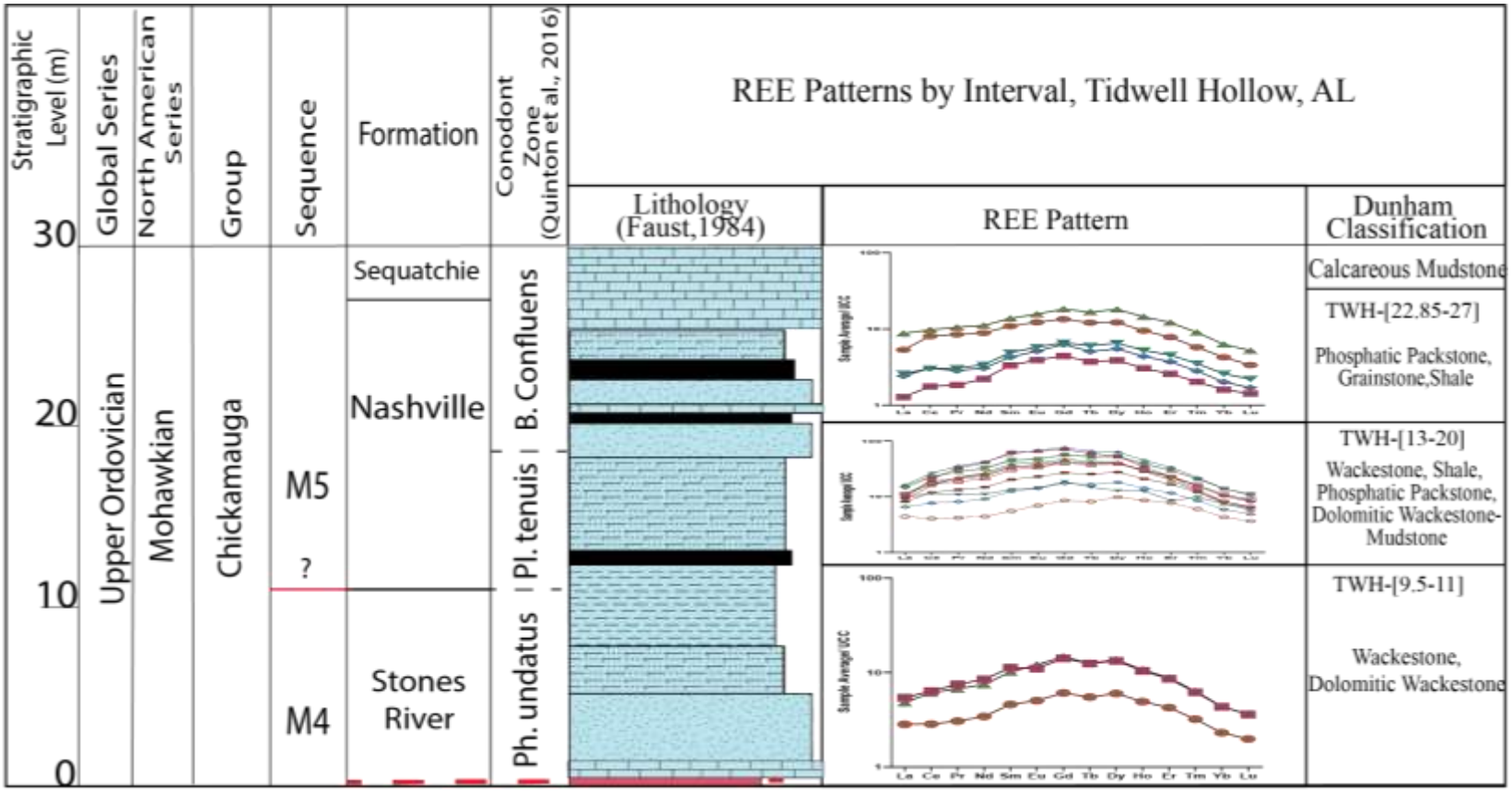

Figure 12. REE patterns by interval and associated lithologies. Wackestone-packstone interval is characterized by lower ∑REE enrichment and dolomitic wackestone interbedded with packstones. The middle interval is enriched in ∑REE and is represented by predominantly wackestones and packstones. The final interval is represented by a return to lower ∑REE values and phosphatic packstones and grainstones.

The REE patterns of this interval TWH-[9.5,10,11] are all MREE enriched (Figure 12). The geochemical analysis was not conducted on the full interval (TWH-[-5-11]) since samples were analyzed based on phosphogenesis, so it is impossible to compare changes in REE systematics across the entire interval. Nevertheless, MREE enrichment is commonly seen in authigenic and biogenic apatites (Bright et al., 2009). As was discussed previously, this pattern may be caused by several potential diagenetic and dynamic pore water conditions (Bright et al., 2009; Haley et al., 2004). However, MREE patterns have been interpreted as occurring in the presence of phosphorous enrichment and iron redox cycling which preferentially scavenges MREE's from the water column (Auer et al., 2017; Föllmi, 1996; Haley et al., 2004). However, due to the low amounts of phosphatic material in this interval and the close proximity of samples TWH-[9.5,10] to the siliciclastic sample TWH-[11], Fe coated quartz grains could have supplied Fe to the overlying water column and pore waters which may have led to MREE enrichment of these apatites during Fe reduction (Haley et al., 2004).

Wackestone-Packstone Interval REE Data

This interval begins with the sudden occurrence of phosphate as partial replacement of skeletal fragments and dissemintated phosphate that likely formed *in situ* via microbial mediation (Fonseca, 2000). Increase in fossil abundance occurs in sample TWH-[12.5] and continues through the 7.5m interval to sample TWH-[20]. Wackestones are fine-grained, argillaceous, lack bioturbation, and are thin bedded, while shale is also present (Benson, 1986a; Faust, 1984). Dolomitic mudstones are concentrated in intervals TWH-[13.5-17.5] and were interpreted as offshore facies occurring at depths >40m in the Nashville Dome area by (Holland & Patzkowsky, 1997). These petrographic observations combined with the highest Th concentrations in the studied interval may represent subtidal facies (Bábek et al., 2013) that

occurred as a shift from peritidal to sub-tidal- basinal deposition in a response abrupt deepening (Burchette & Wright, 1992). Accompanying the shift in lithofacies, diverse biota including presence of suspension feeders such as echinoderms and gastropods as well as trilobites, bivalves, and bryozoan fossils suggests a dramatic environmental change that could be indicative of sea level rise and platform drowning caused by rapid subsidence occurring at this time (Flügel, 2004; Holland & Patzkowsky, 1997). Fragments of various organisms are seen in thin section in the primarily wackestone facies suggesting these organism may have been transported from the shelf to their depositional location rather than buried in place.

The occurrence of abundant phosphate requires a mechanism to supply phosphorous to the sediment (organic matter and P escape) and conditions that allow preservation of the phosphate in the sediment (P trapping) (Benitez-Nelson, 2000; Filippelli, 2008; Fonseca, 2000; Tribovillard et al., 2006). Upwelling is frequently associated with subsiding basins such as the Peru margin where phosphorous concentrated in deep waters reaches the surface via upwelling spurring biological productivity (Encinas et al., 2008; Filippelli, 2008; Suess, Kulm, & Killingley, 1987). The water mass along the southern margin of Laurentia exhibited cool (approximately 10ºC at 1,000m) in deep waters and above 20ºC across the shallow epieric sea (Herrmann et al., 2010) with deep waters likely exhibiting higher levels of dissolved O_2 in addition to phosphorus than the warm surface waters. This scenario would promote an increase in phosphorous and organic matter which is the most important supply of phosphorous to marine sediments where it is incorporated through various processess and conditions such as microbial mediation in suboxic-anoxic conditions (Auer et al., 2017; Faul et al., 2005; Filippelli, 2008; Föllmi, 1996). However, under anoxic conditions, a fraction of P that reaches the sediment can be cycled back to the zone of primary productivity via bacterial mediation (P escape) promoting

additional productivity and supply of organic matter to the sediments (Benitez-Nelson, 2000; Tribovillard et al., 2006). Preservation of the phosphate would occur as a result of these processes where porewaters are supersaturated in P leading to the precipitation of authigenic phosphates (P trapping) (Benitez-Nelson, 2000; Tribovillard et al., 2006).

A scenario such as the one described above and perturbations in the C cycle are commonly linked with organic-rich deposits and anoxic events (Bjørlykke, 1994; Filippelli, 2008; Föllmi, 1996; Jacobs et al., 1996; McManus et al., 1997; Vincent & Berger, 1985). Increasing $\delta^{13}C$ values before the unconformity at Tidwell Hollow are followed by a 2 ‰ decrease in $\delta^{13}C$ at TWH-[10.5] (Quinton et al., 2016). This drop in $\delta^{13}C$ coincides with the lithologic changes at the base of this interval and onset of abundant phosphate deposition. Following the 2‰ decrease in $\delta^{13}C$ values is a dramatic shift to high (4.76) Th/U ratio in sample TWH-[13] and elevated U cocentrations in the apatites that may signify a shift to anoxic conditions (Brennecka et al., 2011; Tribovillard et al., 2006).

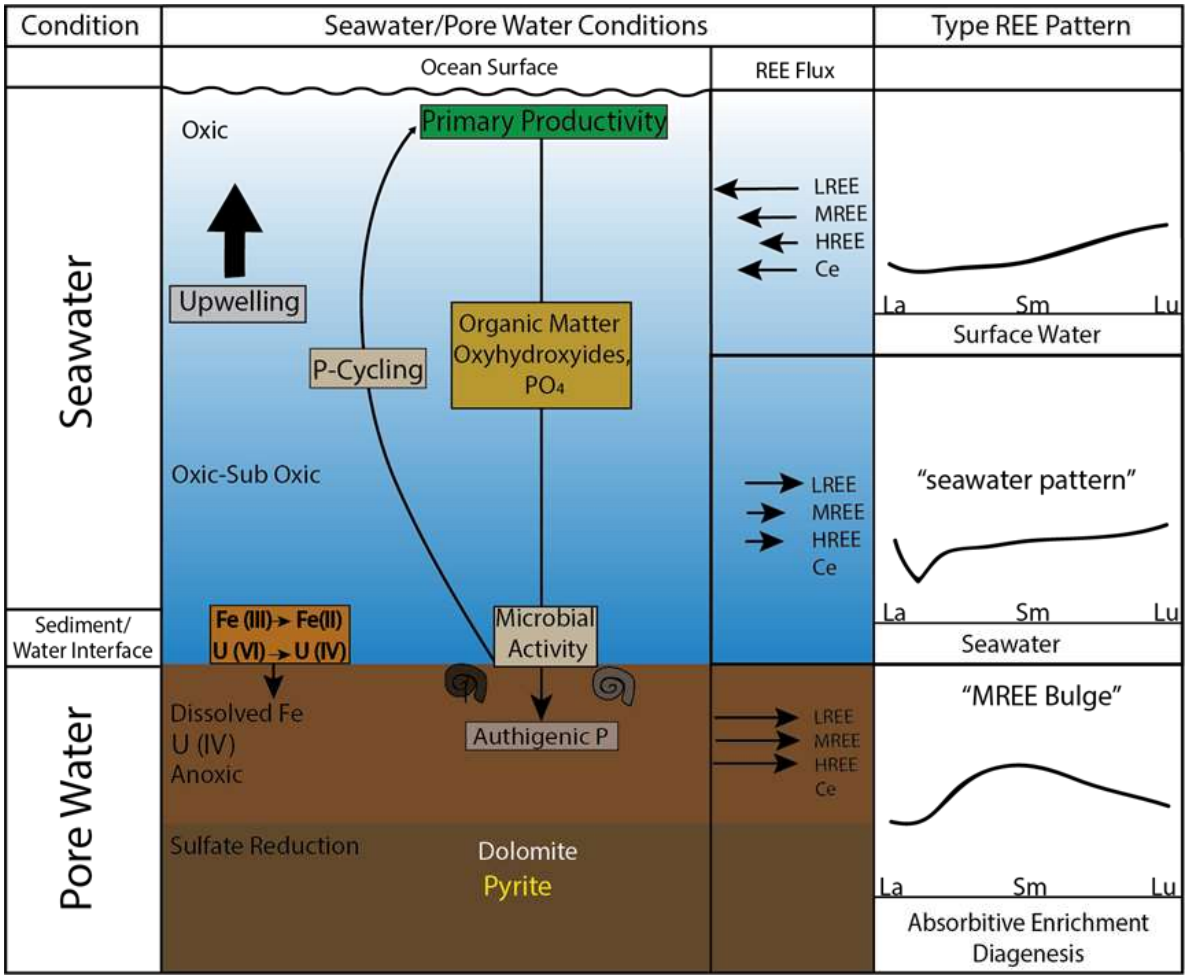

Figure 13. Pore water model for Tidwell Hollow, Alabama. P is delivered to surface waters via upwelling and transported to sediments by descending organic matter or as coatings on oxyhydroxides but a fraction is returned to the surface. Soluble U^{+6} is stored as insoluble U^{+4} in anoxic conditions at or near the Fe^{+3} Fe^{+2} redox boundary. REE are incorporated in the water column by Fe-Mn oxyhydroxides, organic matter, and phosphate. MREE are preferentially released in anoxic pore waters by Fe-oxyhydroxides below the Fe^{+3} to Fe^{+2} transition. REE flux to and from solids and type patterns from (Haley et al., 2004). Dolomite forms in the presence of pyrite in the sulfate reduction zone where Fe combines with S and releases HCO_3- promoting dolomitization.

The observed increase in the Th/U ratio in this interval may have occurred in response to an increase in sequestration of U in the sediments due to anoxic conditions (Figure 13). High levels of primary productivity in the surface waters leading up to the GICE depleting the water column of oxygen accompanied with rising sea level and shifting carbonate facies in response to

a rapidly subsiding basin (Bábek et al., 2013; Brennecka et al., 2011; Burchette & Wright, 1992). Bábek et al. (2013) suggested that facies shifts that accompany sea level rise can be interpreted by variations in U and Th with higher concentrations of these elements occurring in basinal mudstones which agrees with petrographic and geochemical interpratations in this study with the subtidal dolomitic wackestones containing the highest concentrations of Th (27-95ppm) and elevated U concentrations (11-17ppm). Alternatively, the increased level of anoxia may be due to inhibition of bottom circulation in the rapidly subsiding basin as suggested by (Shanmugam & Walker, 1983). Y/Ho ratios in this interval range from 27 at the bottom of the interval to 51 at the top of the interval which further suggests a progression from restricted circulation to open marine conditions during this interval of deposition supporting this interpretation (Bau & Dulski, 1994; Tostevin et al., 2016).

The REE patterns of this interval do not reflect seawater like conditions that are incorporated into most carbonates (Byrne & Sholkovitz, 1996; Sholkovitz & Shen, 1995). The range of Ce anomalies from .94 to 1.16 is fairly neutral and due to the high level of siliciclastic contamination, cannot be employed as a reliable proxy of redox conditions during this period. The very high Th concentrations may be partially responsible for alteration of the REE patterns in this interval. However, this interval does not exhibit the “flat” REE pattern associated with siliciclastic contamination (Nothdurft et al., 2004; Webb & Kamber, 2000). Instead, this interval displays a similar MREE bulge pattern as the underlying interval . However, this interval has an overall much higher ∑REE and MREE enrichment. One explanation for the increase in ∑REE and MREE over the adjacent intervals can be explained by preferential scavenging of MREE from seawater due to a prolonged period of exposure caused by sediment starvation that occurred due to rapid subsidence (Auer et al., 2017; Shanmugam & Walker, 1980).

Another explanation for the MREE enriched pattern is an increase in dissolved Fe in the sediment pore waters as discussed earlier (Haley et al., 2004). The Taconic Highlands to the east of the carbonate platform were undergoing rapid uplift and erosion of silicate rocks during this time that in addition to erosion, where according to (Kump et al., 1999), responsible for pCO_2 drawdown and global cooling before the Hirnantian. As was previously stated, this section also exhibits the highest concentrations of Th of the studied section and therefore increased delivery of silicates to the basin during this period may have increased the amount of available Fe that preferentially scavenges MREE's and releases them to the pore waters leading to the MREE enriched pattern (Haley et al., 2004). Further,the increased availability of Fe from the eroding highlands may also have led to the preferential burial of phosphates through Fe-P cycling (McManus et al., 1997) however this prediction relies on high bottom oxygen concentrations which do not agree with the Th/U ratios or U concentrations of this interval.

Packstone-Grainstone Interval

A reduction in Th/U ratios and decrease in U concentration at the base of this interval marks a period of decreased anoxia from the underlying sediments (Brennecka et al., 2011). The lowest Ce anomaly of the entire interval (.65) in sample TWH-[23.5] is present in this interval however based on the Ce/Ce* vs. Pr/Pr* plot, this sample possesses neither a La or Ce anomaly. The phosphatic grainstones and packstones that along with low angled cross bedding suggest a return to higher energy depositional environments than the underlying interval with these lithologies interpreted as occurring between 25-40m depth in the Nashville Dome area (Holland & Patzkowsky, 1997). Phosphate in samples remains abundant as does the diversity of the biota including crinoids and large (15 cm) bryozoan colonies (Faust, 1984) which are present as

heavily phosphatized fossil grains that means although marine conditions shifted, phosphate deposition persisted.

The Y/Ho ratios for this interval have a wide range (56-26) suggesting this period experienced a transition from open marine conditions seen in the underlying interval to a more restricted marine environment (Bau & Dulski, 1994; Tostevin et al., 2016). The decrease in anoxia based on Th/U values in this study suggest a return to more normal marine conditions and is tracked closely by reduced $\delta^{13}C$ values in this interval. Further, this interval possesses a much lower avarage Th concentration (15ppm) compared to the underlying interval (47.7 ppm). The reduction in Th in the sediment may correlate with the shift in lithofacies from basinal/distal wackestone-packstone to more proximal slope carbonate deposition (Bábek et al., 2013; Burchette & Wright, 1992). However, the presence of pyrite and preservation of phosphate seen in thin section suggests that some level of anoxia was still present throughout this interval (Filippelli, 2008; Fonseca, 2000; Loucks & Ruppel, 2007). Two explanations for the decrease in anoxia for these younger lithologies is ventilation of the basin via bottom currents generated by thermohaline differences during late stages of basin development (Shanmugam & Walker, 1983) or a decrease in anoxic deposition related to $\delta^{13}C$ data.

The MREE bulge in this section is less enriched than the underlying interval that was interpreted as acquiring enrichment through prolonged exposure to seawater. As the above discussion suggests, the basin began to shallow from clastic input from the eroding highlands and experience renewed circulation (Shanmugam & Walker, 1983). A higher sedimentation rate may have led to reduced exposure of these apatites to seawater leaving REE enrichment to other sources such as the anoxic porewaters that were likely present based on geochemical evidence discussed previously, the preservation of abundant phosphate, and pyrite framboids (Auer et al.,

2017; Loucks & Ruppel, 2007). Although positive Ce anomolies are to be interpreted with caution, when present they represent the release of Ce in anoxic pore waters (Haley et al., 2004). Following burial, the anoxic pore waters that had abundant phosphate then imparted the MREE enriched pattern overprinting any previous geochemcal signautres the apatite may have obtained from the overlying seawater (Bright et al., 2009).

Origin of Dolomite in Organic Rich Sediments

Dolomite and dolostones (limestone containing >75% of the mineral dolomite) are economically significant due to their influence on the distribution of permeability and porosity in carbonate reservoirs and aquifers (Gregg et al., 2015; Machel, 2004). However, the mechanisms and environments associated with dolomite formation are still poorly understood (Zhang et al., 2015). The formation of dolomite and dolostones is believed to be influenced by a number of chemical and environmental factors such as Ca^{2+}/Mg^{2+} ratios of seawater, salinity, alkalinity, temperature, periods of increased atmospheric and surface pCO_2, and the presence of microbes (Burns et al., 2000; Longstaffe et al., 2003). Although these factors are widely known, there are still several unresolved issues with the formation of dolomite such as dolomites form in a variety of sedimentary and diagenetic settings, a lack of modern analogs, and an inability to synthesize dolomite at near-surface conditions (Machel, 2004).

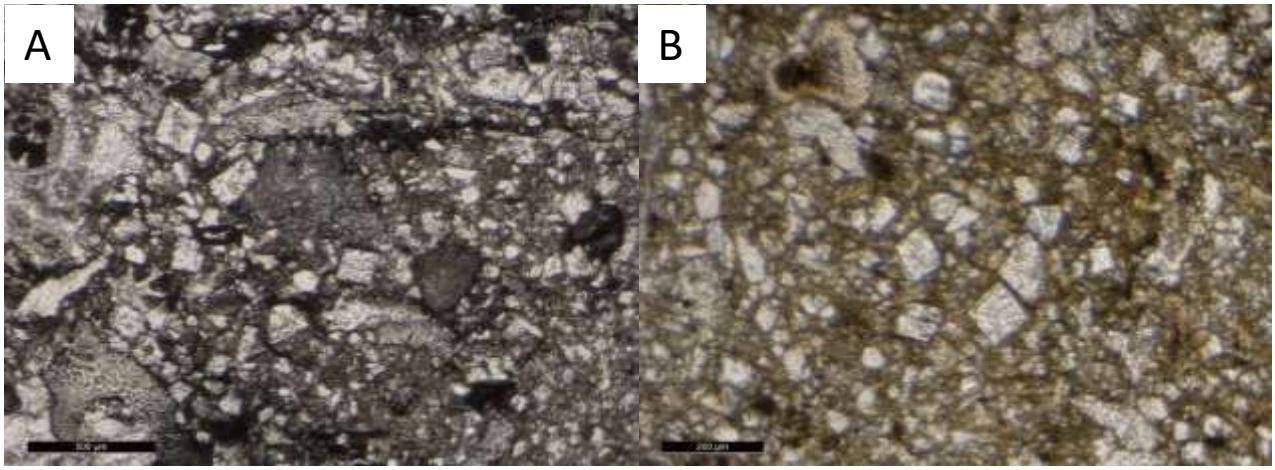

Figure 14. A: TWH- [14] dolomitic wacke-packstone shows signs of abundant biota and disseminated dolomite rhombs. B: TWH- [13.5] exhibits pyrite framboids and some dolomite rhombs. Some echinoderm fragments are present possibly transported from the shelf.

Dolomite within the wackestone-packstone interval at Tidwell Hollow is concentrated in areas that appear to be partially replaced by pyrite and high concentrations of phosphate based on petrographic observations (Figure 14a,b). Dolomitization of organic rich limestones has been observed in numerous studies (Baker & Burns, 1985; Compton, 1988; Mazzullo, 2000; Moore et al., 2004). These dolomitic mud-wackestones were previously interpreted as a subtidal-deep ramp facies of the Nashville Dome area by (S. M. Holland & Patzkowsky, 1997). As discussed previously, there are several barriers that inhibit dolomite formation including sulfate and alkalinity of porewaters (Baker & Burns, 1985; Baker & Kastner, 1981). Sulfate reducing bacteria use oxygen in dissolved SO_4 as an oxidant during the breakdown of organic matter thereby removing sulfate from pore waters (Mazzullo, 2000). In the presence of Fe, a by product of sulfate reduction is pyrite and to a lesser extent, marcasite or pyrhotite shown by the chemical equation Berner (1980) via:

$$15CH_2O + 8SO_4^{2-} + 2Fe_2O_3 \rightarrow 4FeS_2 + H_2O + 15HCO_3^- + OH^-$$

Or

$$CH_2O + 3SO_4^{2-} + 2FeOOH \rightarrow FeS_2 + FeS + 4H_2O + 6HCO_3^-$$

As can be seen from the above equations, a byproduct of these reactions is HCO_3^- capable of increasing alkalinity further promoting dolomitization (Baker & Burns, 1985; Burns et al., 1988; Mazzullo, 2000).

Bacteria sulfate reduction described above and methanogensis both occur in anoxic, organic rich sediments (Baker & Burns, 1985; Mazzullo, 2000). The interval over which dolomitic mudstones occur at Tidwell Hollow exhibit elevated Th/U ranging from .7 to 5.7 with an average of 2.8 which confirms the sediments were likely deposited in an anoxic environment. Based on geochemical evidence found in these intervals, it appears that anoxia may have been

present that would facilitate the onset of bacterial sulfate reduction/methanogenesis that would promote favorable conditions for dolomite formation (Baker & Burns, 1985; Mazzullo, 2000). Once sulfate and alkalinity of pore waters are altered by sulfate reduction and methanogenesis, another major factor leading to dolomitization is magnesium which was suggested by Baker and Burns (1985) to be supplied by diffusion of overlying seawater into the sediments.

Conclusions

The addition of petrographic and geochemical analysis to the Middle-Upper Ordovician carbonate ramp deposits of Tidwell Hollow has resulted in evidence that has multiple implications. The addition of REE and trace element geochemistry provides new insights for the complex relationship between phosphate depostion and paleoenvironmental conditions present during the Middle-Upper Ordovician along the southeast margin of Laurentia.

It was found through geochemical analysis that the REE patterns of this interval were all MREE enriched (Garnit et al., 2012). Further, these apatites were likely subjected to diagenetic and REE enrichment due to pore water conditions, high levels of siliciclastic contamination, and prolonged exposure to seawater (Auer et al., 2017; Bright et al., 2009; Haley et al., 2004; Lécuyer et al., 2004; Nothdurft et al., 2004; Sell et al., 2015). Ce/Ce* and Eu/Eu* were calculated in order to better understand changes in redox conditions through time at Tidwell Hollow but were also likely affected by diagenesis and are more likely to reflect pore water conditions than the overlying water column (Bright et al., 2009). These findings suggest that although REE's are potent tracers of many geological processes, application of REE geochemistry to authigenic and biogenic apatites must be done with caution and screening for diagenetic alteration must be conducted (Bright et al., 2009; Nothdurft et al., 2004).

Even with the limited application of REE's to this study, petrographic analysis as well as the redox sensitive element U and stable Th proved valuable indicators of changes in carbonate facies and redox conditions. A distinct shift in redox conditions from slightly anoxic in the peritdal interval to anoxic in the wackestone-packstone interval is illustrated by abrupt sequestration of U in the sediment which was reflected in the higher U concentrations in this

interval. An abrupt shift in the Th/U ratios coincides with the abrupt change in lithology from tropical to cool water carbonates and shales is seen across much of the Nashville Dome area (Holland & Patzkowsky, 1997; Holland et al., 1996). This is interpreted as an abrupt change in anoxia that occurs following peak $\delta^{13}C$ values that were likely related to an increase in productivity and phosphate cycling and deposition in the presence of cool waters along the southern margin of Laurentia. Anaerobic conditions would have been supported in a rapidly subsiding basin due to inhibition of bottom circulation (Shanmugam & Walker, 1983) thereby preserving phosphatic sediments.

Direct evidence for subsidence such as soft sediment deformation, slumping or turbidite deposits at Tidwell Hollow is not present. However, based on previous studies conducted across Laurentia, glaciation and the GICE are not likely to have caused the changes seen at Tidwell Hollow (Quinton et al., 2016; Quinton et al., 2017). Further, it has already been shown that cool nutrient-rich waters could have been present along the south east margin of Laurentia during the period that these environmental changes occurred (Herrmann, et al., 2010). Finally, backstripping analysis was applied to the Nashville Dome area, and these results suggest that sea level rose at approximately 10.3 m/m.y until decreasing in the Upper Ordovician (Holland & Patzkowsky, 1997). The argument for eustatic causes was argued against by Shanmugam and Walker (1983) citing that even during later larger scale transgressions such as that in the Late Cretaceous, the rapid subsidence rate was a fraction of that occurring during the Middle-Upper Ordovican and changes seen in the basin cannot be attributed to eustatic sea level in the absence of glaciation. Finally, it is unlikely that cool waters from the adjacent Sebree Trough were able to access the eastward-sloping carbonate ramp due to the elevated shoals of the Nashville Dome and Cincinnati Arch to the west (Holland & Patzkowsky, 1997).

Dolomitic wackestones found between intervals TWH-[13-17.5] were likely deposited in anoxic, deep ramp environments (Baker & Burns, 1985; Holland & Patzkowsky, 1997; Mazzullo, 2000). This is supported by the presence of pyrite which is a byproduct bacteria sulfate reduction and promotes the uptake of S and release of HCO_3^- which removes chemical barriers that inhibit the formation of dolomite (Baker & Burns, 1985; Mazzullo, 2000).

The evidence provided above suggests that rapid subsidence may have been the cause of these lithologic changes, however because this study was conducted at a single location, spatial correlations along the Laurentian margin are impossible. Future work would necessitate a shelf to basin transect, paleoenvironmental investigation at a broader scale, a more in depth look at the influence of siliciclastics and climatic changes, and would benefit from modified geochemical methods that either carefully screen for contamination and diagenesis before implementing REE geochemistry or adopt other methods.

References

Ainsaar, L., Kaljo, D., Martma, T., Meidla, T., Männik, P., Nõlvak, J., & Tinn, O. (2010). Middle and Upper Ordovician carbon isotope chemostratigraphy in Baltoscandia: a correlation standard and clues to environmental history. *Palaeogeography, Palaeoclimatology, Palaeoecology, 294*(3-4), 189-201.

Alibo, D. S., & Nozaki, Y. (1999). Rare earth elements in seawater: particle association, shale-normalization, and Ce oxidation. *Geochimica Et Cosmochimica Acta, 63*(3-4), 363-372.

Auer, G., Reuter, M., Hauzenberger, C. A., & Piller, W. E. (2017). The impact of transport processes on rare earth element patterns in marine authigenic and biogenic phosphates. *Geochimica Et Cosmochimica Acta, 203*, 140-156.

Bábek, O., Kalvoda, J., Cossey, P., Šimíček, D., Devuyst, F.-X., & Hargreaves, S. (2013). Facies and petrophysical signature of the Tournaisian/Viséan (Lower Carboniferous) sea-level cycle in carbonate ramp to basinal settings of the Wales-Brabant massif, British Isles. *Sedimentary Geology, 284*, 197-213.

Bábek, O., Přikryl, T., & Hladil, J. (2007). Progressive drowning of carbonate platform in the Moravo-Silesian Basin (Czech Republic) before the Frasnian/Famennian event: facies, compositional variations and gamma-ray spectrometry. *Facies, 53*(2), 293-316.

Baker, P. A., & Burns, S. J. (1985). Occurrence and formation of dolomite in organic-rich continental margin sediments. *AAPG bulletin, 69*(11), 1917-1930.

Baker, P. A., & Kastner, M. (1981). Constraints on the formation of sedimentary dolomite. *Science, 213*(4504), 214-216.

Baranov, V. I. i., Ronov, A., & Kinashova, K. (1956). On Geochemistry Of Dispersed Thorium And Uranium In Clays And Carbonate Rocks Of Russian Platform. *Geokhimiya (USSR) For English translation 1956-63 see Geochemistry (USSR)*.

Bau, M., & Dulski, P. (1994). Evolution of the yttrium–holmium systematics of seawater through time. *Mineral. Mag. A, 58*, 61-62.

Bau, M., & Dulski, P. (1996). Distribution of yttrium and rare-earth elements in the Penge and Kuruman iron-formations, Transvaal Supergroup, South Africa. *Precambrian Research, 79*(1-2), 37-55.

Benitez-Nelson, C. R. (2000). The biogeochemical cycling of phosphorus in marine systems. *Earth-Science Reviews, 51*(1-4), 109-135.

Benson, D. J. (1986a). Depositional Setting and History of the Middle Ordovician of the Alabama Appalachians. *Alabama Geological Society*.

Benson, D. J. (1986b). Stratigraphic Setting of the Middle Ordovician of the Alabama Appalachians. *Alabama Geological Society*.

Benson, D. J., & Mink, R. M. (1983). Depositional History and Petroleum Potential of the Middle and Upper Ordovician of the Alabama Appalachians.

Bergström, S. M., Saltzman, M. R., Leslie, S. A., Ferretti, A., & Young, S. A. (2015). Trans-Atlantic application of the Baltic Middle and Upper Ordovician carbon isotope zonation. *Estonian Journal of Earth Sciences, 64*(1), 6-10.

Berner, R. A. (1980). *Early diagenesis: a theoretical approach*: Princeton University Press.

Bjørlykke, K. (1994). Fluid-flow processes and diagenesis in sedimentary basins. *Geological Society, London, Special Publications, 78*(1), 127-140.

Bolhar, R., & Van Kranendonk, M. J. (2007). A non-marine depositional setting for the northern Fortescue Group, Pilbara Craton, inferred from trace element geochemistry of stromatolitic carbonates. *Precambrian Research, 155*(3), 229-250.

Brenchley, P., Marshall, J., Carden, G., Robertson, D., Long, D., Meidla, T., . . . Anderson, T. (1994). Bathymetric and isotopic evidence for a short-lived Late Ordovician glaciation in a greenhouse period. *Geology, 22*(4), 295-298.

Brennecka, G. A., Herrmann, A. D., Algeo, T. J., & Anbar, A. D. (2011). Rapid expansion of oceanic anoxia immediately before the end-Permian mass extinction. *Proceedings of the National Academy of Sciences, 108*(43), 17631-17634.

Bright, C. A., Cruse, A. M., Lyons, T. W., MacLeod, K. G., Glascock, M. D., & Ethington, R. L. (2009). Seawater rare-earth element patterns preserved in apatite of Pennsylvanian conodonts? *Geochimica Et Cosmochimica Acta, 73*(6), 1609-1624.

Burchette, T., & Wright, V. (1992). Carbonate ramp depositional systems. *Sedimentary Geology, 79*(1-4), 3-57.

Burdige, D. J. (1993). The biogeochemistry of manganese and iron reduction in marine sediments. *Earth-Science Reviews, 35*(3), 249-284.

Burnett, W. C., Beers, M. J., & Roe, K. K. (1982). Growth rates of phosphate nodules from the continental margin off Peru. *Science, 215*(4540), 1616-1618.

Burns, S. J., Baker, P. A., & Showers, W. J. (1988). The factors controlling the formation and chemistry of dolomite in organic rich sediments Miocene Drakes Bay Formation California.

Burns, S. J., Mckenzie, J. A., & Vasconcelos, C. (2000). Dolomite formation and biogeochemical cycles in the Phanerozoic. *Sedimentology, 47*, 49-61.

Byrne, R., & Sholkovitz, E. (1996). Marine chemistry and geochemistry of the lanthanides. *Handbook on the physics and chemistry of rare earths, 23*, 497-593.

Calvert, S., & Pedersen, T. (1993). Geochemistry of recent oxic and anoxic marine sediments: implications for the geological record. *Marine geology, 113*(1-2), 67-88.

Carter, B. D., & Chowns, T. M. (1986). Stratigraphic and Environmental Relationships of Middle and Upper Ordovician Rocks in Northwestern Georgia and Northeastern Alabama.

Castle, J. (2001). Appalachian basin stratigraphic response to convergent-margin structural evolution. *Basin Research, 13*(4), 397-418.

Chew, D. M., Sylvester, P. J., & Tubrett, M. N. (2011). U–Pb and Th–Pb dating of apatite by LA-ICPMS. *Chemical Geology, 280*(1-2), 200-216.

Chowns, T. M., & McKinney, F. K. (1980). Depositional facies in middle-upper Ordovician and Silurian rocks of Alabama and Georgia. *Excursions in southeastern geology, 2*, 323-347.

Compton, J. S. (1988). Sediment Composition and Precipitation of Dolomite and Pyrite in the Neogene Monterey and Sisquoc Formations Santa Maria Basin Area California.

Compton, J. S., Hall, D. L., Mallinson, D. J., & Hodell, D. A. (1994). Origin of dolomite in the phosphatic Miocene Hawthorn Group of Florida. *Journal of Sedimentary Research, 64*(3a), 638-649.

Compton, J. S., & Siever, R. (1986). Diffusion and mass balance of Mg during early dolomite formation, Monterey Formation. *Geochimica Et Cosmochimica Acta, 50*(1), 125-135.

Drahovzal, J. A., & Neathery, T. L. (1971). *The Middle and Upper Ordovician of the Alabama Appalachians* (Vol. 9): Alabama Geological Society.

Drahovzal, J. A., & Neathery, T. L. (1971). The Middle and upper Ordovician of the Alabama Appalachians. Road Log.

Duncan F. Sibley, J. M. G. (1987). Classification of Dolomite Rock Textures. *Journal of Sedimentary Petrology, 57*(6), 9.

Dunham, R. J. (1962). *Classification of Carbonate Rocks According to Depositional Texture*.

Elderfield, H. (1988). The oceanic chemistry of the rare-earth elements. *Phil. Trans. R. Soc. Lond. A, 325*(1583), 105-126.

Elderfield, H., & Greaves, M. J. (1982). The rare earth elements in seawater. *Nature, 296*(5854), 214-219.

Elderfield, H., & Pagett, R. (1986). Rare earth elements in ichthyoliths: variations with redox conditions and depositional environment. *Science of the Total Environment, 49*, 175-197.

Elderfield, H., & Sholkovitz, E. t. (1987). Rare earth elements in the pore waters of reducing nearshore sediments. *Earth and Planetary Science Letters, 82*(3-4), 280-288.

Encinas, A., Finger, K. L., Nielsen, S. N., Lavenu, A., Buatois, L. A., Peterson, D. E., & Le Roux, J. P. (2008). Rapid and major coastal subsidence during the late Miocene in south-central Chile. *Journal of South American Earth Sciences, 25*(2), 157-175.

Esteban, M., & Klappa, C. F. (1983). Subaerial Exposure Environment: Chapter 1: PART 2.

Ettensohn, F. R. (2010). Origin of Late Ordovician (mid-Mohawkian) temperate-water conditions on southeastern Laurentia: glacial or tectonic. *The Ordovician Earth System. Geological Society of America Special Paper, 466*, 163-175.

Fanton, K., & Holmden, C. (2007). Sea-level forcing of carbon isotope excursions in epeiric seas: implications for chemostratigraphy. *Canadian Journal of Earth Sciences, 44*(6), 807-818.

Faul, K. L., Paytan, A., & Delaney, M. L. (2005). Phosphorus distribution in sinking oceanic particulate matter. *Marine Chemistry, 97*(3-4), 307-333.

Faust, R. J. (1984). *Geology of Blount County, Alabama*: Geological Survey of Alabama.

Filippelli, G. M. (2008). The global phosphorus cycle: past, present, and future. *Elements, 4*(2), 89-95.

Fisher, C. M., McFarlane, C. R., Hanchar, J. M., Schmitz, M. D., Sylvester, P. J., Lam, R., & Longerich, H. P. (2011). Sm–Nd isotope systematics by laser ablation-multicollector-inductively coupled plasma mass spectrometry: Methods and potential natural and synthetic reference materials. *Chemical Geology, 284*(1-2), 1-20.

Flügel, E. (2004). *Microfacies of Carbonate Rocks*

Föllmi, K. (1996). The phosphorus cycle, phosphogenesis and marine phosphate-rich deposits. *Earth-Science Reviews, 40*(1-2), 55-124.

Fonseca, C. (2000). Upwelling, sedimentation and anoxia control on deposition of phosphates in the Late Cretaceous California margin.

Frimmel, H. E. (2009). Trace element distribution in Neoproterozoic carbonates as palaeoenvironmental indicator. *Chemical Geology, 258*(3), 338-353.

Garnit, H., Bouhlel, S., Barca, D., & Chtara, C. (2012). Application of LA-ICP-MS to sedimentary phosphatic particles from Tunisian phosphorite deposits: Insights from trace elements and REE into paleo-depositional environments. *Chemie der Erde-Geochemistry, 72*(2), 127-139.

German, C., Klinkhammer, G., Edmond, J., Mura, A., & Elderfield, H. (1990). Hydrothermal scavenging of rare-earth elements in the ocean. *Nature, 345*(6275), 516-518.

German, C., Masuzawa, T., Greaves, M., Elderfield, H., & Edmond, J. (1995). Dissolved rare earth elements in the Southern Ocean: Cerium oxidation and the influence of hydrography. *Geochimica Et Cosmochimica Acta, 59*(8), 1551-1558.

Glenn, C., Follmi, K., Riggs, S., Baturin, G., Grimm, K., Trappe, J., . . . Siegmund, H. (1994). Phosphorus and phosphorites: sedimentology and environments of formation. *Eclogae Geologicae Helvetiae, 87*(3), 747788.

Gregg, J. M., Bish, D. L., Kaczmarek, S. E., & Machel, H. G. (2015). Mineralogy, nucleation and growth of dolomite in the laboratory and sedimentary environment: a review. *Sedimentology, 62*(6), 1749-1769.

Haley, B. A., Klinkhammer, G. P., & McManus, J. (2004). Rare earth elements in pore waters of marine sediments. *Geochimica Et Cosmochimica Acta, 68*(6), 1265-1279.

Hall, J. C., Bergstrom, S. M., & Schmidt, M. A. (1986). Conodont biostratigraphy of the Middle Ordovician Chickamauga Group and related strata of the Alabama Appalachians.

Hallock, P., & Schlager, W. (1986). Nutrient excess and the demise of coral reefs and carbonate platforms. *Palaios*, 389-398.

Hellstrom, J., Paton, C., Woodhead, J., & Hergt, J. (2008). Iolite: software for spatially resolved LA-(quad and MC) ICPMS analysis.

Herrmann, A., & Haynes, J. T. (2015). *Ordovician of the Southern Appalachians, USA, Pre-symposium Field Trip*: Micropaleontology Press.

Herrmann, A. D., Haupt, B. J., Finney, S., & Berry, W. (2010). Toward identifying potential causes for stratigraphic change in subtropical to tropical Laurentia during the Mohawkian (early Late Ordovician). *The Ordovician Earth System. Geological Society of America Special Paper, 466*(193), 29-35.

Herrmann, A. D., Macleod, K. G., & Leslie, S. A. (2010). Did a volcanic mega-eruption cause global cooling during the Late Ordovician? *Palaios, 25*(12), 831-836.

Holland, S., & Patzkowsky, M. (1998). Sequence stratigraphy and relative sea-level history of the Middle and Upper Ordovician of the Nashville Dome, Tennessee. *Journal of Sedimentary Research, 68*(4), 684-699.

Holland, S. M., & Patzkowsky, M. E. (1997). Distal orogenic effects on peripheral bulge sedimentation; Middle and Upper Ordovician of the Nashville Dome. *Journal of Sedimentary Research, 67*(2), 250-263.

Holland, S.M., and Patzkowsky, M.E., 1996, Sequence stratigraphy and long-term paleoceanographic change in the Middle and Upper Ordovician of the eastern United States, in Witzke, B.J., Ludvigson, G.A., and Day, J., eds., Paleozoic sequence stratigraphy: Views from the North American craton: *Geological Society of America Special Paper* 306, p. 117-129. Holmden, C., Creaser, R., Muehlenbachs, K., Leslie, S., & Bergström, S. (1998). Isotopic evidence for geochemical decoupling between ancient epeiric seas and bordering oceans: implications for secular curves. *Geology, 26*(6), 567-570.

Jacobs, E., Weissert, H., Shields, G., & Stille, P. (1996). The Monterey event in the Mediterranean: A record from shelf sediments of Malta. *Paleoceanography, 11*(6), 717-728.

Jarvis, I. (1995). Phosphorite geochemistry: state-of-the-art and environmental concerns. *Eclogae Geologicae Helvetiae, 87*(3), 656-664.

Kim, J.-H., Torres, M. E., Haley, B. A., Kastner, M., Pohlman, J. W., Riedel, M., & Lee, Y.-J. (2012). The effect of diagenesis and fluid migration on rare earth element distribution in

pore fluids of the northern Cascadia accretionary margin. *Chemical Geology, 291*, 152-165.

Kolata, D. R., Huff, W. D., & Bergström, S. M. (2001). The Ordovician Sebree trough: an oceanic passage to the Midcontinent United States. *Geological Society of America Bulletin, 113*(8), 1067-1078.

Kowal-Linka, M., Jochum, K. P., & Surmik, D. (2014). LA-ICP-MS analysis of rare earth elements in marine reptile bones from the Middle Triassic bonebed (Upper Silesia, S Poland): Impact of long-lasting diagenesis, and factors controlling the uptake. *Chemical Geology, 363*, 213-228.

Kump, L., Arthur, M., Patzkowsky, M., Gibbs, M., Pinkus, D., & Sheehan, P. (1999). A weathering hypothesis for glaciation at high atmospheric pCO2 during the Late Ordovician. *Palaeogeography, Palaeoclimatology, Palaeoecology, 152*(1-2), 173-187.

Lécuyer, C., Reynard, B., & Grandjean, P. (2004). Rare earth element evolution of Phanerozoic seawater recorded in biogenic apatites. *Chemical Geology, 204*(1-2), 63-102.

Liang, Q., & Grégoire, D. C. (2000). Determination of trace elements in twenty six Chinese geochemistry reference materials by inductively coupled plasma-mass spectrometry. *Geostandards Newsletter, 24*(1), 51-63.

Longstaffe, F. J., Hardie, L. A., Coniglio, M., Church, M. J., & Middleton, G. V. (2003). *Encyclopedia of sediments and sedimentary rocks*: Springer Netherlands.

Lottermoser, B. G., & Ashley, P. M. (1996). Geochemistry and exploration significance of ironstones and barite-rich rocks in the Proterozoic Willyama Supergroup, Olary Block, South Australia. *Journal of Geochemical Exploration, 57*(1-3), 57-73.

Loucks, R. G., & Ruppel, S. C. (2007). Mississippian Barnett Shale: Lithofacies and depositional setting of a deep-water shale-gas succession in the Fort Worth Basin, Texas. *AAPG bulletin, 91*(4), 579-601.

Machel, H. G. (2004). Concepts and models of dolomitization: a critical reappraisal. *Geological Society, London, Special Publications, 235*(1), 7-63.

MacRae, N., Nesbitt, H., & Kronberg, B. (1992). Development of a positive Eu anomaly during diagenesis. *Earth and Planetary Science Letters, 109*(3-4), 585-591.

Marenco, P. J., Martin, K. R., Marenco, K. N., & Barber, D. C. (2016). Increasing global ocean oxygenation and the Ordovician Radiation: Insights from Th/U of carbonates from the Ordovician of western Utah. *Palaeogeography, Palaeoclimatology, Palaeoecology, 458*, 77-84.

Mazzullo, S. (2000). Organogenic dolomitization in peritidal to deep-sea sediments. *Journal of Sedimentary Research, 70*(1), 10-23.

McDowell, F. W., McIntosh, W. C., & Farley, K. A. (2005). A precise 40Ar–39Ar reference age for the Durango apatite (U–Th)/He and fission-track dating standard. *Chemical Geology, 214*(3-4), 249-263.

McLennan, S. M. (1989). Rare earth elements in sedimentary rocks: influence of provenance and sedimentary processes. *Geochemistry and Minerology of Rare Earth Elements*, 169-200.

McManus, J., Berelson, W. M., Coale, K. H., Johnson, K. S., & Kilgore, T. E. (1997). Phosphorus regeneration in continental margin sediments. *Geochimica Et Cosmochimica Acta, 61*(14), 2891-2907.

McManus, J., Berelson, W. M., Severmann, S., Poulson, R. L., Hammond, D. E., Klinkhammer, G. P., & Holm, C. (2006). Molybdenum and uranium geochemistry in continental margin sediments: paleoproxy potential. *Geochimica Et Cosmochimica Acta, 70*(18), 4643-4662.

Metzger, J. G., Fike, D. A., & Smith, L. (2014). Applying carbon-isotope stratigraphy using well cuttings for high-resolution chemostratigraphic correlation of the subsurface. *AAPG bulletin, 98*(8), 1551-1576.

Moore, T. S., Murray, R., Kurtz, A., & Schrag, D. (2004). Anaerobic methane oxidation and the formation of dolomite. *Earth and Planetary Science Letters, 229*(1), 141-154.

Nothdurft, L. D., Webb, G. E., & Kamber, B. S. (2004). Rare earth element geochemistry of Late Devonian reefal carbonates, Canning Basin, Western Australia: confirmation of a

seawater REE proxy in ancient limestones. *Geochimica Et Cosmochimica Acta*, *68*(2), 263-283.

Paton, C., Hellstrom, J., Paul, B., Woodhead, J., & Hergt, J. (2011). Iolite: Freeware for the visualisation and processing of mass spectrometric data. *Journal of Analytical Atomic Spectrometry*, *26*(12), 2508-2518.

Piepgras, D. J., & Wasserburg, G. (1982). Isotopic composition of neodymium in waters from the Drake Passage. *Science*, *217*(4556), 207-214.

Piper, D., Perkins, R., & Rowe, H. (2007). Rare-earth elements in the Permian Phosphoria Formation: Paleo proxies of ocean geochemistry. *Deep Sea Research Part II: Topical Studies in Oceanography*, *54*(11-13), 1396-1413.

Piper, D. Z., & Bau, M. (2013). Normalized rare earth elements in water, sediments, and wine: identifying sources and environmental redox conditions. *American Journal of Analytical Chemistry*, *4*(10), 69.

Pollack, G. D., Krogstad, E. J., & Bekker, A. (2009). U–Th–Pb–REE systematics of organic-rich shales from the ca. 2.15 Ga Sengoma Argillite Formation, Botswana: Evidence for oxidative continental weathering during the Great Oxidation Event. *Chemical Geology*, *260*(3-4), 172-185.

Pomar, L. (2001). Types of carbonate platforms: a genetic approach. *Basin Research*, *13*(3), 313-334.

Pope, M., & Read, J. F. (1998). Ordovician metre-scale cycles: implications for climate and eustatic fluctuations in the central Appalachians during a global greenhouse, non-glacial to glacial transition. *Palaeogeography, Palaeoclimatology, Palaeoecology*, *138*(1-4), 27-42.

Pope, M. C., Holland, S. M., Patzkowsky, M. E., Swart, P., Eberli, G., & McKenzie, J. (2009). The Cincinnati Arch: a stationary peripheral bulge during the Late Ordovician. *Perspectives in Carbonate Geology: A Tribute to the Career of Robert Nathan Ginsburg*, 255-275.

Pope, M. C., & Steffen, J. B. (2003). Widespread, prolonged late Middle to Late Ordovician upwelling in North America: A proxy record of glaciation? *Geology*, *31*(1), 63-66.

Quinton, P. C., Herrmann, A. D., Leslie, S. A., & MacLeod, K. G. (2016). Carbon cycling across the southern margin of Laurentia during the Late Ordovician. *Palaeogeography, Palaeoclimatology, Palaeoecology, 458*, 63-76. doi:10.1016/j.palaeo.2015.08.020

Quinton, P. C., Law, S., Macleod, K. G., Herrmann, A. D., Haynes, J. T., & Leslie, S. A. (2017). Testing the early Late Ordovician cool-water hypothesis with oxygen isotopes from conodont apatite. *Geological Magazine*, 1-15.

Reynard, B., Lécuyer, C., & Grandjean, P. (1999). Crystal-chemical controls on rare-earth element concentrations in fossil biogenic apatites and implications for paleoenvironmental reconstructions. *Chemical Geology, 155*(3-4), 233-241.

Rudnick, R., & Gao, S. (2003). Composition of the continental crust. *Treatise on geochemistry, 3*, 659.

Saller, A. H., Dickson, J., & Boyd, S. A. (1994). Cycle stratigraphy and porosity in Pennsylvanian and Lower Permian shelf limestones, eastern Central Basin Platform, Texas. *AAPG bulletin, 78*(12), 1820-1842.

Saltzman, M. R., & Young, S. A. (2005). Long-lived glaciation in the Late Ordovician? Isotopic and sequence-stratigraphic evidence from western Laurentia. *Geology, 33*(2), 109-112.

Sell, B. K., Samson, S. D., Mitchell, C. E., McLaughlin, P. I., Koenig, A. E., & Leslie, S. A. (2015). Stratigraphic correlations using trace elements in apatite from Late Ordovician (Sandbian-Katian) K-bentonites of eastern North America. *Geological Society of America Bulletin, 127*(9-10), 1259-1274. doi:10.1130/b31194.1

Sell, B. K., Samson, S. D., Mitchell, C. E., McLaughlin, P. I., Koenig, A. E., & Leslie, S. A. (2015). Stratigraphic correlations using trace elements in apatite from Late Ordovician (Sandbian-Katian) K-bentonites of eastern North America. *Bulletin, 127*(9-10), 1259-1274.

Shanmugam, G., & Walker, K. R. (1980). Sedimentation, subsidence and evolution of a foredeep basin in the Middle Ordovician, southern Appalachians. *American Journal of Science, 280*, 479-496.

Shanmugam, G., & Walker, K. R. (1983). Anatomy of the middle Ordovician Sevier Shale basin, eastern Tennessee. *Sedimentary Geology, 34*(4), 315-337.

Shields, G., & Stille, P. (2001). Diagenetic constraints on the use of cerium anomalies as palaeoseawater redox proxies: an isotopic and REE study of Cambrian phosphorites. *Chemical Geology, 175*(1-2), 29-48.

Shields, G. A., & Webb, G. E. (2004). Has the REE composition of seawater changed over geological time? *Chemical Geology, 204*(1-2), 103-107.

Sholkovitz, E., Shaw, T. J., & Schneider, D. (1992). The geochemistry of rare earth elements in the seasonally anoxic water column and porewaters of Chesapeake Bay. *Geochimica Et Cosmochimica Acta, 56*(9), 3389-3402.

Sholkovitz, E., & Shen, G. T. (1995). The incorporation of rare earth elements in modern coral. *Geochimica Et Cosmochimica Acta, 59*(13), 2749-2756.

Sloss, L. (1963). Sequences in the cratonic interior of North America. *Geological Society of America Bulletin, 74*(2), 93-114.

Soares, C. J., Mertz-Kraus, R., Guedes, S., Stockli, D. F., & Zack, T. (2015). Characterisation of Apatites as Potential Uranium Reference Materials for Fission-track Dating by LA-ICP-MS. *Geostandards and Geoanalytical Research, 39*(3), 305-313.

Suess, E., Kulm, L., & Killingley, J. (1987). Coastal upwelling and a history of organic-rich mudstone deposition off Peru. *Geological Society, London, Special Publications, 26*(1), 181-197.

Swart, P. K. (2015). The geochemistry of carbonate diagenesis: The past, present and future. *Sedimentology, 62*(5), 1233-1304.

Taylor, S. R., & McLennan, S. M. (1985). The continental crust: its composition and evolution.

Taylor, S. R., & McLennan, S. M. (1995). The geochemical evolution of the continental crust. *Reviews of Geophysics, 33*(2), 241-265.

Thomas, W. A. (1985). The Appalachian-Ouachita connection: Paleozoic orogenic belt at the southern margin of North America. *Annual Review of Earth and Planetary Sciences, 13*(1), 175-199.

Thomas, W. A., & Bayona, G. (2002). Palinspastic restoration of the Anniston transverse zone in the Appalachian thrust belt, Alabama. *Journal of Structural Geology, 24*(4), 797-826.

Thomson, S. N., Gehrels, G. E., Ruiz, J., & Buchwaldt, R. (2012). Routine low-damage apatite U-Pb dating using laser ablation–multicollector–ICPMS. *Geochemistry, Geophysics, Geosystems, 13*(2).

Tobin, K. J., Walker, K. R., & Goldberg, S. G. (1997). Burial diagenesis of middle Ordovician carbonate buildups (Alabama, USA): documentation of the dominance of shallow burial conditions. *Sedimentary Geology, 114*(1), 223-236.

Tostevin, R., Shields, G. A., Tarbuck, G. M., He, T., Clarkson, M. O., & Wood, R. A. (2016). Effective use of cerium anomalies as a redox proxy in carbonate-dominated marine settings. *Chemical Geology, 438*, 146-162.

Tribovillard, N., Algeo, T. J., Lyons, T., & Riboulleau, A. (2006). Trace metals as paleoredox and paleoproductivity proxies: an update. *Chemical Geology, 232*(1-2), 12-32.

Vincent, E., & Berger, W. H. (1985). Carbon dioxide and polar cooling in the Miocene: The Monterey hypothesis. *The carbon cycle and atmospheric CO2: Natural variations Archean to present, 32*, 455-468.

von Huene, R., Suess, E., & Emeis, K.-C. (1987). Convergent tectonics and coastal upwelling: a history of the Peru continental margin. *Episodes: Journal of International Geoscience, 10*(2), 87-93.

Webb, G. E., & Kamber, B. S. (2000). Rare earth elements in Holocene reefal microbialites: A new shallow seawater proxy. *Geochimica Et Cosmochimica Acta, 64*(9), 1557-1565. doi:10.1016/s0016-7037(99)00400-7

Wignall, P. B., & Twitchett, R. J. (1996). Oceanic anoxia and the end Permian mass extinction. *Science, 272*(5265), 1155-1158.

Yang, Y.-H., Wu, F.-Y., Yang, J.-H., Chew, D. M., Xie, L.-W., Chu, Z.-Y., . . . Huang, C. (2014). Sr and Nd isotopic compositions of apatite reference materials used in U–Th–Pb geochronology. *Chemical Geology, 385*, 35-55.

Zhang, F., Xu, H., Shelobolina Evgenya, S., Konishi, H., Converse, B., Shen, Z., & Roden Eric, E. (2015). The catalytic effect of bound extracellular polymeric substances excreted by anaerobic microorganisms on Ca-Mg carbonate precipitation: Implications for the "dolomite problem". In *American Mineralogist* (Vol. 100, pp. 483).

Zhang, W., Guan, P., Jian, X., Feng, F., & Zou, C. N. (2014). In situ geochemistry of Lower Paleozoic dolomites in the northwestern Tarim basin: Implications for the nature, origin, and evolution of diagenetic fluids. *Geochemistry Geophysics Geosystems, 15*(7), 2744-2764. doi:10.1002/2013gc005194

Zhao, L., Chen, Z.-Q., Algeo, T. J., Chen, J., Chen, Y., Tong, J., . . . Liu, Y. (2013). Rare-earth element patterns in conodont albid crowns: evidence for massive inputs of volcanic ash during the latest Permian biocrisis? *Global and Planetary Change, 105*, 135-151.

Appendix 1: Petrographic Analysis

Interval/Dunham Classification	Biota /Features	Comments	Thin Section Images by Interval
27 Phosphatic grainstone	Phosphate, echinoderms, bryozoans, pyrite.	Bryozoan replaced with partially pyritized phosphatic matter under PPL, reflected light photomicrograh of phosphatic material and a partially phosphatized echinoderm under reflectd light.	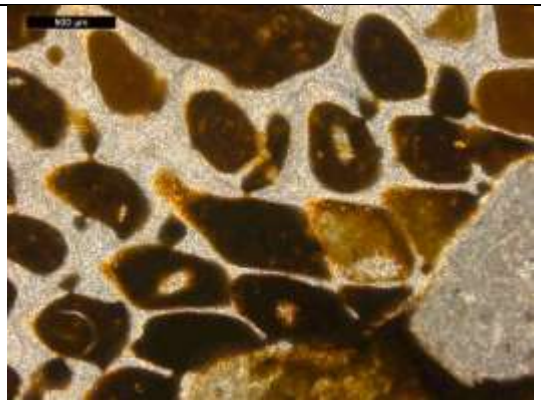 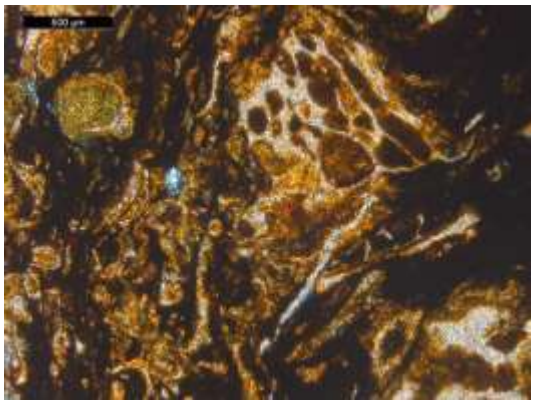 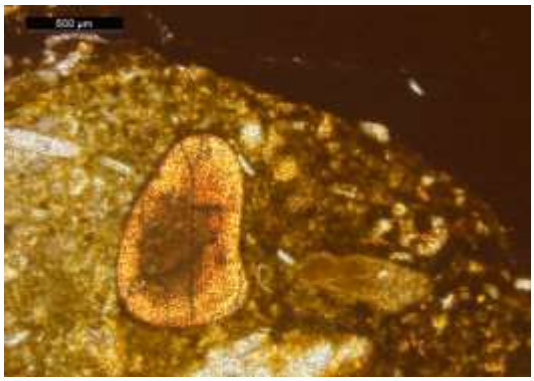

Interval/Dunham Classification	Biota /Features	Comments	Thin Section Images by Interval
26.35 Grainstone	Gastropods, Echinoderms	A gastropod that appears partially phosphatized as well as an echinoderm.	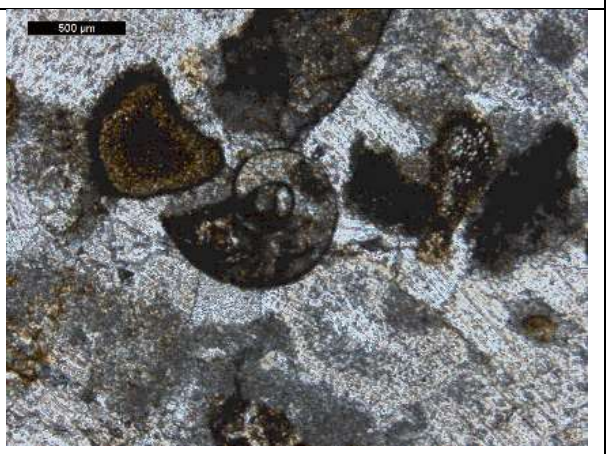
26 Phosphatic packstone	Echinoiderms, gastropod	Phosphatized echinoderm and gastropod.	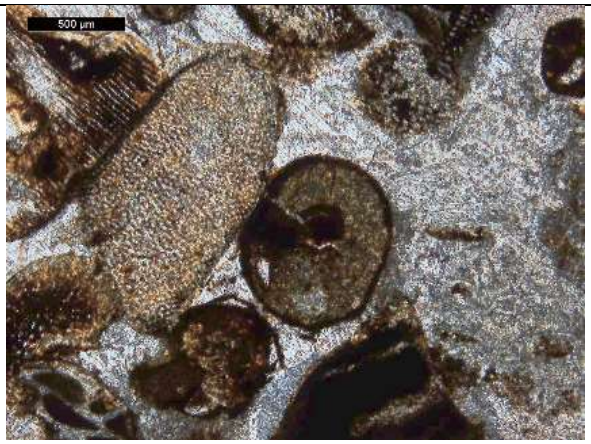
24.5 Packstone	Phosphate, gastropods.	Gastropod fragments replaced by calcite and scattered phosphate grains.	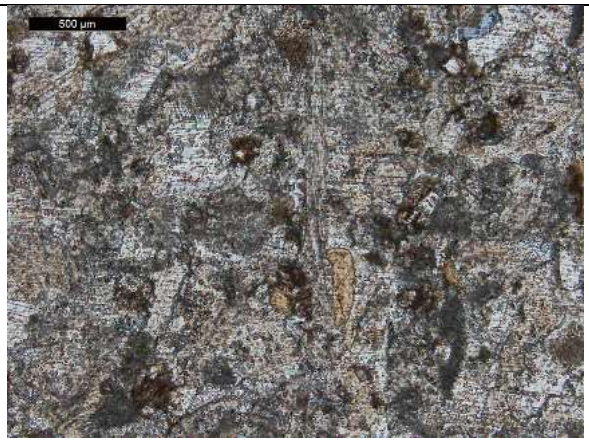

Table continued

Interval/Dunham Classification	Biota /Features	Comments	Thin Section Images by Interval
23.5 Phospahtic packstone	Phosphate, pyrite,trilobites,bryozoans, and echinoderms.	Phosphatic material with minor pyrite and with major pyrite also occuring near phosphatic material.	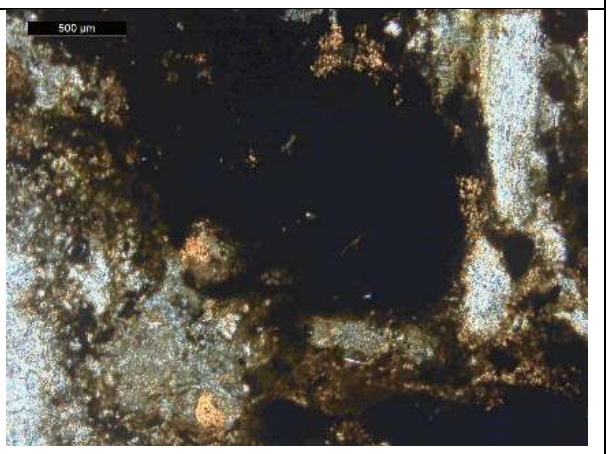 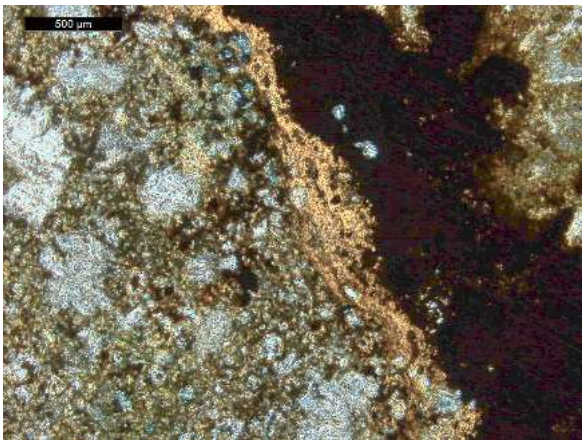 

Table continued

Interval/Dunham Classification	Biota /Features	Comments	Thin Section Images by Interval
			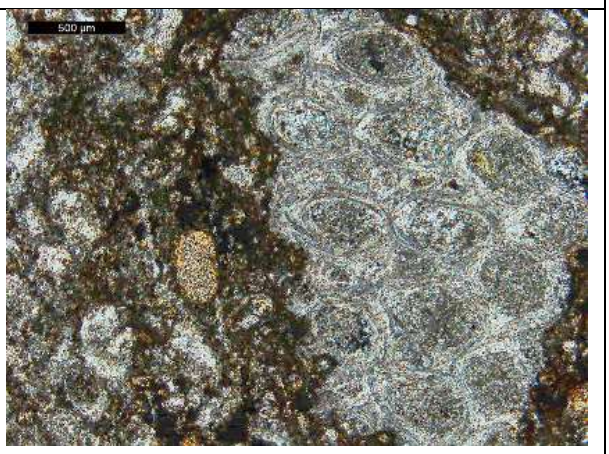 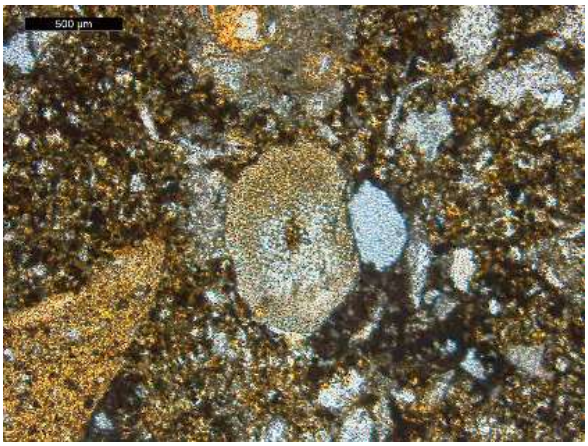
23 Phosphatic packstone	Phosphate,echinoderms	Phosphatized echinoderm and phosphatized grains.	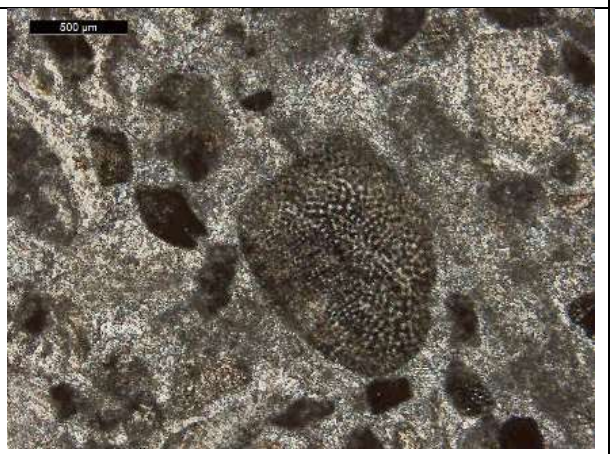

Table continued

Interval/Dunham Classification	Biota /Features	Comments	Thin Section Images by Interval
21 Phosphatic packstone	Phosphatized gastropods.	Scattered phosphatic material and phosphatized gastropod fossils.	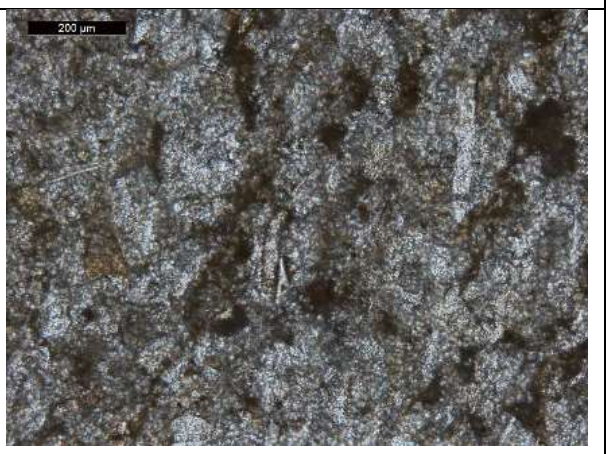 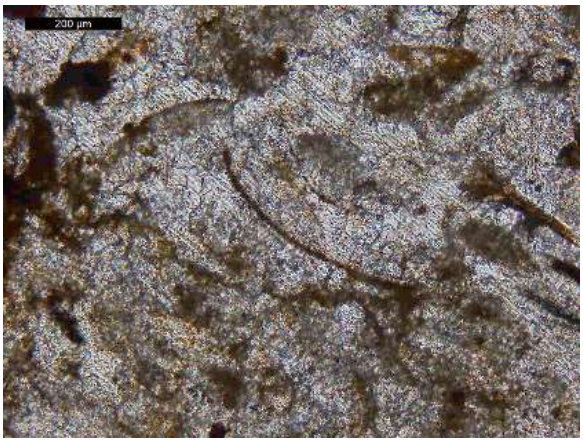 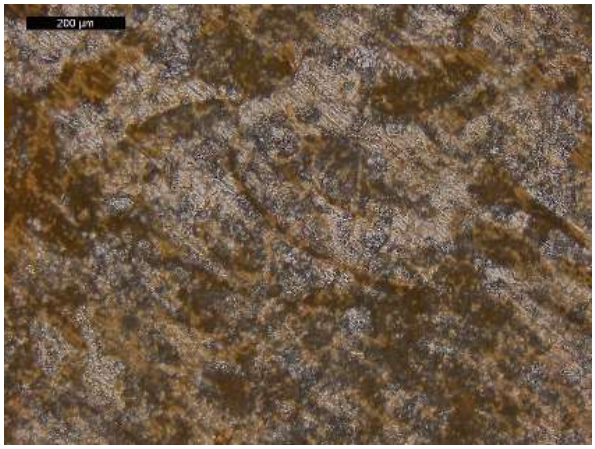

Table continued

Interval/Dunham Classification	Biota /Features	Comments	Thin Section Images by Interval
20.5 Phosphatic packstone	Phosphatized fossils, bryozoans, bivalves, trilobites,gastropods.	Bryozoan and bivalve fossils replaced by phosphatic material, trilobite and gastropod fossils also present.	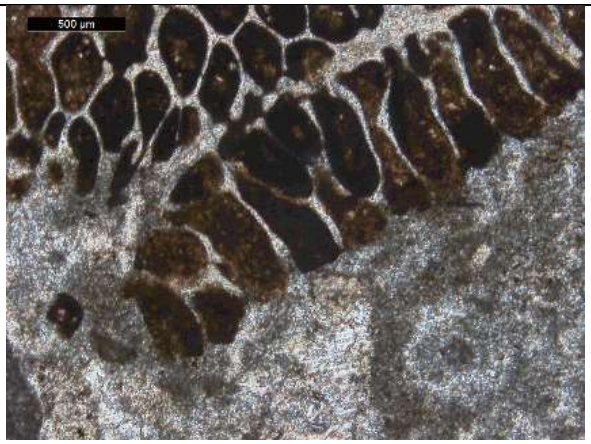 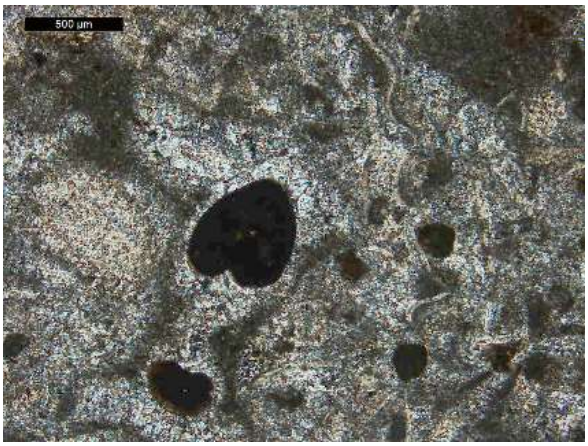 

Table continued

			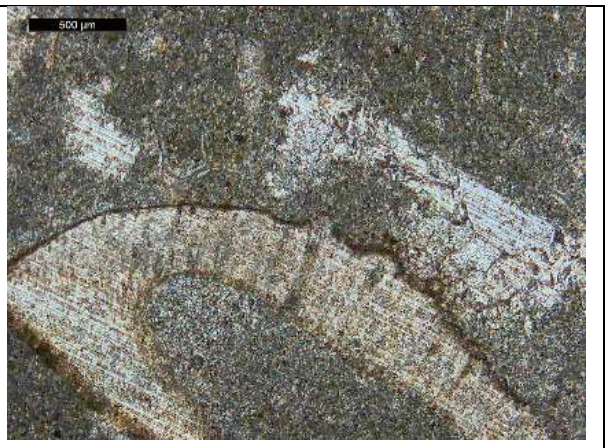
20 Phosphatic packstone	Phosphatized echinoderms, micrite encrusteed brachiopods	Phosphatized grains and echinoderms, bivalve fossils with micrite lining also present.	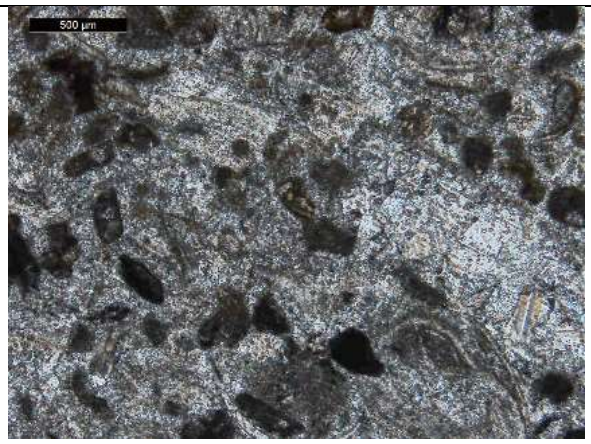 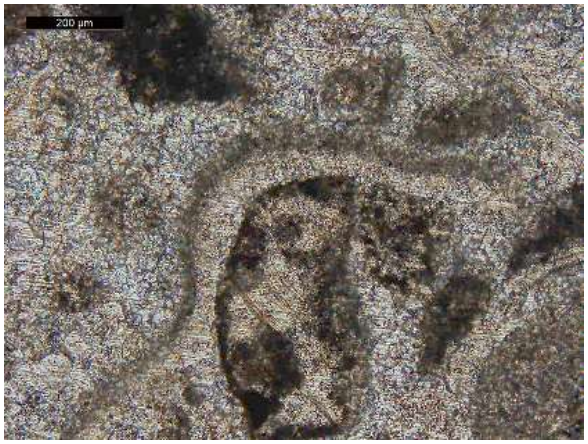

Table continued

Interval/Dunham Classification	Biota /Features	Comments	Thin Section Images by Interval
19 Phosphatic packstone	Brachiopods, bivalves, and gastropods.	Limestone with abundant fine grained matrix with abundant gastropod and brachiopod fossils.	
18.5 Phosphatic packstone	Phosphatized bryozoans, bivalves.	Bryozoan that has beein partially replaced by phosphate and bivalve fragement.	
18 Grainstone	Bryozoans	Bryozoan that have been micritized and replaced with calcite.	

Table continued

17.5 Dolomitic-grain-packstone	Phosphatized shell fragments, echinoderms, pyrite, and dolomite	Phosphatized echinoderm fragment along with bivalve fragment followed by matrix that has been extensively dolomitized under PPL and reflected light.	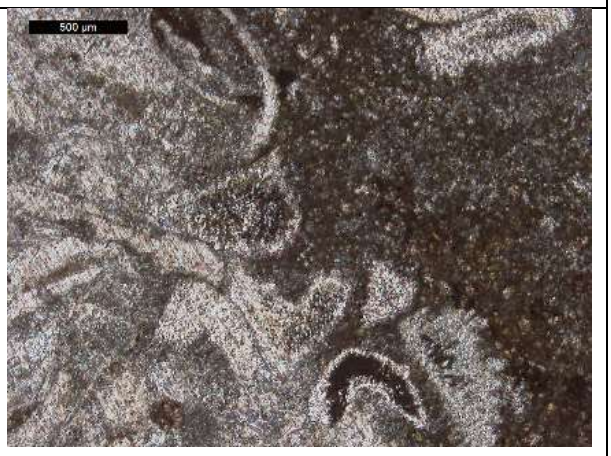 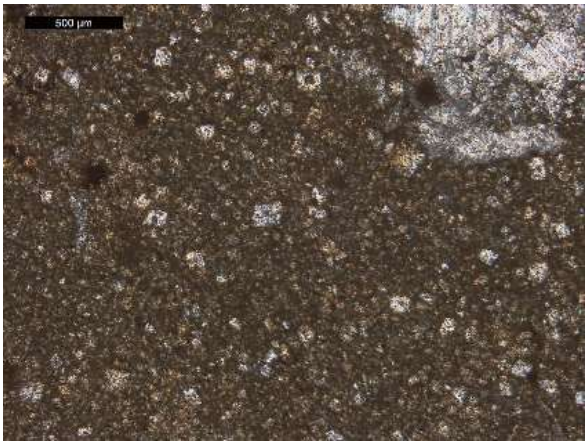 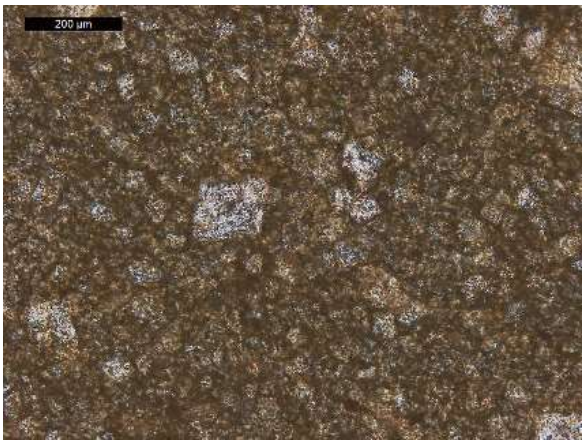

Table continued

Interval/Dunham Classification	Biota /Features	Comments	Thin Section Images by Interval
17 Packstone	Phosphate, dissolution seams,siliciclastics, pyrite, gastropods.	Limestone with abundant dissolution seems and phosphate followed by a gastropod fragment and opaque pyrite grain and then same pyrite grain under reflected light .	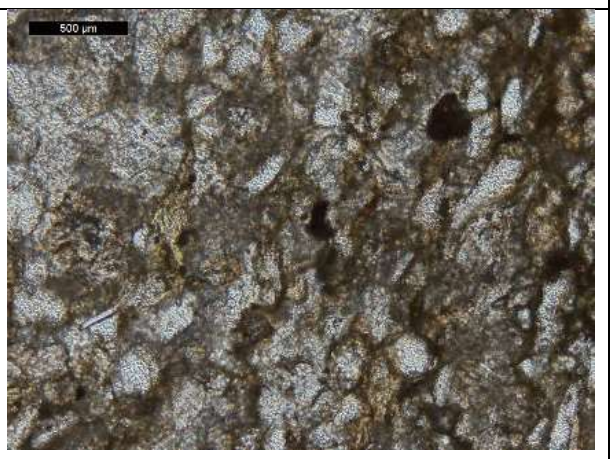 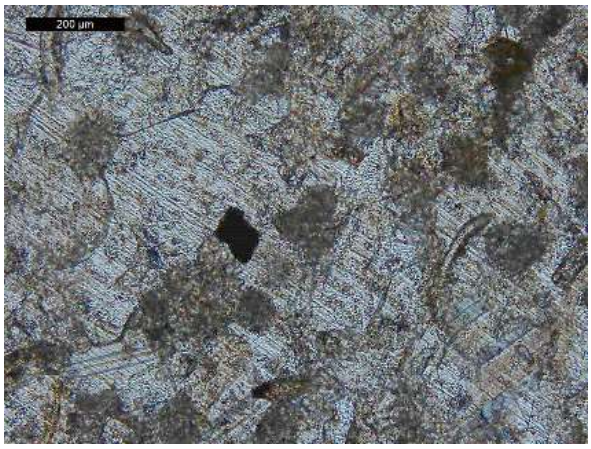 

Table continued

Interval/Dunham Classification	Biota /Features	Comments	Thin Section Images by Interval
16.5 Nodular packstone	Phosphate,bryozoans, echinoderm, gastropods,trilobites, and bivalves.	Bryozoans partially replaced by pyrite and burrows containing minor pyrite followed by trilobite and bivalve fragments that are also appear to have been replaced by pyrite followd by micritic echinoderm fragments.	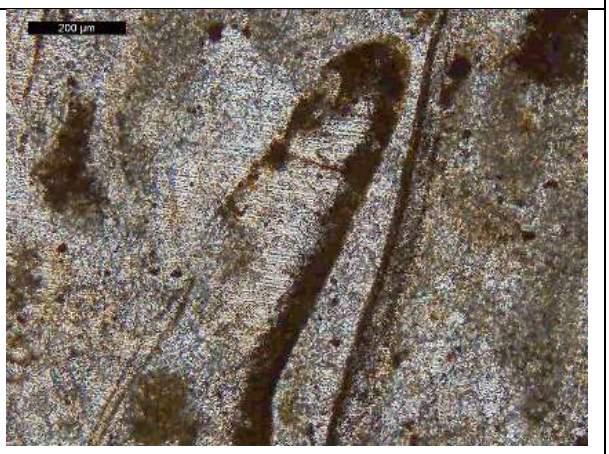 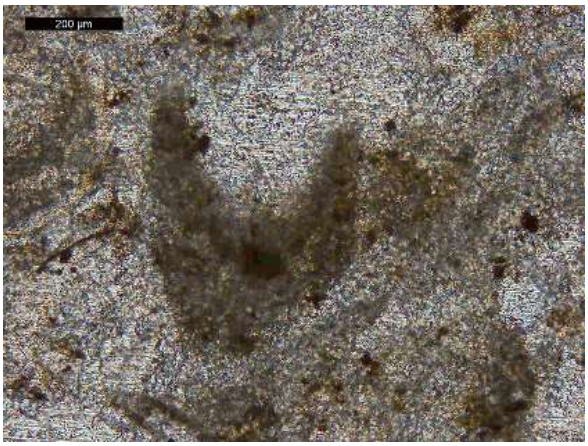 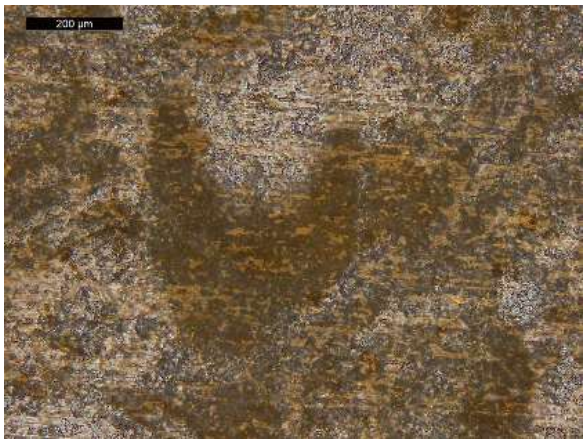

Table continued

Interval/Dunham Classification	Biota /Features	Comments	Thin Section Images by Interval
			 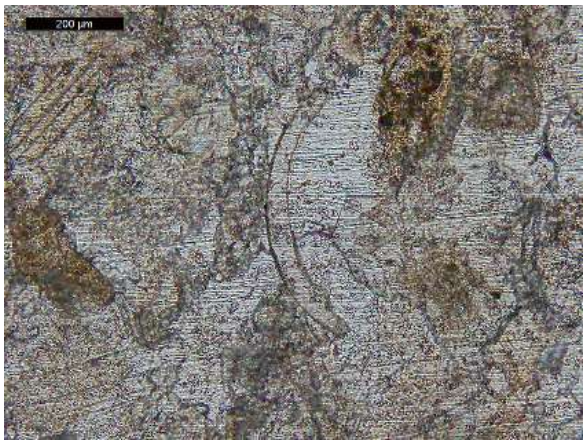

Table continued

Interval/Dunham Classification	Biota /Features	Comments	Thin Section Images by Interval
15.5 Wackestone	Gastropods, echinoderms, brachiopods.	Partially phosphatized gastropod and brachipod fragment, phosphatized echinoderms also present.	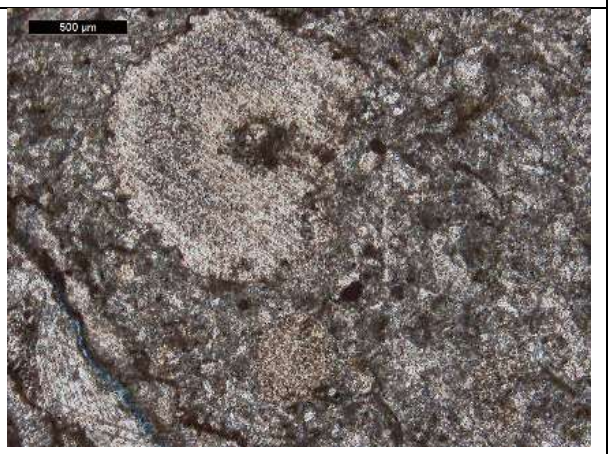 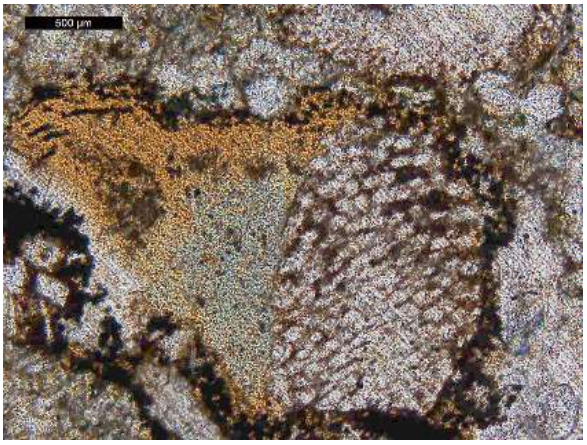

Table continued

Interval/Dunham Classification	Biota /Features	Comments	Thin Section Images by Interval
15 Wackestone	Phosphatic material and pyrite.	Phosphatic material scattered in limestone matrix followed by more concentrated phosphatic material showing partial pyritization under reflected light also seen in thin section.	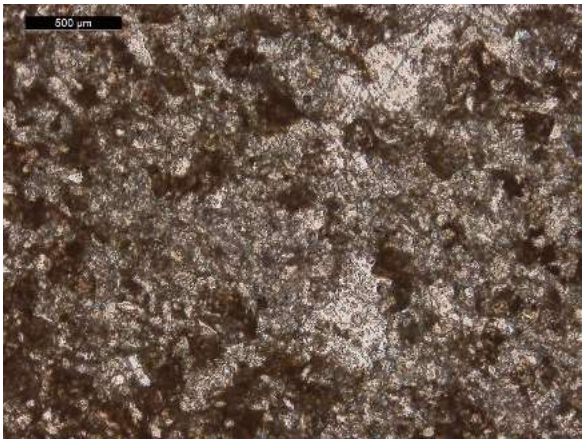 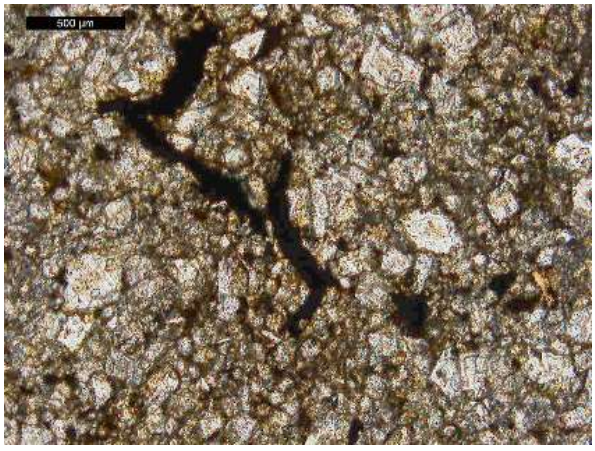

Table continued

Interval/Dunham Classification	Biota /Features	Comments	Thin Section Images by Interval
			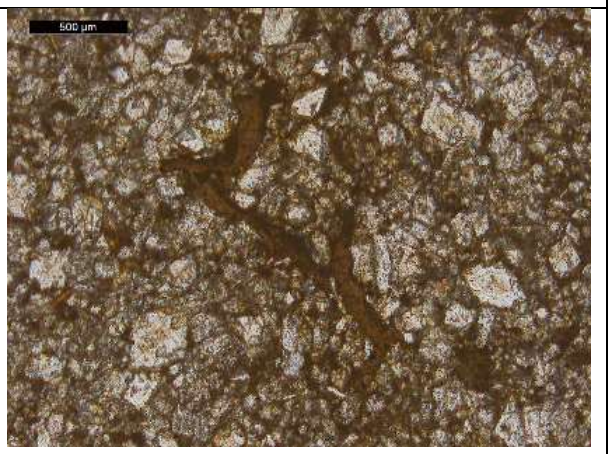
14.55 Packstone	Phospahate,echinoderm, bryozoans,gastropods, pyrite.	Echinoderms, gastropods, and bryozoans occur as partially phosphatized fossils. Phosphatized echinoderm fragments using reflected light reveals patial pyritization of phosphatized grains.	

Table continued

Interval/Dunham Classification	Biota /Features	Comments	Thin Section Images by Interval
			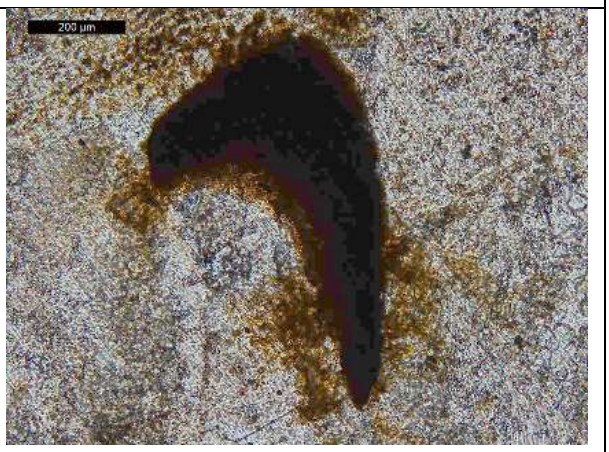

Table continued

Interval/Dunham Classification	Biota /Features	Comments	Thin Section Images by Interval
14 Dolomitic wackestone	Echinoderms, phosphate, dolomite, pyrite.	Echinoderm fragment that has been phosphatized followed by the same echinoderm under reflected light, and image of dolomite associated with phosphate occurrence under PPL, and reflected light .	 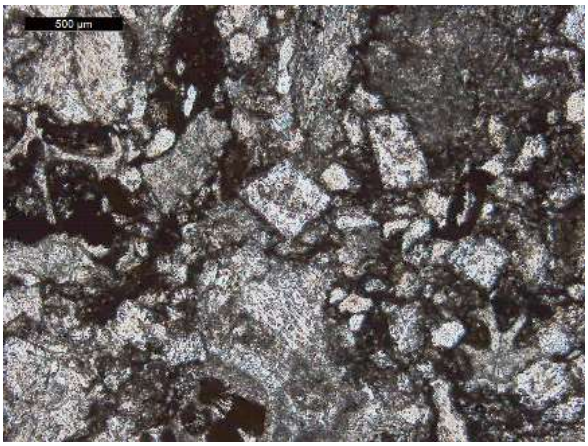

Table continued

Interval/Dunham Classification	Biota /Features	Comments	Thin Section Images by Interval
			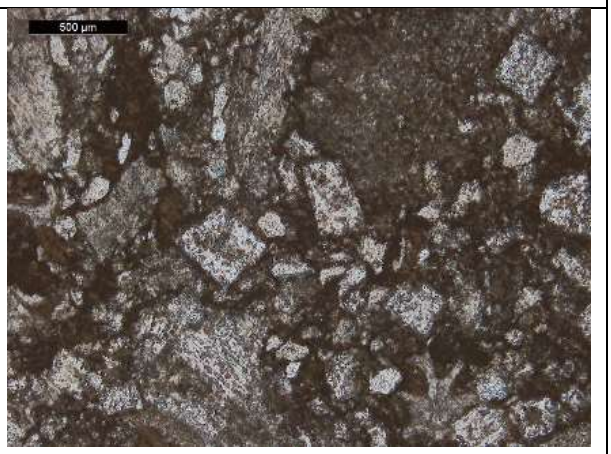
13.5 Dolomitic packstone	Phosphatic material, echinoderms, brachiopods, gastropods.	Phosphatized fossils gastropods and echinoderm fragments as well as phosphatized green algae within a dolomitized organic mud matrix that is partially pyritized .	

Table continued

Interval/Dunham Classification	Biota /Features	Comments	Thin Section Images by Interval
			
12.5 Packstone	Phosphatic material, echinoderms, gastropods.	Phosphatized fossils including gastropods and echinoderms.	

Table continued

Interval/Dunham Classification	Biota /Features	Comments	Thin Section Images by Interval
11 Argillaceous wackestone	Siliciclastics	Abundant silicastic grains with little to no carbonate grains.	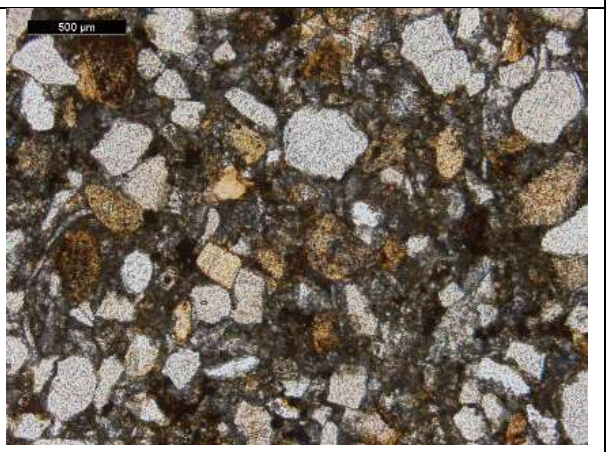 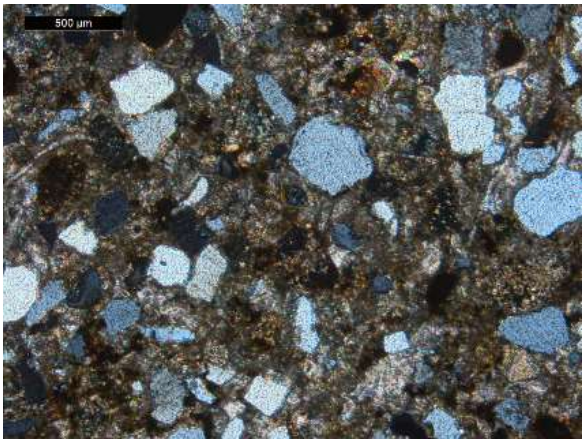

Table continued

Interval/Dunham Classification	Biota /Features	Comments	Thin Section Images by Interval
10.5 Peloidal wackestone	Peloids	Abundant peloids and calcite cement.	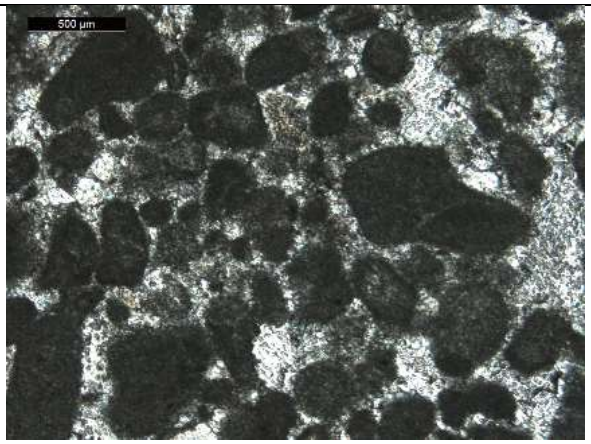

Table continued

Interval/Dunham Classification	Biota /Features	Comments	Thin Section Images by Interval
10 Wackestone	Gastropods, echinoderms, siliciclastic grains	Abundant carbonate and siliciclastic grains. Fossils include gastropods and echinoderm fragments.	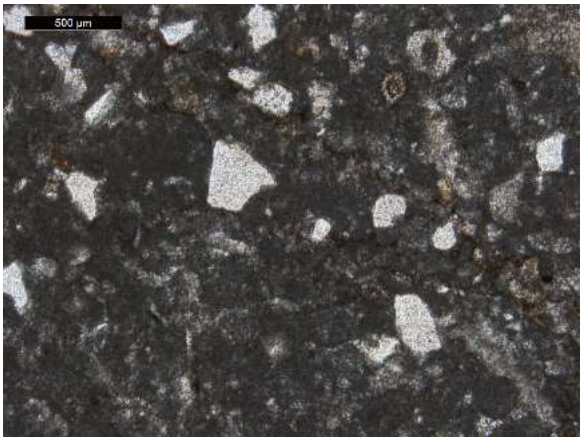 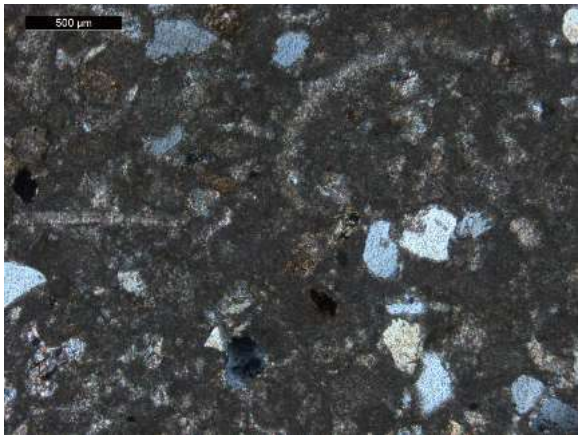

Table continued

Interval/Dunham Classification	Biota /Features	Comments	Thin Section Images by Interval
9.75 Wackestone	Peloids, echinoderm fragments, and gastropods.	Abundant peloids with scattered echinoderm and gastropod fragments.	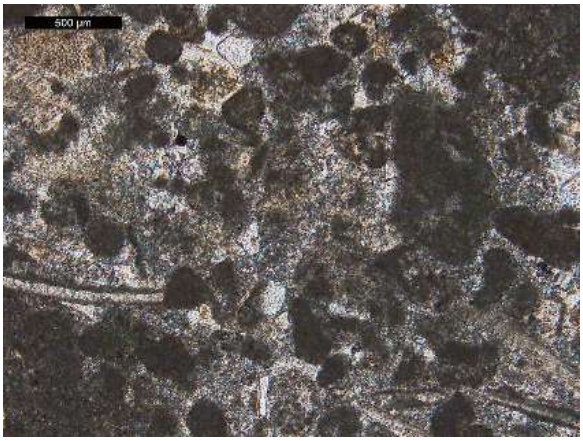
9 Wackestone	Bivalves	Bivalve shell preserved in fine grained limestone.	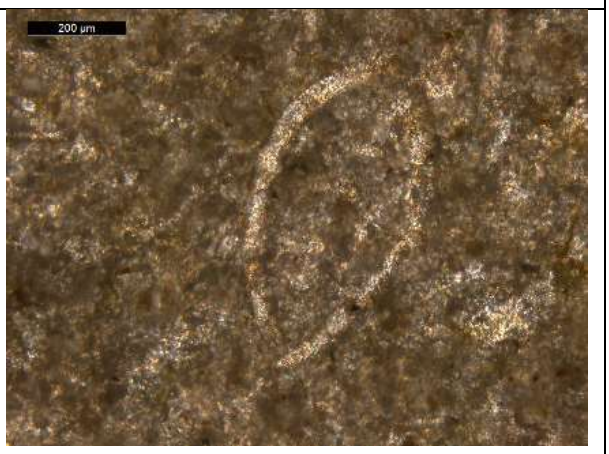

Table continued

Interval/Dunham Classification	Biota /Features	Comments	Thin Section Images by Interval
8.5 Wackestone	Gastropods, bivalves	Scattered gastropod and bivalve fossils in largely lime mud matrix.	 

Table continued

Interval/Dunham Classification	Biota /Features	Comments	Thin Section Images by Interval
8 Wackestone	Gastropods,Pyrite	Scattered gastropods fossils in lime mud matrix. Large pyrite framboids identified in plain and reflected light.	 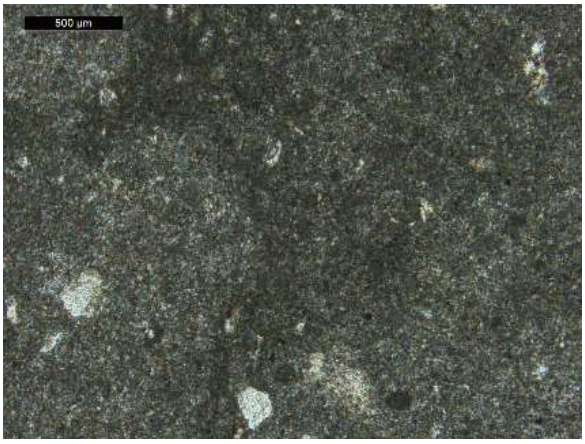

Table continued

Interval/Dunham Classification	Biota /Features	Comments	Thin Section Images by Interval
			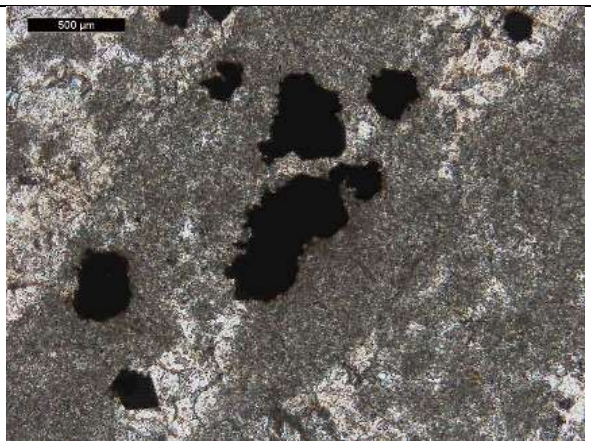 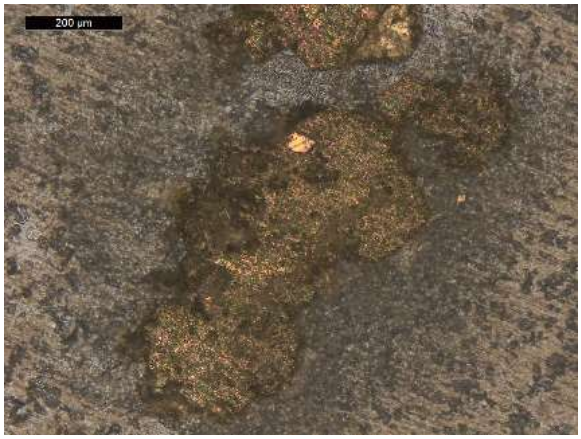

Table continued

Interval/Dunham Classification	Biota /Features	Comments	Thin Section Images by Interval
5 Wackestone	Coral, siliciclastics	Coral and siliciclastic material in fine grained matrix.	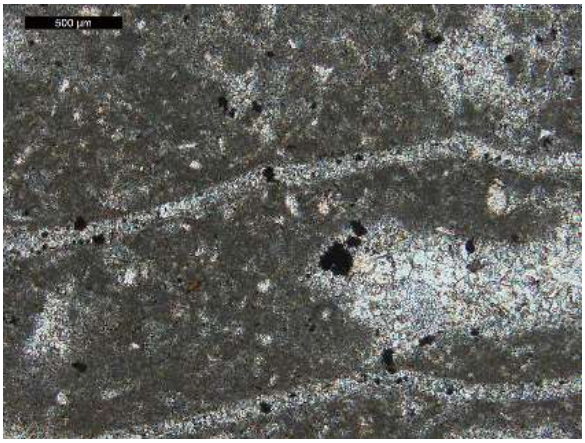 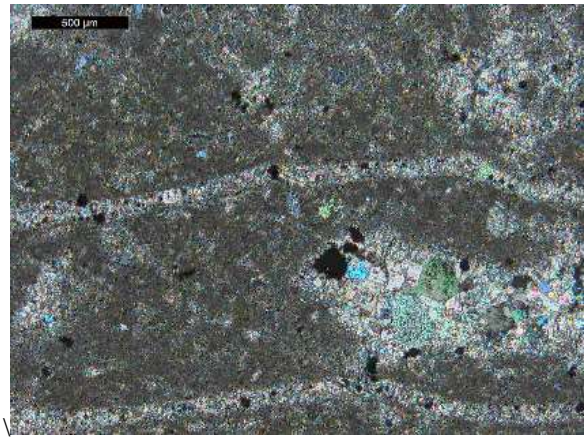

Table continued

Interval/Dunham Classification	Biota /Features	Comments	Thin Section Images by Interval
4.75 Wackestone	Echinoderm fragments, and siliciclastics.	Grains and fossils appear in a fine grained, micritic limestone.	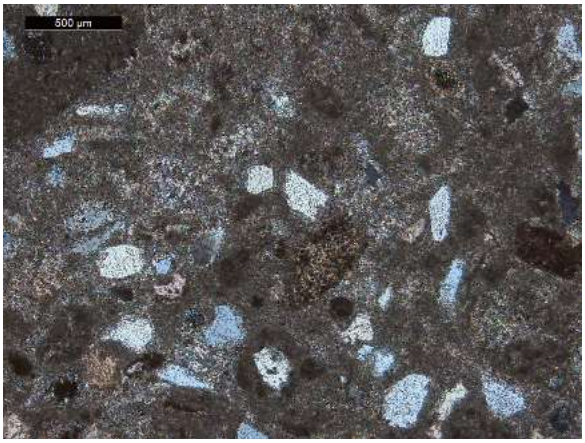
3 Packstone	Gastropods, and brachiopods.	Abundant gastropods and brachiopod fossils with micritic envelops.	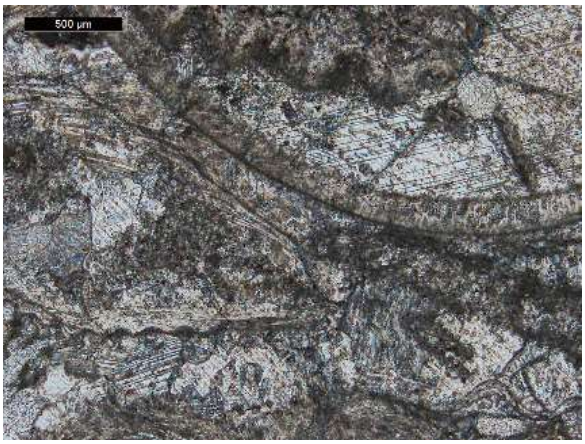

Table continued

Interval/Dunham Classification	Biota /Features	Comments	Thin Section Images by Interval
1.5 Packstone	Echinoderm fragments and siliciclastic material	Echinoderm fragments with abundant siliciclastic grains present in thin section.	 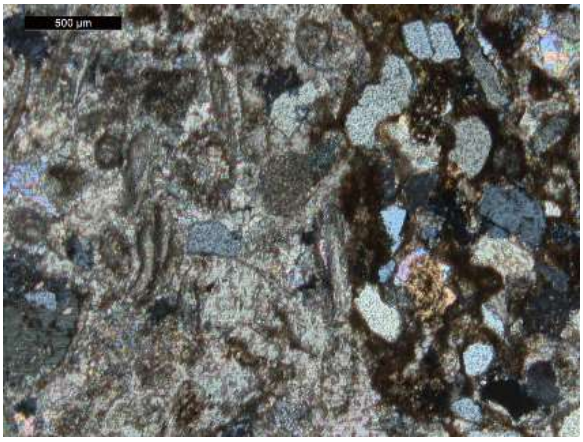

Table continued

Interval/Dunham Classification	Biota /Features	Comments	Thin Section Images by Interval
1 Packstone	Gastropods, echinoderms.	Gastropods and echinoderm fragments present.	

Table continued

Interval/Dunham Classification	Biota /Features	Comments	Thin Section Images by Interval
0 Wackestone	Peloids	Abundant peloids and calcite cement.	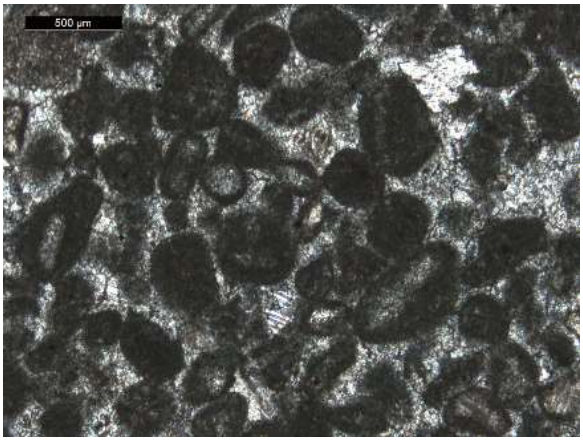
-0.5 Wackestone	Peloids	No phosphate, abundant peloids, and some dolomite rhombs occuring within the matrix.	

Table continued

Interval/Dunham Classification	Biota /Features	Comments	Thin Section Images by Interval
-1 Wackestone	Peloids	No phosphate, no fossils present, abundant peloids and calcite cement.	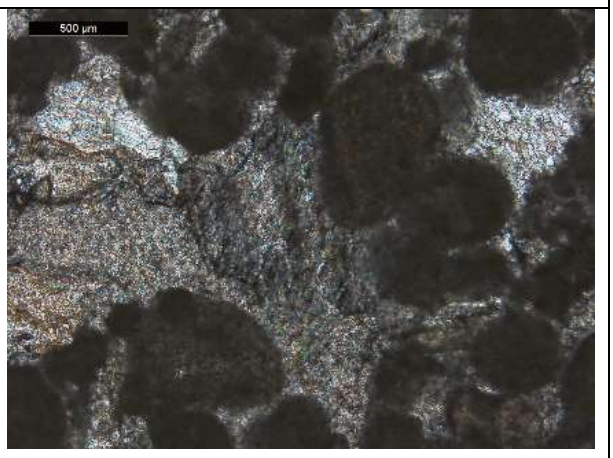
-1.5 Wackestone	None	No phosphate or fossils present in interval, minute evidence of meteoric diagenesis as well as scattered dolomite rhombs.	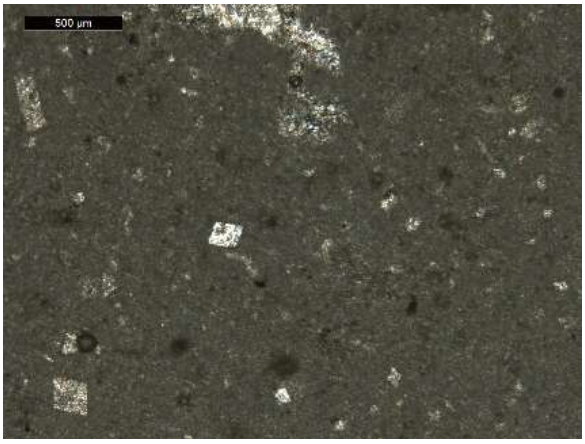

Table continued

Interval Data/Dunham Classification	Biota /Features	Comments	Thin Section Images by Interval
-3 Wackestone	None	No fossils, abundant dolomite present, no organic/phosphatic material.	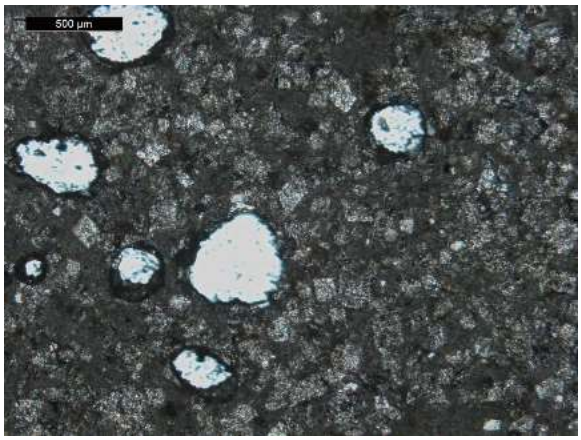
-3.5 Wackestone	None	No fossils present, fine grained limestone with small amounts of dolomite.	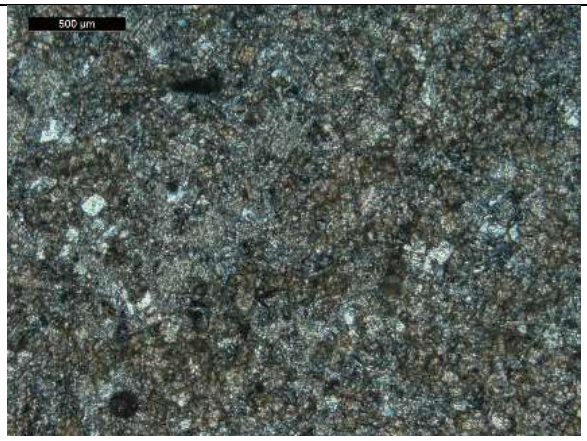

Table continued

Interval/Dunham Classification	Biota /Features	Comments	Thin Section Images by Interval
-4.5 Wackestone	Peloids	Wackestone possesing abundant dolomite grains with no organic content.	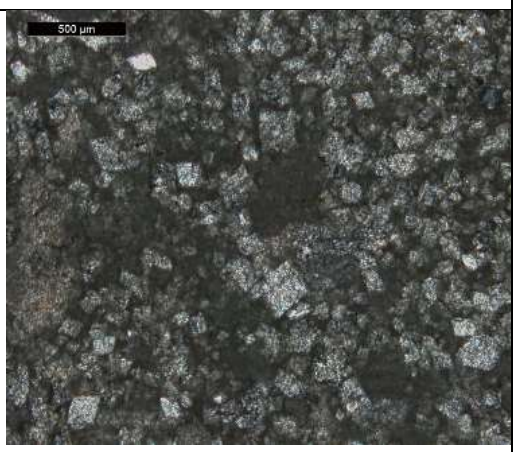
-5 Wackestone	None	No phosphate, dolomite rhombs share crystal boundaries.	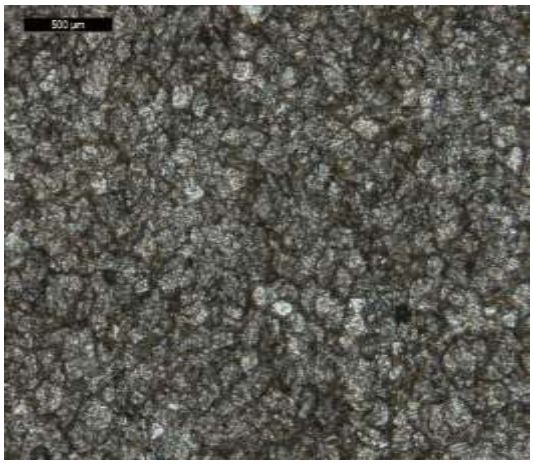

Appendix 2: Apatite Data

Key: TWH_27_S1_1=Interval 27_Steinkern 1_Shot 1

Run 1														
Sample ID	La	Ce	Pr	Nd	Sm	Eu	Gd	Tb	Dy	Ho	Er	Tm	Yb	Lu
Rafael_TWH_27_S1_1	90	226	26.13	94.7	19.7	4.8	24.09	3.96	24.67	4.77	11.99	1.372	6.6	0.81
Rafael_TWH_27_S1_2	96.9	245.4	27.82	99.4	21.09	5.27	26.7	4.503	27.54	5.35	13.75	1.528	7.61	0.937
Rafael_TWH_27_S1_3	96.1	248.1	27.49	96.3	20.15	5.22	25.87	4.36	26.6	5.22	12.99	1.495	7.39	0.91
Rafael_TWH_27_S2_1	187.1	527	61.4	234.2	50.3	11.88	54	8.66	48.7	8.84	21.36	2.3	11.36	1.289
Rafael_TWH_27_S2_2	181.2	532	60.5	220.9	47.4	11.3	50.3	8.16	45.83	8.24	19.6	2.155	10.55	1.22
Rafael_TWH_27_S2_3	170.7	524	58.5	208.1	44.2	10.82	48.6	7.68	43	7.76	18.52	2.012	9.74	1.146
Rafael_TWH_27_S3_1	171.8	554	65.2	238.3	48.7	10.9	51.6	7.98	43.8	7.72	18.25	1.967	9.26	1.137
Rafael_TWH_27_S3_2	172.7	572	66.5	238	49.8	11.23	51.5	8.04	43.4	7.75	18.4	1.908	9.36	1.1
Rafael_TWH_27_S3_3	183.7	563	65.6	246.8	51.8	11.2	52.9	8.21	43.61	7.79	18.3	1.997	9.56	1.137
Rafael_TWH_27_S4_1	173.3	533	54.7	196.4	41.3	9.97	43.5	6.86	38.3	6.86	16.6	1.857	9.42	1.11
Rafael_TWH_27_S4_2	176.7	498	55.3	203.1	43	9.98	46.4	7.32	41.46	7.69	19.14	2.098	10.67	1.257
Rafael_TWH_27_S4_3	167.8	477.9	54.6	194.7	40.63	9.75	45.4	7.13	40.35	7.5	18.22	2.039	10.51	1.225
Rafael_TWH_27_S5_1	131.3	495	58.8	229.2	50.9	12.47	46.9	7.19	36.08	6.09	13.85	1.384	6.78	0.771
Rafael_TWH_27_S5_2	135.7	508	61.5	241.6	53.5	12.73	50.5	7.57	39.1	6.48	14.59	1.448	7.09	0.821
Rafael_TWH_27_S5_3	141	481	60.5	245.4	54.3	12.71	52.5	8	41.03	6.92	15.33	1.52	7.53	0.824
Rafael_TWH_27_S6_1	170.7	569	61.3	217.3	46.2	11.48	50.1	7.67	42.5	7.76	19.05	2.04	10.2	1.146
Rafael_TWH_27_S6_2	173.7	565	62.8	223.5	48.4	11.53	52.1	8.27	45.5	8.27	19.56	2.137	10.84	1.204
Rafael_TWH_27_S6_3	176.2	593	65.8	231.4	50.2	11.81	54.3	8.33	46.6	8.44	20.03	2.141	10.62	1.202
Rafael_TWH_27_S7_1	187.4	547	65.4	237.4	50.8	12.13	54.5	8.63	46.86	8.61	20.2	2.122	10.68	1.161
Rafael_TWH_27_S7_2	177.2	553	62.7	223.2	47.6	11.53	51.4	8.05	45.3	8.13	19.33	2.027	9.95	1.108
Rafael_TWH_27_S7_3	167.9	542	60.1	247	51.1	11.31	50.4	7.84	42.2	7.82	18.69	1.905	9.43	1.007
Rafael_TWH_27_S8_1	155.9	562	63.4	255	52.4	10.98	50.6	7.83	42	7.81	18.81	1.916	9.78	1.117
Rafael_TWH_27_S8_2	228.1	408.6	67.4	392.5	91.4	14.81	98.4	16.13	89.8	16.62	39.9	4.155	19.74	2.31

Rafael_TWH_27_S8_3	232.8	411.6	68.27	404.6	93.8	15.43	107.4	17.32	96.3	17.78	41.9	4.39	21	2.49
Rafael_TWH_27_S9_1	184.8	579	65.2	282.4	54.3	11.03	52.1	7.81	42.1	7.55	18.07	1.871	9.45	1.048
Rafael_TWH_27_S9_2	211.9	376.1	59.9	363.8	85.1	13.51	92.3	14.94	83.5	15.46	36.1	3.86	18.3	2.2
Rafael_TWH_27_S9_3	167.4	627	65.1	287.9	54.6	10.97	49	7.5	39.4	6.84	15.99	1.643	8.23	0.909
Rafael_TWH_27_S10_1	145	490	51.8	222.1	43.5	9.12	42.2	6.61	35.9	6.66	16.5	1.788	9.28	1.02
Rafael_TWH_27_S10_2	139.5	487	50.3	215.3	41.4	8.9	42.2	6.44	34.6	6.47	15.54	1.67	8.7	0.988
Rafael_TWH_27_S10_3	136.1	470	48.4	205.3	38.7	8.13	37.7	5.63	30.8	5.66	14.16	1.517	8.07	0.918
Rafael_TWH_27_S11_1	145.4	482	55.5	250.2	46.8	8.49	45.1	6.65	34.56	5.97	13.58	1.333	6.11	0.718
Rafael_TWH_27_S11_2	143.6	505	57.3	246.5	46.2	8.85	45	6.41	33.4	5.74	12.93	1.269	5.85	0.651
Rafael_TWH_27_S11_3	142.6	513	55.6	242.1	46.4	9.02	44.2	6.37	33.5	5.76	13.3	1.283	6.13	0.683
Rafael_TWH_27_S12_1	138.6	467	53.7	225.7	44.2	8.25	41.6	6.14	31.5	5.46	12.34	1.182	5.67	0.648
Rafael_TWH_27_S12_2	147.3	405	49.8	231.4	47.4	9.98	48.4	7.75	42.6	7.56	17.9	1.932	9.78	1.14
Rafael_TWH_27_S12_3	170.1	526	60.1	256.7	49.8	10.57	48.7	7.34	40.1	7.03	16.58	1.74	9.2	1.024
Rafael_TWH_27_S13_1	164.1	566	64.7	261	49.9	10.72	49.8	7.51	39.6	7.07	16.6	1.759	8.6	0.96
Rafael_TWH_27_S13_2	192.2	636	71.3	284.4	54.8	11.09	54.8	7.8	42.75	7.27	16.87	1.715	8.67	1.002
Rafael_TWH_27_S13_3	184.8	654	73.8	279.8	57.3	12.35	55.2	8.15	42.5	7.37	16.82	1.706	8.58	0.97
Rafael_TWH_27_S14_1	158.2	431.3	65.3	298.6	65.3	13.97	62.3	8.99	46.8	7.92	17.63	1.766	9.08	1.022
Rafael_TWH_27_S14_2	141.6	543	66.4	264	57.7	12.79	52.5	7.67	39.1	6.55	14.49	1.438	7.41	0.794
Rafael_TWH_27_S14_3	143.7	551	66.7	227.6	52.5	12.47	55.2	7.8	40.6	6.8	15.62	1.515	7.66	0.863
Rafael_TWH_27_S15_1	147	581	69.7	228.3	53.8	12.8	54.1	7.83	40.6	6.77	15.03	1.463	7.21	0.799
Rafael_TWH_27_S15_2	131.8	519	63.1	214.1	51.5	12.42	52.7	7.61	40.56	6.86	15.64	1.537	7.73	0.893
Rafael_TWH_27_S15_3	148	554	66.1	224.1	54.1	12.37	55.4	8.13	42.4	7.35	16.62	1.679	8.25	0.929
Rafael_TWH_27_S16_1	132.4	499	62.4	213	51.8	12.32	53.8	7.99	42.37	7.21	16.29	1.621	8.03	0.903
Rafael_TWH_27_S16_2	148.5	388.2	50.2	175.5	42.3	10.28	52.8	8.4	48	8.76	21	2.222	11.07	1.319
Rafael_TWH_27_S16_3	140	484	52.4	159.3	36.4	9.21	43.8	6.68	38.2	6.95	16.73	1.821	9.09	1.093
Rafael_TWH_27_S17_1	148.8	490	55.4	172.6	38.8	9.86	46	6.99	39.7	7.27	17.32	1.828	9.17	1.022

Rafael_TWH_27_S17_2	103.8	338	38.2	121.9	27.37	7.26	33.7	5.17	29	5.47	13.42	1.495	7.88	0.935
Rafael_TWH_27_S17_3	99.5	331	37	119.3	26.73	7.03	32.5	5.1	29.16	5.54	13.63	1.545	8.11	0.978
Rafael_TWH_27_S18_1	98.2	318.8	37.26	119.2	27.15	7.12	33.25	5.14	29.53	5.61	13.55	1.531	7.98	0.975
Rafael_TWH_27_S18_2	151.7	611	70.8	234.6	51.4	12.77	56.8	8.18	43.6	7.76	17.69	1.757	8.49	0.959
Rafael_TWH_27_S18_3	148.1	600	70.2	235.5	52	12.25	53.4	7.84	41.1	7.25	16.76	1.704	7.98	0.894
Rafael_TWH_27_S19_1	146.3	529	66.8	232	51.3	11.88	51.6	7.56	40.76	7.2	16.6	1.696	8.36	0.959
Rafael_TWH_27_S19_2	194.4	601	64.9	213.1	44.3	9.9	49.9	7.55	42.4	7.84	18.91	2.007	9.64	1.101
Rafael_TWH_27_S19_3	183.5	563	62.6	202.6	41	9.96	49.3	7.14	40.32	7.54	18.1	1.924	9.36	1.09
Rafael_TWH_27_S20_1	187.2	606	64	198.8	39	9.73	47.4	6.85	38.9	7.13	17.53	1.868	9.2	1.06
Rafael_TWH_27_S20_2	192.7	676	76.5	264.5	56.2	12.25	60.7	8.65	46.3	8.44	20.13	2.146	10.69	1.253
Rafael_TWH_27_S20_3	179.5	619	69.2	229.5	47.9	11.41	51.7	7.94	43.2	7.73	18.69	1.899	9.56	1.056
Rafael_TWH_27_S21_1	178.6	618	68	229.3	48.4	11.45	52.9	8.04	43.2	7.79	18.68	1.986	9.74	1.1
Rafael_TWH_27_S21_2	163.5	545	65.9	245.2	53.1	11.62	57.1	8.41	48.6	8.39	20.09	2.192	10.23	1.192
Rafael_TWH_27_S21_3	195.8	646	76.7	283	61.3	13.28	64.7	9.66	55.1	9.59	22.51	2.443	11.64	1.298
Rafael_TWH_27_S22_1	175.5	584	71.4	261.6	56.3	12.41	61	9	52.9	9.09	21.38	2.334	11.06	1.272
Rafael_TWH_27_S22_2	178.9	651	83.9	341.5	76.1	16.12	70.6	10.16	55.1	9.05	20.55	2.049	9.63	1.077
Rafael_TWH_27_S22_3	200.4	720	89.4	355.4	76.1	14.91	73.1	10.06	54.7	9.02	20.7	2.054	9.58	1.067
Rafael_TWH_27_S23_1	204.1	735	93.3	360.7	78.9	16.19	75	10.6	57.4	9.38	21.35	2.082	9.56	1.055
Rafael_TWH_27_S23_2	136.4	406	49.3	178.1	38	8.21	39.4	6.09	36.2	6.45	16.04	1.803	9.05	1.08
Rafael_TWH_27_S23_3	127.5	390	45.1	167	35.3	8.04	38.8	5.81	35.08	6.2	15.55	1.744	8.92	1.068
Rafael_TWH_27_S24_1	133.1	414	45.9	178.5	37.1	8.15	39.7	6.03	35.5	6.29	15.29	1.701	8.72	1.014
Rafael_TWH_27_S24_2	98.4	303	32.4	120.3	24.76	5.87	28.58	4.43	27.45	5.15	13.35	1.56	8.4	1.034
Rafael_TWH_27_S24_3	100.5	298.7	34.74	124.8	27.1	6.16	30.7	4.8	29.63	5.44	14.1	1.649	8.7	1.059
Rafael_TWH_27_S25_1	103.7	317	35.2	127.7	27.59	6.2	31	4.74	29.13	5.55	14.1	1.67	8.66	1.065
Rafael_TWH_27_S25_2	220.7	709	79.8	303	61.7	13.16	62.2	8.94	50.2	8.51	20.11	2.08	9.74	1.076
Rafael_TWH_27_S25_3	226.1	740	81.3	306.2	62.8	13.07	61.1	8.82	50.4	8.79	20.47	2.103	9.92	1.123

Rafael_TWH_27_S26_4	218.6	702	81.5	290.9	59.8	12.54	61.4	8.71	49.2	8.45	19.86	2.082	9.8	1.115

Run 2														
Sample ID	La	Ce	Pr	Nd	Sm	Eu	Gd	Tb	Dy	Ho	Er	Tm	Yb	Lu
Rafael_TWH 26.35_S2_1	40.82	115.9	13.33	60.7	17.7	3.51	18.79	2.639	14.62	2.613	6.8	0.61	3.42	0.452
Rafael_TWH 26.35_S2_2	38.9	118.8	13.21	57.9	15.57	3.572	17.78	2.495	13.96	2.456	5.75	0.634	3.27	0.441
Rafael_TWH 26.35_S3_1	35	114.6	12.76	54.9	14.05	3.35	15.85	2.199	12.29	2.149	5.12	0.575	3	0.381
Rafael_TWH 26.35_S3_2	32.35	114	12.3	50.1	12.17	3.23	13.67	1.954	11.29	1.92	4.57	0.523	2.6	0.313
Rafael_TWH 26.35_S3_3	30.36	105.2	11.91	52.9	13.52	3.25	15.46	2.066	11.39	1.96	4.62	0.51	2.58	0.313
Rafael_TWH 26.35_S5_1	30.21	93.2	10.62	47.5	13.05	3.25	15.09	2.155	12.38	2.217	5.24	0.586	3.29	0.429
Rafael_TWH 26.35_S5_2	34.8	98.8	11.64	53.9	15.02	3.42	15.98	2.288	13.02	2.33	5.38	0.64	3.46	0.453
Rafael_TWH 26.35_S5_3	30.6	96.3	11.1	49.6	13.08	3.4	15.11	2.16	11.89	2.067	5.07	0.555	2.9	0.38
Rafael_TWH 26.35_S6_1	49.1	108.9	16.34	85	22.57	4.64	25.28	3.618	20.95	3.652	8.91	1.055	5.54	0.714
Rafael_TWH 26.35_S6_2	49	158.5	18.66	79.2	18.94	4.16	19.78	2.742	15.2	2.643	6.29	0.683	3.53	0.432
Rafael_TWH 26.35_S6_3	45.24	119.1	16.26	77.7	20.01	4.29	20.56	2.822	16.21	2.879	7.02	0.771	4.16	0.51
Rafael_TWH 26.35_S7_1	31.7	101.4	11.37	47.9	12.74	3.13	14.58	2.089	11.79	2.148	5.18	0.584	3.06	0.392
Rafael_TWH 26.35_S7_2	36.6	102.7	11.74	53.5	15.1	3.425	17.16	2.451	14.02	2.537	6.2	0.658	3.47	0.446
Rafael_TWH 26.35_S7_3	31.38	107.5	11.61	49.8	13.37	3.22	15.62	2.146	11.92	2.155	5.13	0.582	3.03	0.384
Rafael_TWH 26.35_S8_1	33.59	101.6	11.81	50.6	13.2	3.114	15.64	2.257	13	2.35	5.8	0.644	3.27	0.402
Rafael_TWH 26.35_S8_2	35.2	105.3	11.93	51.1	14.02	3.26	15.91	2.293	13.39	2.424	5.9	0.658	3.36	0.426
Rafael_TWH 26.35_S8_3	34.8	101.4	11.48	50.1	12.87	3.19	15.19	2.172	12.78	2.334	5.73	0.655	3.46	0.453
Rafael_TWH 26.35_S9_1	31.48	91.6	10.64	47.7	12.7	2.927	14.57	2.109	11.78	2.102	5.1	0.552	2.88	0.368
Rafael_TWH 26.35_S9_2	31.1	99.2	11.05	47.4	12.72	3.027	14.62	2.071	11.78	2.115	4.96	0.559	2.767	0.357
Rafael_TWH 26.35_S9_3	29.33	92.4	10.4	45.7	12.03	2.9	13.98	1.979	11.54	2.1	4.95	0.545	2.79	0.35
Rafael_TWH 26.35_S11_2	50.6	157	18.48	80.2	20.62	4.43	21.3	2.91	17.2	3.17	7.7	0.857	4.43	0.557
Rafael_TWH 26.35_S11_3	53	161.2	19.56	79.9	20.15	4.37	22.3	3.033	17.74	3.27	7.84	0.92	4.95	0.61
Rafael_TWH 26.35_S12_1	37.4	126.8	13.78	58.7	15.64	3.67	18.3	2.627	15.06	2.69	6.31	0.714	3.62	0.464

Rafael_TWH 26.35_S12_2	37.1	132	13.85	58.1	15.06	3.61	18.26	2.545	14.81	2.64	6.57	0.694	3.47	0.449
Rafael_TWH 26.35_S12_3	38.2	124	13.64	59.2	15.09	3.58	18.81	2.528	14.32	2.603	6.35	0.696	3.55	0.454
Rafael_TWH 26.35_S13_1	54.4	152.9	19.07	83	20.78	4.49	21.88	3	16.94	3.02	7.19	0.79	4	0.48
Rafael_TWH 26.35_S13_2	52.6	163.4	19.33	81.7	20.6	4.45	22.66	3.232	18.84	3.402	8.11	0.913	4.51	0.568
Rafael_TWH 26.35_S13_3	54.5	164.9	20.28	85.8	20.63	4.79	22.73	3.383	19.36	3.52	8.41	0.908	4.49	0.563
Rafael_TWH 26.35_S14_1	40.5	135.3	15.85	64.6	16.31	3.96	20.6	2.85	16.66	2.88	7.26	0.754	3.56	0.57
Rafael_TWH 26.35_S14_2	42.2	143.5	16.25	68.3	17.16	4.07	20.66	2.903	16.38	2.908	6.73	0.717	3.44	0.43
Rafael_TWH 26.35_S14_3	42	136.3	15.89	66.8	17.63	4.01	20.35	2.866	16.46	2.961	7.1	0.758	3.6	0.451
Rafael_TWH 26.35_S15_1	34.13	104.8	11.45	50.3	13.1	3.15	15.49	2.174	12.21	2.214	5.39	0.606	3.11	0.394
Rafael_TWH 26.35_S15_2	34.98	101.7	11.52	50.4	13.19	3.026	15.66	2.221	12.42	2.273	5.42	0.578	2.88	0.356
Rafael_TWH 26.35_S15_3	35.72	103.1	11.91	51.4	13.62	3.118	16.06	2.251	12.96	2.355	5.57	0.6	2.863	0.361
Rafael_TWH 26.35_S16_1	20.8	49.4	5.88	27.5	6.67	1.56	7.04	0.99	6.15	1.23	3.24	0.461	2.87	0.388
Rafael_TWH 26.35_S16_2	9.1	25.9	2.9	14.1	3.66	0.99	4.47	0.582	3.41	0.614	1.43	0.161	0.94	0.123
Rafael_TWH 26.35_S16_3	30.5	86.4	10.08	48.1	12.36	3.06	15.2	2.22	11.67	2.19	5.68	0.783	4.81	0.607
Rafael_TWH 26.35_S17_1	32.5	87.2	10.2	48.5	12.94	3.1	14.62	2.066	11.87	2.112	5.17	0.579	3.22	0.395
Rafael_TWH 26.35_S17_2	44.3	100.7	11.35	52.5	13.71	3.22	16.4	2.21	12.91	2.44	5.71	0.669	3.83	0.484
Rafael_TWH 26.35_S17_3	34.1	92.2	10.69	50.2	14.23	3.25	16	2.47	14.8	2.76	7.51	1.037	5.87	0.839
Rafael_TWH 26.35_S18_1	33.3	90	10.56	52.5	14.61	3.19	17.4	2.53	14.7	2.64	6.53	0.753	3.67	0.462
Rafael_TWH 26.35_S18_2	38.6	109.7	12.45	58.2	15.8	3.86	18.6	2.67	15.11	2.73	6.6	0.735	4.01	0.525
Rafael_TWH 26.35_S18_3	38.7	109.4	13.18	59	17.1	3.68	18.9	2.65	15.26	2.66	6.28	0.738	3.94	0.527
Rafael_TWH 26.35_S18_4	39.2	112.4	13.33	60.5	16.3	3.79	18	2.96	17.12	3.25	8.88	1.13	6.26	0.882
Rafael_TWH 26.35_S19_1	73	136	14	57.1	14.43	3.27	14.97	2.042	11.09	1.999	4.67	0.524	2.96	0.388
Rafael_TWH 26.35_S19_2	29.9	80.1	9.76	43.4	12.22	2.76	12.87	1.779	9.87	1.82	4.52	0.563	3.12	0.405
Rafael_TWH 26.35_S19_3	43.6	99.6	10.71	50	13.38	3.26	13.97	2.08	12.76	2.4	6.52	0.832	4.99	0.699
Rafael_TWH 26.35_S20_1	41.7	126	15.48	70.1	16.6	3.67	16.5	2.444	13.96	2.476	5.98	0.652	3.4	0.431
Rafael_TWH 26.35_S20_2	40.17	126.2	15.68	66.5	16.06	3.65	17.02	2.427	13.69	2.453	5.88	0.655	3.47	0.432

Rafael_TWH 26.35_S20_3	41.23	121.4	15.05	66.2	16.01	3.67	17.38	2.467	14.28	2.559	6.34	0.705	3.54	0.45
Rafael_TWH 26.35_S21_1	42.03	112.9	13.42	56.7	14.68	3.27	16.19	2.269	12.79	2.265	5.42	0.593	2.99	0.383
Rafael_TWH 26.35_S21_2	39.9	120.4	13.18	54.7	13.49	3.084	14.66	2.037	11.58	2.078	5.03	0.535	2.82	0.344
Rafael_TWH 26.35_S21_3	38.55	118.2	13.03	53.3	13.45	2.999	15.12	2.126	12.5	2.29	5.73	0.681	3.7	0.498
Rafael_TWH 26.35_S21_4	38.7	128.7	13.35	53	13.35	2.985	14.03	1.998	11.13	1.977	4.7	0.529	2.68	0.331
Rafael_TWH 27_S21_1	163.5	545	65.9	245.2	53.1	11.62	57.1	8.41	48.6	8.39	20.09	2.192	10.23	1.192
Rafael_TWH 27_S21_2	195.8	646	76.7	283	61.3	13.28	64.7	9.66	55.1	9.59	22.51	2.443	11.64	1.298
Rafael_TWH 27_S21_3	175.5	584	71.4	261.6	56.3	12.41	61	9	52.9	9.09	21.38	2.334	11.06	1.272
Rafael _TWH27_S22_1	178.9	651	83.9	341.5	76.1	16.12	70.6	10.16	55.1	9.05	20.55	2.049	9.63	1.077
Rafael_TWH 27_S22_2	200.4	720	89.4	355.4	76.1	14.91	73.1	10.06	54.7	9.02	20.7	2.054	9.58	1.067
Rafael_TWH 27_S22_3	204.1	735	93.3	360.7	78.9	16.19	75	10.6	57.4	9.38	21.35	2.082	9.56	1.055
Rafael_TWH 27_S23_1	136.4	406	49.3	178.1	38	8.21	39.4	6.09	36.2	6.45	16.04	1.803	9.05	1.08
Rafael_TWH 27_S23_2	127.5	390	45.1	167	35.3	8.04	38.8	5.81	35.08	6.2	15.55	1.744	8.92	1.068
Rafael_TWH 27_S23_3	133.1	414	45.9	178.5	37.1	8.15	39.7	6.03	35.5	6.29	15.29	1.701	8.72	1.014
Rafael_TWH 27_S24_1	98.4	303	32.4	120.3	24.76	5.87	28.58	4.43	27.45	5.15	13.35	1.56	8.4	1.034
Rafael_TWH 27_S24_2	100.5	298.7	34.74	124.8	27.1	6.16	30.7	4.8	29.63	5.44	14.1	1.649	8.7	1.059
Rafael_TWH 27_S24_3	103.7	317	35.2	127.7	27.59	6.2	31	4.74	29.13	5.55	14.1	1.67	8.66	1.065
Rafael_TWH 27_S25_1	220.7	709	79.8	303	61.7	13.16	62.2	8.94	50.2	8.51	20.11	2.08	9.74	1.076
Rafael_TWH 27_S25_2	226.1	740	81.3	306.2	62.8	13.07	61.1	8.82	50.4	8.79	20.47	2.103	9.92	1.123
Rafael_TWH 27_S25_3	218.6	702	81.5	290.9	59.8	12.54	61.4	8.71	49.2	8.45	19.86	2.082	9.8	1.115

Run 3														
Sample ID	La	Ce	Pr	Nd	Sm	Eu	Gd	Tb	Dy	Ho	Er	Tm	Yb	Lu
Rafael_TWH 23_S1_1	46.88	117	14.03	62.3	16.61	3.8	19.25	2.928	17.17	3.074	7.66	0.801	3.808	0.474
Rafael_TWH 23_S1_2	41.02	109.4	13.41	58.1	15.96	3.59	18.1	2.738	15.91	2.837	6.63	0.643	2.721	0.312
Rafael_TWH 23_S1_3	43.4	112.3	13.3	58.8	15.8	3.57	18.49	2.753	15.78	2.824	6.91	0.713	3.346	0.402

Rafael_TWH 23_S2_1	88.2	195.6	20.96	84.7	21.89	4.44	25.34	3.813	22.96	4.17	10.33	1.106	4.89	0.617
Rafael_TWH 23_S2_2	78.3	176.3	18.93	76.9	19.96	4.4	23.74	3.554	21.15	3.983	9.78	1.05	4.92	0.616
Rafael_TWH 23_S3_3	79.3	177.1	19.07	80.6	20.22	4.38	24.81	3.703	22.39	4.177	10.2	1.124	5.15	0.632
Rafael_TWH 23_S4_1	55.7	159.6	17.2	70.4	17.99	4.46	20.82	3.169	18.73	3.39	8.46	0.949	4.85	0.588
Rafael_TWH 23_S4_2	60.4	157.6	17.9	74.4	19.22	4.49	22.2	3.33	20.27	3.615	9.08	1.027	5.01	0.621
Rafael_TWH 23_S4_3	55.7	146	16.71	68.4	18.5	4.48	21.52	3.27	19.35	3.53	8.66	0.991	5.08	0.632
Rafael_TWH 23_S5_1	118.5	265.6	28.78	111.5	26.67	5.76	29.39	4.57	27.34	5.11	13.25	1.522	7.41	0.941
Rafael_TWH 23_S5_2	106.9	248.3	26.97	105.6	25.27	5.48	28.6	4.41	26.96	5.04	12.79	1.449	6.98	0.888
Rafael_TWH 23_S5_3	103.8	250.5	26.53	104.8	25.08	5.75	28.76	4.44	26.13	4.98	12.69	1.461	7.45	0.907
Rafael_TWH 23_S6_1	59.4	148.2	15.91	63.6	16.65	3.84	18.84	2.962	17.74	3.34	8.3	0.925	4.62	0.592
Rafael_TWH 23_S6_2	60.4	149.6	15.99	66.5	17.03	3.85	19.23	3.011	17.8	3.32	8.39	0.916	4.61	0.594
Rafael_TWH 23_S6_3	58.7	145.1	15.67	64.7	16.58	3.74	19.39	2.987	18.05	3.339	8.53	0.941	4.61	0.593
Rafael_TWH 23_S7_1	100.1	250.4	29.86	122.9	30.27	6.9	33.98	5.16	29.86	5.36	12.9	1.375	6.42	0.777
Rafael_TWH 23_S7_2	97.2	258.7	30.18	124.2	30.1	6.97	33.5	5.08	30.26	5.36	12.91	1.387	6.52	0.81
Rafael_TWH 23_S7_3	96.2	252.4	30.49	121.1	30.17	6.96	32.93	5.08	29.85	5.28	12.74	1.366	6.61	0.801
Rafael_TWH 23_S8_1	95.3	244.6	28.49	114.2	28.39	6.09	32.4	4.81	28.31	5.12	12.36	1.351	6.41	0.826
Rafael_TWH 23_S8_2	87	229.6	26.64	108.7	26.85	5.82	29.75	4.58	26.23	4.89	11.86	1.282	6.16	0.78
Rafael_TWH 23_S8_3	81.1	210.2	24.81	100.4	27.9	6.67	29.2	4.68	25.51	3.99	11.01	1.222	5.82	0.754
Rafael_TWH 23_S9_1	97.3	219.8	25.22	106	26.3	5.39	28.9	4.565	27.04	5.01	12.5	1.379	6.74	0.873
Rafael_TWH 23_S9_2	83.7	197.8	22.7	95	23.24	5.12	27.78	4.307	25.95	4.89	12.3	1.363	6.39	0.832
Rafael_TWH 23_S9_3	87.6	200.9	23.17	97.8	24.15	5.43	27.81	4.29	25.6	4.79	12.31	1.372	6.97	0.871
Rafael_TWH 23_S10_1	79.7	190.5	19.97	81.3	20.57	4.55	26.84	3.775	23.11	4.309	10.72	1.199	5.74	0.739
Rafael_TWH 23_S10_2	79.3	196.1	20.76	81.8	21.2	5.11	25.9	3.89	23.31	4.3	10.85	1.259	6.42	0.853
Rafael_TWH 23_S10_3	83.7	192.1	20.75	80.5	20.03	4.42	23.91	3.79	22.33	4.23	10.49	1.182	5.59	0.719
Rafael_TWH 23_S11_1	54.3	142.9	15.53	65.6	16.74	4.14	20.09	3.155	18.2	3.443	8.45	0.958	4.86	0.616
Rafael_TWH 23_S11_2	56.3	139.2	15.7	63.3	16.65	4.08	19.44	2.943	17.65	3.31	8.38	0.922	4.61	0.581

Rafael_TWH23_S11_3	59	150.6	16.24	65.7	16.8	4.2	19.5	2.94	17.92	3.27	8.22	0.917	4.7	0.584
Rafael_TWH23_S12_1	43.83	114	13.09	56.9	15.25	4.02	17.88	2.65	16.22	2.949	7.53	0.855	4.5	0.574
Rafael_TWH23_S12_2	45.7	117.4	13.43	59	16.03	3.96	17.85	2.733	16.01	2.973	7.61	0.882	4.63	0.597
Rafael_TWH23_S12_3	52.2	129.6	14.78	63.6	16.87	4.28	17.98	2.806	16.41	3.155	7.87	0.911	4.72	0.596
Rafael_TWH23_S13_1	47.6	118.2	12.58	50.9	13.45	3.36	16.23	2.453	14.93	2.78	7.15	0.807	4.09	0.524
Rafael_TWH23_S13_2	52.3	134.2	14.25	56.6	14.22	3.61	16.37	2.516	15.27	2.846	6.97	0.771	3.77	0.472
Rafael_TWH23_S13_3	79.8	201.8	21.31	87	21.36	5.28	25.93	3.94	23.39	4.32	11.2	1.302	6.82	0.893
Rafael_TWH23_S14_1	82.2	192.1	20.63	79.3	18.69	4.64	21.47	3.337	20.16	3.79	9.68	1.096	5.52	0.689
Rafael_TWH23_S14_2	77.6	190.2	19.81	80.6	18.35	4.51	22.29	3.292	19.86	3.78	9.61	1.071	5.21	0.621
Rafael_TWH23_S14_3	76.4	177.6	18.63	72.3	17.36	4.22	20.67	3.23	18.95	3.64	9.42	1.058	5.16	0.62
Rafael_TWH23_S15_1	72.8	200.2	21.97	88.4	22.45	5.26	23.74	3.64	21.36	3.94	9.76	1.091	5.34	0.642
Rafael_TWH23_S15_2	71.3	196.8	21.33	86.7	21.38	4.85	23.81	3.689	21.45	3.972	9.62	1.074	5.31	0.636
Rafael_TWH23_S15_3	74.8	210.4	22.48	92.1	22.5	5.03	24.94	3.67	21.57	3.98	9.94	1.143	5.6	0.68
Rafael_TWH23_S16_1	118.7	347	39.18	155.5	37.6	8.52	40.7	6.48	37.5	6.73	16.63	1.801	8.87	1.086
Rafael_TWH23_S16_2	121.6	343	40.16	159.6	38	8.19	41.9	6.61	38.66	6.9	16.65	1.793	8.53	1.03
Rafael_TWH23_S16_3	136.4	374.9	44.71	178.4	42.2	8.85	45.4	6.95	41.9	7.39	17.94	1.906	8.98	1.1
Rafael_TWH23_S17_1	74.1	187.8	21.09	85.8	21.91	5.18	24.77	3.681	21.64	3.895	9.77	1.101	5.64	0.692
Rafael_TWH23_S17_2	72.2	188.1	21.71	87.1	22.4	5.38	25.1	3.71	21.33	3.94	9.79	1.088	5.45	0.673
Rafael_TWH23_S17_3	75.9	192.9	21.89	88.8	22.6	5.43	24.51	3.86	22.21	4.01	10.02	1.2	5.91	0.709
Rafael_TWH23_S18_1	82.2	188.6	22.36	93.8	24.12	5.37	26.92	4.212	25.42	4.624	11.65	1.318	6.53	0.798
Rafael_TWH23_S18_2	74	187.1	21.72	88.3	22.24	5.28	25.16	3.997	23.77	4.35	10.98	1.235	6.06	0.76
Rafael_TWH23_S18_3	72.9	188.1	21.4	87.9	21.36	5.24	24.32	3.8	22.62	4.12	10.54	1.161	5.86	0.72
Rafael_TWH23_S19_1	76.4	185.8	20.61	83	20.34	4.83	24.04	3.637	21.66	4.02	10.1	1.121	5.59	0.669
Rafael_TWH23_S19_2	80.3	182.2	20.55	85.7	20.5	4.76	23.77	3.701	21.74	3.999	10	1.102	5.43	0.671
Rafael_TWH23_S19_3	81	182.3	21.11	85.6	21.28	4.99	25.57	3.93	23.74	4.4	10.97	1.238	5.95	0.709
Rafael_TWH23_S20_1	85	203.7	23.55	92.8	22.76	5.7	27.3	4.08	24.96	4.73	11.83	1.351	6.79	0.822

Rafael_TWH 23_S20_2	88.3	205.5	23.74	97	23.25	5.47	27.44	4.33	26.36	4.78	11.86	1.349	6.51	0.793
Rafael_TWH 23_S20_3	87.5	207.7	23.91	96.9	23.8	5.46	27.3	4.24	25.18	4.77	11.73	1.289	6.16	0.778
Rafael_TWH 23_S21_1	86.6	215.7	24.83	98.7	23.87	5.72	26.17	4.09	24.56	4.53	11.4	1.279	6.51	0.814
Rafael_TWH 23_S21_2	85.5	210.5	24.63	96.7	24.16	5.94	28.54	4.276	24.69	4.74	11.81	1.367	6.88	0.833
Rafael_TWH 23_S21_3	95.9	237	26.4	108.1	26.1	6.07	27.7	4.24	25.61	4.72	12.24	1.334	6.9	0.813
Rafael_TWH 23_S22_1	59.4	144	15.32	63.8	16.25	3.96	19.72	2.919	17.6	3.307	8	0.895	4.27	0.537
Rafael_TWH 23_S22_2	59.8	140	15.3	63.5	16.49	3.88	19.71	2.977	17.69	3.377	8.29	0.957	4.58	0.55
Rafael_TWH 23_S22_3	70.3	165.6	17.88	75	18.9	4.04	22.29	3.33	19.89	3.627	9	0.959	4.52	0.561
Rafael_TWH 23_S23_1	99.6	248.6	26.78	111.7	25.19	6.01	29.7	4.54	26.81	4.97	12.32	1.386	6.67	0.832
Rafael_TWH 23_S23_2	105.8	252	28.82	111.4	27.34	6.14	29.78	4.79	27.84	5.19	12.65	1.403	6.75	0.814
Rafael_TWH 23_S23_3	95.5	240.6	26.84	106.3	25.99	6.1	30.3	4.57	27.31	5.02	12.53	1.337	6.59	0.792
Rafael_TWH 23_S24_1	70.3	181.5	19.6	79.7	20.57	4.71	22.43	3.5	21.14	3.89	9.75	1.102	5.45	0.654
Rafael_TWH 23_S24_2	73.5	179.7	20.21	87.5	21.2	5.31	25.4	3.72	23.01	4.25	10.57	1.154	5.73	0.705
Rafael_TWH 23_S24_3	70.8	176.9	20.88	82.9	20.99	4.82	23.3	3.68	22.45	4.07	10.17	1.104	5.5	0.684
Rafael_TWH 23_S25_1	69.6	180.2	20.42	81.1	19.92	4.38	22.97	3.4	19.66	3.62	8.93	0.963	4.52	0.568
Rafael_TWH 23_S25_2	75.7	183.6	20.68	83.5	21.15	4.41	23.72	3.55	21.25	3.965	9.54	1.06	4.91	0.605
Rafael_TWH 23_S25_3	75.4	188	20.97	84.7	20.86	4.55	24.36	3.746	21.44	4.02	9.75	1.06	5.09	0.656
Rafael_TWH 23.5_S1_1	235.4	552	61.6	247	50.2	11.78	57.4	8.74	52.8	9.75	24.4	2.61	12.16	1.519
Rafael_TWH 23.5_S1_2	225.7	521	57.9	220.5	46.4	11.49	55.2	8.42	52.2	9.79	24.58	2.61	12.1	1.498
Rafael_TWH 23.5_S1_3	223.1	481	55.8	219.3	47.7	11.05	57.9	8.92	54.1	10.35	25.84	2.76	13.2	1.609
Rafael_TWH 23.5_S2_1	301	765	81.4	320	65.6	15.67	73.9	11.32	68.3	12.09	29.8	3.21	15.54	1.84
Rafael_TWH 23.5_S2_2	301.2	732	83.9	323.2	66.1	16.22	77.7	12.05	71.6	13.26	32	3.41	15.95	1.916
Rafael_TWH 23.5_S2_3	302.6	767	86.2	312.1	66.1	15.93	74.2	11.53	67.8	12.35	30.1	3.18	15.54	1.86
Rafael_TWH 23.5_S3_1	245	568	68.6	260.9	56.5	13.43	63.6	10.14	62.1	11.34	28.5	3.16	14.18	1.77
Rafael_TWH 23.5_S3_2	248.2	568	67.2	265.4	55.9	13.1	63.6	9.79	58.6	10.99	27	2.97	14.15	1.664
Rafael_TWH 23.5_S3_3	265.1	582	69.8	268.6	58.2	13.23	61.8	9.69	58.7	10.72	26.22	2.833	13.53	1.638

Rafael_TWH 23.5_S4_1	240 .4	589	67. 8	269 .3	58. 2	13. 51	64. 3	9.9	58. 8	10. 74	25. 7	2.7 2	13. 55	1.6 2
Rafael_TWH 23.5_S4_2	234 .9	559	68. 8	259 .1	56. 4	13. 77	63. 9	9.3 7	56. 1	10. 36	25	2.7 2	13. 36	1.5 5
Rafael_TWH 23.5_S4_3	263 .1	685	77. 5	300	60. 5	14. 9	71. 7	10. 82	66. 1	12. 15	28. 9	3.0 3	14. 1	1.6 1
Rafael_TWH 23.5_S5_1	269 .9	611	69. 5	250 .3	52	11. 91	57. 7	8.8 8	54. 6	10. 28	25. 3	2.6 9	12. 25	1.4 37
Rafael_TWH 23.5_S5_2	277 .8	659	70. 1	263 .2	51. 2	12. 27	60. 1	8.8 8	54. 9	10. 44	25. 1	2.6 8	12. 13	1.5 04
Rafael_TWH 23.5_S5_3	283 .4	653	73. 9	269 .8	53. 3	12. 93	61. 6	9.7 8	57. 4	10. 79	26. 9	2.8	12. 7	1.5 69
Rafael_TWH 23.5_S6_1	227 .1	508	58. 6	224 .8	48. 4	11. 26	55. 3	8.6 6	52. 2	9.7	23. 73	2.5 71	11. 74	1.4 58
Rafael_TWH 23.5_S6_2	243 .1	552	64. 7	245 .4	52. 2	12. 29	61. 1	9.4 1	56. 7	10. 6	25. 7	2.7 1	12. 27	1.4 35
Rafael_TWH 23.5_S6_3	253 .9	557	65. 8	247 .4	54. 1	12. 57	62	9.4 9	58	10. 74	25. 78	2.7 69	12. 32	1.5 06
Rafael_TWH 23.5_S7_1	204 .8	421	51. 8	201 .3	44. 8	11. 04	53. 9	8.6 3	53. 1	10. 37	25. 9	2.9 6	13. 73	1.6 92
Rafael_TWH 23.5_S7_3	197 .8	436	50. 7	194	42. 5	10. 56	52. 2	8.0 6	50. 8	9.6 1	23. 64	2.6 42	12. 35	1.4 58
Rafael_TWH 23.5_S8_1	293 .3	756	102 .8	422 .1	93. 3	17. 52	96. 4	14. 87	83. 8	14. 41	33. 3	3.3 2	15. 05	1.8 35
Rafael_TWH 23.5_S8_2	190 .2	413	48	190 .2	41. 4	10. 35	48. 6	7.8 4	49. 8	9.2 9	23	2.5 9	12. 76	1.5 19
Rafael _TWH 23.5_S8_3	198 .6	437	51. 3	196 .8	42. 4	10. 42	51. 1	7.8	48. 3	9.3 5	24. 1	2.6 7	13. 41	1.5 9
Rafael_TWH 23.5_S9_1	280 .6	759	101 .2	386	84. 5	17. 12	88. 7	13. 47	78. 2	13. 79	31. 7	3.3	15. 09	1.7 62
Rafael_TWH 23.5_S9_2	255 .9	683	90	364	81. 8	17. 65	85. 8	13. 38	76. 2	13. 56	31. 7	3.2 7	15. 63	1.8
Rafael_TWH 23.5_S9_3	242 .8	633	84. 6	339 .5	76. 7	16. 41	82	12. 68	73. 7	13. 16	31. 05	3.2 4	15. 47	1.7 85
Rafael_TWH 23.5_S10_1	271 .1	648	79. 2	296 .3	64. 1	13. 17	69. 7	10. 61	63. 2	11. 53	27. 2	2.8 8	13. 13	1.5 89
Rafael_TWH 23.5_S10_2	301 .5	560	75. 5	323	70. 8	14. 86	82. 2	12. 77	75. 1	13. 76	33. 09	3.4 75	16. 1	1.9 73
Rafael_TWH 23.5_S10_3	269 .4	591	74. 4	295 .1	63. 7	13. 72	70. 5	10. 8	64. 4	11. 69	27. 69	2.9 28	13. 46	1.6 57
Rafael_TWH 23.5_S11_1	197 .9	494	54. 6	208 .9	44. 6	10. 33	50. 3	7.7 9	46. 8	8.8 8	21. 57	2.3 67	11. 39	1.3 85
Rafael_TWH 23.5_S11_2	215	455 .5	54	209 .1	45. 1	10. 6	52. 4	8.1 9	50. 4	9.5 7	23. 9	2.6 43	12. 9	1.5 51
Rafael_TWH 23.5_S11_3	220 .5	510	57. 7	216 .3	45. 2	10. 71	51. 4	8.1 8	49. 5	9.3	23. 9	2.5 1	12. 98	1.5 4
Rafael_TWH 23.5_S12_1	249 .3	514	57. 1	223 .5	46. 5	11. 79	58. 1	9.4 5	58. 9	10. 86	28. 6	3.0 5	14. 9	1.7 4
Rafael_TWH 23.5_S12_2	233 .1	470	51. 5	195 .8	41. 2	10. 38	52. 7	8.5	50. 9	9.7 8	24. 7	2.7 6	13. 33	1.5 9
Rafael_TWH 23.5_S12_3	239 .1	496	54. 1	208 .7	44. 2	11. 2	54. 9	8.8 1	54. 7	10. 37	25. 6	2.8 6	13. 9	1.7 1

Rafael_TWH 23.5_S13_1	243.5	560	65.4	249.8	54.6	11.72	59.3	9.64	56.2	10.96	26.7	2.86	13.18	1.61
Rafael_TWH 23.5_S13_2	242.7	556	64.5	236.2	49.8	11.07	56.5	8.92	53.3	10.14	25.1	2.62	12.15	1.543
Rafael_TWH 23.5_S13_3	215.1	483	57.3	226.2	50.4	10.76	56.3	8.64	52.7	9.67	24.3	2.57	12.42	1.528
Rafael_TWH 23.5_S14_1	206.9	465	53.9	205.6	44.8	10.6	53.9	8.19	50.9	9.77	23.6	2.58	12.32	1.48
Rafael_TWH 23.5_S14_2	210.4	475	54.4	206.1	45.9	10.9	53.4	8.39	50.5	9.66	23.54	2.565	12.3	1.49
Rafael_TWH 23.5_S14_3	214.8	472	55.9	214	46.2	12.1	58.1	8.8	52.9	10.42	26.4	3.28	13.8	1.44
Raael_TWH 23.5_S15_1	282.8	646	74.3	277.4	57.3	11.6	66.3	10.22	61.4	11.56	28.22	3.02	13.4	1.732
Raael_TWH 23.5_S15_2	279	644	74.3	270.5	55.1	11.11	61.1	9.39	54.9	10.05	24.96	2.64	11.99	1.529
Raael_TWH 23.5_S15_3	293.6	656	77.1	284.1	58.3	11.69	67.2	10.31	61.8	11.67	28.43	2.988	13.3	1.688
Raael_TWH 23.5_S16_1	326	860	103.2	387	79.7	16.15	91.3	13.64	78.8	13.93	32.3	3.3	14.7	1.728
Raael_TWH 23.5_S16_2	325.7	792	95.8	383.6	83.5	16.6	93.1	14.17	81.7	14.7	34.6	3.45	15.12	1.871
Raael_TWH 23.5_S16_3	328.2	808	98	385.4	83.9	16.29	93.4	14.24	83.2	14.92	34.8	3.54	15.28	1.825
Raael_TWH 23.5_S17_1	203.9	509	60.6	236	54.2	11.79	62.7	9.35	52.8	9.54	22.46	2.276	10.12	1.243
Raael_TWH 23.5_S17_2	263.8	651	70.9	264.9	54.6	11.8	62.4	9.51	57.7	10.72	26.04	2.753	12.39	1.533
Raael_TWH 23.5_S17_3	263.7	675	71.2	259.9	52.4	11.2	60.3	9.21	56.5	10.68	25.43	2.753	12.33	1.514
Rafael_TWH 23.5_S18_1	283.8	625	72.5	281.3	58.6	13.39	65.4	10.05	62.1	11.47	28.5	3.04	14.06	1.723
Raael_TWH 23.5_S18_2	260.8	537	64.4	254.3	55.6	12.46	61.4	9.78	59.4	11.11	27.3	2.95	14.27	1.73
Raael_TWH 23.5_S18_3	255.9	573	68.6	253.1	54.7	12.69	58.8	9.03	54.7	10.23	25.16	2.7	13.5	1.579
Raael_TWH 23.5_S19_1	255.6	654	86.6	334	75.6	15.16	78.3	11.9	67.7	11.57	27.6	2.84	13.13	1.559
Raael_TWH 23.5_S19_2	254.4	656	84.8	341	75.6	15.66	80.8	12.19	69.7	12.05	28.2	2.96	14	1.64
Raael_TWH 23.5_S19_3	229.3	644	79.4	313.4	70	14.98	74.4	11.49	66.6	11.96	27.5	2.8	12.87	1.564
Raael_TWH 23.5_S20_1	388	1047	136.2	539	115.9	24.42	119.6	18.08	101.5	17.78	40.4	4.26	19.5	2.33
Raael_TWH 23.5_S20_2	405	1007	132.2	541	116	24.6	118.4	18.17	104.8	17.77	41.3	4.32	19.9	2.34
Raael_TWH 23.5_S20_3	346.5	942	122.2	488	108.9	22.58	114.2	17.38	98.5	16.99	38.6	3.98	17.94	2.109
Raael_TWH 23.5_S20_4	359	1007	125.1	476	103	22.46	112	16.62	94.4	16.43	38.2	3.8	17.86	2.105
Raael_TWH 23.5_S20_5	356	1027	121.9	471	101	22.43	109.2	15.85	90	15.45	35.8	3.66	16.57	1.97

Rafael_TWH 26.35_S22_1	49	146.8	18.88	83.7	21.38	4.43	21.66	3.078	17.1	2.965	7.29	0.807	4.16	0.511
Rafael_TWH 26.35_S22_2	47.7	145.2	18.65	83.1	21	4.36	21.6	2.943	16.59	2.94	7.22	0.771	4.02	0.524
Rafael_TWH 26.35_S23_1	35.3	102.4	11.23	48.5	13.06	3.11	14.41	2.04	11.53	2.049	4.94	0.537	2.77	0.365
Rafael_TWH 26.35_S23_2	28.48	92	10.24	47	13.37	3.08	15.23	2.098	12.06	2.161	5.3	0.578	3.09	0.408
Rafael_TWH 26.35_S23_3	28.64	92.2	10.08	46.8	12.59	2.91	14.01	2.071	11.48	2.067	5.11	0.566	2.95	0.376

Run 4														
Sample ID	La	Ce	Pr	Nd	Sm	Eu	Gd	Tb	Dy	Ho	Er	Tm	Yb	Lu
Rafael_TWH 22.85_S1_1	70.5	174.9	17.39	72.2	17.33	4.38	20.38	3.1	18.7	3.453	8.69	0.975	4.8	0.578
Rafael_TWH 22.85_S1_2	73.5	178.4	18.46	70.1	16.95	3.97	19.63	2.956	18.03	3.359	8.21	0.9	4.41	0.54
Rafael_TWH 22.85_S1_3	68.6	183.6	17.54	66.1	15.43	3.79	18.53	2.891	17.17	3.16	8.01	0.89	4.36	0.523
Rafael_TWH 22.85_S2_1	71.7	204	21.43	85.1	21.1	4.83	22.68	3.339	19.06	3.328	8.14	0.853	4.05	0.502
Rafael_TWH 22.85_S2_2	82.3	219.7	23.65	95.3	22.68	5.07	24.26	3.6	20.98	3.63	8.61	0.916	4.28	0.501
Rafael_TWH 22.85_S2_3	76.3	227.9	21.95	88.3	20.64	4.75	22.22	3.25	19.17	3.4	8.34	0.881	4.11	0.507
Rafael_TWH 22.85_S3_1	65.2	192	18.86	72	17.47	4.32	20.18	3.07	17.79	3.322	8.21	0.889	4.35	0.537
Rafael_TWH 22.85_S3_2	71.4	194.5	19.95	79	19.81	4.6	21.73	3.332	19.9	3.658	9.19	1.02	5.08	0.615
Rafael_TWH 22.85_S3_3	69.5	187.2	19.47	75.9	18.47	4.59	20.81	3.199	19.26	3.517	8.82	0.982	4.92	0.601
Rafael_TWH 22.85_S4_1	67.8	181.5	19.36	78.7	19.04	4.67	21.82	3.25	19.27	3.54	8.59	0.906	4.42	0.539
Rafael_TWH 22.85_S4_2	66.3	190.6	19.64	76	18.67	4.36	20.97	3.138	18.65	3.345	8.28	0.884	4.26	0.526
Rafael_TWH 22.85_S4_3	74.7	197.7	21.73	84.1	19.75	4.37	21.89	3.247	18.45	3.35	8.17	0.872	4.11	0.508
Rafael_TWH 22.85_S5_1	78.8	207.5	20.71	83.9	20.63	4.79	22.7	3.51	20.98	3.75	9.09	1.019	4.94	0.596
Rafael_TWH 22.85_S5_2	78.1	212.5	20.68	82.6	20.13	4.85	23.23	3.472	20.28	3.62	8.98	0.998	4.88	0.594
Rafael_TWH 22.85_S5_3	70.6	190.2	19.35	74	17.99	4.66	21.09	3.198	19.14	3.61	9.01	0.999	4.94	0.587
Rafael_TWH 22.85_S6_1	78.3	219.1	22.15	88.2	21.38	5.8	57.9	3.757	21.88	4.055	9.65	1.032	4.53	0.566
Rafael_TWH 22.85_S6_2	71.4	208.5	21	82.3	19.81	4.57	22.4	3.32	20.35	3.559	8.69	0.946	4.52	0.525
Rafael_TWH 22.85_S6_3	70.6	195.1	20.94	85.1	19.76	4.83	23.19	3.3	19.73	3.57	8.79	0.948	4.62	0.54

Rafael_TWH 22.85_S7_1	75.8	205.4	18.98	73.2	17.24	4.39	20.02	3.06	18.37	3.41	8.73	0.945	4.59	0.555
Rafael_TWH 22.85_S7_2	76.4	210.8	20.16	74.7	17.35	4.45	20.19	2.96	18.35	3.45	8.36	0.936	4.37	0.555
Rafael_TWH 22.85_S7_3	72.2	190.3	19.14	74.5	17.52	4.32	20.29	3.006	18.26	3.365	8.43	0.915	4.51	0.554
Rafael_TWH 22.85_S8_1	79.3	218.7	21.81	85.2	19.4	4.39	21.48	3.085	18.27	3.33	8.02	0.879	4.31	0.511
Rafael_TWH 22.85_S8_2	73.7	194.2	20.57	81.2	19.2	4.44	21.4	3.273	19.26	3.461	8.54	0.943	4.61	0.569
Rafael_TWH 22.85_S8_3	75	191.8	20.61	81.1	19.16	4.37	21.32	3.233	19.14	3.468	8.28	0.888	4.35	0.51
Rafael_TWH 22.85_S9_1	76.8	214.8	22.7	88.7	21.86	4.83	23.16	3.473	20.16	3.72	9.3	1.013	4.98	0.622
Rafael_TWH 22.85_S9_2	75	216.6	22.66	87.6	20.36	4.42	23.15	3.471	20.55	3.73	9.07	0.997	4.65	0.577
Rafael_TWH 22.85_S9_3	79.7	213.7	23.09	88.5	21.24	4.73	23.84	3.611	21.13	3.845	9.29	1.004	4.77	0.603
Rafael_TWH 22.85_S10_1	71	207.9	20.96	83.6	20.13	4.72	22.36	3.314	18.88	3.393	8.26	0.892	4.36	0.532
Rafael_TWH 22.85_S10_2	67.6	188.3	20	78.6	19.68	4.59	22.12	3.316	19.46	3.52	8.58	0.939	4.55	0.553
Rafael_TWH 22.85_S10_3	68.8	152	18.65	80.9	20.35	4.85	23.73	3.615	21.88	3.998	9.7	1.06	5.17	0.645
Rafael_TWH 22.85_S11_1	73.1	203.5	19.29	74.4	17.73	4.08	20.66	3.046	18.1	3.328	8.08	0.864	3.96	0.487
Rafael_TWH 22.85_S11_2	68.5	181.6	18.24	71.6	17.4	3.87	19.72	3.032	18.08	3.313	8.08	0.864	4	0.505
Rafael_TWH 22.85_S11_3	65.6	172.6	17.35	69.8	16.39	3.97	19.9	2.93	17.43	3.241	8.07	0.851	4.12	0.497
Rafael_TWH 22.85_S12_1	83	208.7	21.93	87.8	20.54	4.87	23.85	3.39	20.22	3.676	9.18	0.996	4.76	0.604
Rafael_TWH 22.85_S12_2	78.2	223.7	22	86	19.74	4.85	20.96	3.11	17.85	3.23	8.05	0.894	4.41	0.528
Rafael_TWH 22.85_S12_3	80.9	213.2	22.4	85.7	20.37	4.61	21.77	3.174	18.27	3.313	8.05	0.863	4.19	0.496
Rafael_TWH 22.85_S13_1	81.6	215.8	23.97	93.4	22.62	4.37	24.17	3.628	21.16	3.854	9.19	0.988	4.35	0.535
Rafael_TWH 22.85_S13_2	83.5	212.2	23.52	95.8	22.35	4.51	23.97	3.65	21.07	3.9	9.45	1.027	4.62	0.58
Rafael_TWH 22.85_S13_3	80.5	225.1	23.59	90.5	21.3	4.43	24.15	3.478	20.27	3.653	8.73	0.908	4.12	0.502
Rafael_TWH 22.85_S14_1	75.5	193.4	20.93	83.8	20.44	4.26	22.6	3.38	19.98	3.64	8.93	1.014	5.1	0.623
Rafael_TWH 22.85_S14_2	71.1	190.6	19.94	80	19.8	4.2	21.94	3.22	19.01	3.29	8.08	0.834	3.7	0.442
Rafael_TWH 22.85_S14_3	73.6	197	19.82	78.1	19	4.17	21.2	3.24	18.41	3.4	7.93	0.846	3.87	0.482
Rafael_TWH 22.85_S15_1	77.4	222.4	23.13	88.3	20.82	4.96	22.82	3.448	20.03	3.61	9.15	1.049	5.2	0.649
Rafael_TWH 22.85_S15_2	73.2	201.2	21.42	85.2	19.56	4.94	22.04	3.304	19.95	3.551	8.91	0.946	4.81	0.601

Rafael_TWH 22.85_S15_3	74.3	212.2	21.52	83.4	20.28	4.89	22.29	3.318	18.97	3.44	8.4	0.908	4.49	0.548
Rafael_TWH 22.85_S16_1	61.7	142.4	14.34	57.1	14.16	3.09	17.08	2.593	15.4	2.92	7.24	0.781	3.53	0.442
Rafael_TWH 22.85_S16_2	61.3	154.7	14.75	56.6	14.41	3.36	17.26	2.594	15.81	3.002	7.51	0.821	3.83	0.47
Rafael_TWH 22.85_S16_3	63	151.2	14.63	59.1	13.79	3.46	17.56	2.645	16.35	2.975	7.56	0.833	3.98	0.475
Rafael_TWH 22.85_S17_1	84.9	207.8	21.98	90.8	21.02	4.62	24.05	3.66	21.43	3.74	9.28	0.961	4.31	0.528
Rafael_TWH 22.85_S17_2	90.1	220.4	23.52	93.4	22.97	4.93	25.37	3.795	21.85	3.93	9.33	0.965	4.44	0.53
Rafael_TWH 22.85_S17_3	88.6	200.8	22.67	94.7	22.59	5.18	26.07	3.85	21.99	3.99	9.31	0.954	4.52	0.545
Rafael_TWH 22.85_S18_1	59.7	169.3	17.34	67.6	16.73	3.85	17.92	2.72	16.33	2.98	7.48	0.815	3.92	0.475
Rafael_TWH 22.85_S18_2	59.6	164.4	15.95	66.8	16.55	4.01	19.4	2.9	16.51	2.97	7.67	0.815	3.99	0.468
Rafael_TWH 22.85_S18_3	58.7	168.4	17.12	64.9	16.11	3.93	18.27	2.741	16.28	2.95	7.22	0.818	4.06	0.506
Rafael_TWH 22.85_S19_1	71.5	187.7	17.18	65.3	15.02	3.37	18.2	2.614	16.13	3.013	7.47	0.852	3.98	0.5
Rafael_TWH 22.85_S19_2	66.3	170	16.41	62.3	14.99	5.34	68	2.738	16.27	3.049	7.6	0.838	3.7	0.47
Rafael_TWH 22.85_S19_3	64.3	159.1	15.63	61.4	14.97	4.55	42.8	2.77	16.76	3.081	7.83	0.838	3.74	0.481
Rafael_TWH 22.85_S20_1	73.1	217.4	22.37	87.2	20.76	4.98	21.54	3.14	18.13	3.22	7.97	0.908	4.77	0.578
Rafael_TWH 22.85_S20_2	63	179.8	19.61	77.3	18.59	4.6	20.67	3.111	18.26	3.334	8.07	0.918	4.53	0.547
Rafael_TWH 22.85_S20_3	60.8	158.7	18.06	74.9	18.82	4.42	20.46	3.058	18.09	3.28	8.07	0.896	4.53	0.543
Rafael_TWH 22.85_S21_1	71.6	193.3	19.33	75.1	18.47	3.78	20.21	3.02	17.93	3.196	7.66	0.792	3.34	0.42
Rafael_TWH 22.85_S21_2	72.1	209.5	19.99	77.6	18.17	3.83	21.23	3.189	18.63	3.296	7.74	0.805	3.52	0.424
Rafael_TWH 22.85_S21_3	71.5	203.9	22.2	89.9	23.1	5.28	34.9	4.05	25.4	4.47	10.68	1.144	5.15	0.664
Rafael_TWH 22.85_S21_4	71.6	215.9	25.8	108.9	28.39	6.75	49.8	5.04	31.85	5.57	13.63	1.497	7.14	0.874
Rafael_TWH_20_S1_1	412	1486	164.1	636	150.3	34.6	169.6	26.26	151.4	26.27	59.1	5.98	26.57	3.058
Rafael_TWH_20_S1_2	441	1443	167.7	651	155.9	33.89	180.3	27.75	159.6	27.63	62.8	6.35	28.22	3.206
Rafael_TWH_20_S1_3	440	1463	165.3	661	152.8	34.34	175.4	27.5	157.3	27.56	63.3	6.23	27.7	3.158
Rafael_TWH_20_S2_1	438.1	1422	188.7	797	194	42.92	213.4	32.97	188	32.19	73.1	7.25	32.26	3.703
Rafael_TWH_20_S2_2	445	1573	195.2	785	195.3	43.4	209	32.35	184.5	31.01	70.7	7.05	31.03	3.554
Rafael_TWH_20_S2_3	457	1598	203.9	792	192.9	43.6	215.2	33.1	186.7	31.35	71.8	7.14	31.95	3.69

Rafael_TWH_20_S3_1	328	1237	153.3	638	154.3	34.9	166.3	25.06	140.3	23.36	51.4	4.91	21.17	2.452
Rafael_TWH 20_S3_2	288	1009	138.2	532	129.8	28.9	141.8	21.13	119.1	19.28	43.1	4.16	17.98	2.061
Rafael_TWH 20_S3_3	355	1347	173.1	690	164.7	37.8	178.7	27.3	149.8	24.52	54.4	5.18	22.12	2.571
Rafael_TWH 20_S4_1	337.3	1243	159	631	153.8	34.8	163.5	25.82	141.6	24.07	53.8	5.36	23.8	2.729
Rafael_TWH 20_S4_2	307.3	1120	146.5	587	147.6	32.5	162.1	24.44	136.4	22.75	50.7	5	22.05	2.54
Rafael_TWH 20_S4_3	285.9	1047	131	529	132.9	29.4	148.5	23.04	129.1	21.75	49.1	4.87	21.36	2.469
Rafael_TWH 20_S5_1	366	1327	171	714	182.5	40.2	202.8	32.82	186.4	31.5	70.4	7.35	35.2	4.31
Rafael_TWH 20_S5_2	358	1330	174.8	715	176.4	38.7	192.2	29.34	164.5	27.37	60.8	5.94	25.6	2.924
Rafael_TWH 20_S5_3	365.9	1370	174.6	725	178.3	39.5	192.4	29.74	167.3	27.63	61.5	6	26.37	3.015
Rafael_TWH 20_S6_1	333.7	1153	142.3	584	140.2	33.9	152	24.7	140.1	24.29	54.8	5.48	24.3	2.72
Rafael_TWH 20_S6_2	321.6	1180	142	585	142.2	32.9	153.5	23.82	135	22.68	50.7	5.09	22.28	2.57
Rafael_TWH 20_S6_3	308.8	1108	136.5	544	134.8	30.9	147.9	23	129.6	22.22	48.9	4.77	21.46	2.42
Rafael_TWH 20_S7_1	320.9	1141	136.7	555	134.3	30.56	145.8	22.21	125.2	21.28	47.3	4.79	21.25	2.412
Rafael_TWH 20_S7_2	289	980	122	505	120.6	27.9	130.3	19.9	114	19.01	43	4.19	19.36	2.17
Rafael_TWH 20_S8_1	361	1402	175.3	714	171.9	37	178.9	27.06	151	25.23	57.4	5.61	25.18	2.82
Rafael_TWH 20_S8_2	394	1397	184.5	748	185.7	39.7	188.7	28.75	161.8	26.55	60.2	5.85	26.46	3.008
Rafael_TWH 20_S8_3	341	1404	173	700	178.3	38.3	190.2	28.89	158.8	26	56.3	5.43	23.5	2.675
Rafael_TWH 20_S9_1	471	1590	198	796	181.4	38.5	185.7	27.77	151.6	25.12	56.5	5.52	24.58	2.798
Rafael_TWH 20_S9_2	348.9	1221	157.4	653	161.9	35.15	173	26.42	148.4	24.65	55.1	5.48	24.52	2.825
Rafael_TWH 20_S9_3	337.1	1210	153.4	675	152.4	33.7	164	25.15	141.4	23.66	52.4	5.1	22.86	2.597
Rafael_TWH 20_S10_1	288	719	91.2	401.8	103.6	21.92	119.6	18.39	106.8	18.52	42.86	4.35	19.01	2.243
Rafael_TWH 20_S10_2	321	728	95.6	426	108.8	22.32	127.5	19.3	111.3	19.67	45.6	4.72	20.87	2.409
Rafael_TWH 20_S10_3	358.4	629	97.2	505	138.6	23.79	178.9	27.8	162.6	28.7	66.4	6.74	28.6	3.56
Rafael_TWH 20_S11_1	378	1397	175.3	706	170.7	37.1	182.4	27.63	155.7	25.67	58.1	5.82	26.2	2.918
Rafael_TWH 20_S11_2	392	1435	177.9	710	171.9	37.2	178.7	27.31	158.2	26.53	60.3	6.17	28.1	3.22
Rafael_TWH 20_S11_3	387	1446	175.3	703	169.6	38	182	27.88	156.2	26.19	58.3	5.78	26.12	2.958

Rafael_TWH 20_S12_1	381	1484	194.7	786	190.9	38.9	199	29.66	161.8	26.3	58.4	5.74	25.09	3
Rafael_TWH 20_S12_2	389	1547	200.5	819	197.6	41.5	206.2	31.78	173.8	28.48	63	6.11	26.68	3.06
Rafael_TWH 20_S12_3	380	1474	189.5	772	187.1	39.7	193.6	28.96	162.2	26.49	58.2	5.8	25.09	2.93
Rafael_TWH 20_S13_1	432	1592	193.7	772	184.3	41.8	204.3	31.07	173.5	29.06	65.2	6.43	28.56	3.361
Rafael_TWH 20_S13_2	367	1462	173.5	689	170.4	38	181.6	27.6	154.5	25.7	56	5.53	24.37	2.849
Rafael_TWH 20_S13_3	374	1470	181.6	717	175.9	37.9	190.8	28.03	154	25.43	55.9	5.34	22.81	2.689
Rafael_TWH 20_S14_1	312.9	1163	150.2	607	148.4	30.87	158.1	24.1	132.2	21.8	47.4	4.6	19.73	2.3
Rafael_TWH 20_S14_2	306.5	1133	144.2	576	145.8	29.8	156	24.2	131.2	21.85	48.1	4.59	19.66	2.304
Rafael_TWH 20_S14_3	324.4	1234	150.5	606	146.2	32.3	161.7	24.29	133.6	22.33	49.6	4.86	20.73	2.408
Rafael_TWH 20_S15_1	319.4	1175	156.3	648	159.8	36.1	172.5	26.9	145.9	23.75	52.5	4.96	21.91	2.459
Rafael_TWH 20_S15_2	272.3	1099	143.5	602	154.4	34.91	161	24.71	136.5	21.69	46.05	4.317	18.14	2.068
Rafael_TWH 20_S15_3	255.7	1031	138.2	561	145.6	33	155.1	23.53	126.5	20.47	41.9	3.88	16.79	1.855
Rafael_TWH 20_S16_1	303	1100	141.2	581	143.3	30.41	152.6	23.18	127.3	20.77	45.8	4.33	19.13	2.208
Rafael_TWH 20_S16_2	264	937	118.7	504	124.6	27.74	140.5	21.17	115.7	19.31	42	3.98	17.28	1.987
Rafael_TWH 20_S16_3	260	954	124.3	529	132.5	28.99	142.4	21.82	119.2	19.72	42.5	3.96	16.69	1.921
Rafael_TWH 20_S17_1	353.4	1231	148.6	578	142.9	32.78	160.4	24.72	141	23.87	53.9	5.38	23.58	2.769
Rafael_TWH 20_S17_2	342	1211	145.4	565	143.4	33.25	155	23.78	136.5	23.22	52.8	5.33	23.64	2.691
Rafael_TWH 20_S17_3	362	1242	150.3	582	142.8	33.7	158.1	24.96	142.5	24.29	55.6	5.54	24.93	2.86
Rafael_TWH 20_S18_1	225	881	114.5	481	121.3	26.04	131.2	19.22	105.4	16.59	34.67	3.165	13.54	1.544
Rafael_TWH 20_S18_2	231.3	957	120.9	500	123.4	26.48	131.8	19.28	104.5	16.39	33.85	3.025	12.83	1.466
Rafael_TWH 20_S18_3	230.9	895	114.5	488	121	26.09	126.7	19.1	100.6	16.15	34.6	3.17	13.74	1.553
Rafael_TWH 20_S19_1	331.1	1176	138.6	562	135.2	32.6	148.8	23.53	134.8	22.69	51.6	5.21	22.85	2.648
Rafael_TWH 20_S19_2	313	1155	131.8	534	127.7	30.25	141.8	22.59	130	21.78	50.6	5.06	22.5	2.633
Rafael_TWH 20_S19_3	306	1142	134	521	128.4	30.6	143	22.29	126.9	21.52	49.4	4.99	22.32	2.58
Rafael_TWH 20_S20_1	218.5	920	120.3	502	127.2	28.18	137.7	19.95	110.4	17.39	36.5	3.37	14.24	1.629
Rafael_TWH 20_S20_2	241.6	994	124	509	130.3	29.42	140.7	21.12	115.3	18.61	39.1	3.62	15.21	1.725

Rafael_TWH 20_S20_3	239 .5	955	122 .1	502	125 .9	28. 44	137 .6	20. 1	112 .5	17. 94	37. 5	3.4 13	14. 68	1.6 76
Rafael_TWH 20_S21_1	289 .6	109 4	130 .9	531	128 .6	27. 97	134 .7	20. 67	115 .3	19. 11	42. 1	4.1 4	18. 25	2.0 84
Rafael_TWH 20_S21_2	268	107 9	123	510	125	27. 2	136 .2	20. 65	113 .2	18. 21	38. 9	3.7 5	16. 53	1.8 74
Rafael_TWH 20_S21_3	308 .3	113 8	139 .3	554	137	30. 33	150 .7	22. 58	127 .2	21. 45	47. 9	4.6 9	20. 19	2.3 56
Rafael_TWH 18.5_S1_1	247 .2	123 4	226 .6	103 6	286 .6	57	272 .1	37. 62	183 .4	26. 52	51. 1	4.1 5	17. 15	1.9 26
Rafael_TWH 18.5_S1_2	255 .3	119 9	229 .4	106 3	293 .8	58. 4	277 .1	38. 32	186 .7	26. 83	52. 8	4.3 1	17. 62	2.0 18
Rafael_TWH 18.5_S1_3	271 .1	122 9	225 .9	106 4	287 .2	58. 4	267 .4	37. 4	181	26. 23	51. 5	4.3 28	18. 05	1.9 96
Rafael_TWH 18.5_S2_1	280 .7	125 4	234 .8	105 9	289	58. 8	275 .5	38. 57	190 .1	27. 45	54. 2	4.5 2	18. 82	2.1 22
Rafael_TWH 18.5_S2_2	281	124 7	227 .5	104 9	289 .9	60. 5	272	38. 47	190 .1	27. 38	53. 8	4.4 6	18. 8	2.0 95
Rafael_TWH 18.5_S2_3	310 .1	130 3	235 .8	108 7	294 .5	61. 8	270 .4	38. 42	191 .2	28. 03	56. 5	4.8 1	20. 33	2.2 62
Rafael_TWH 18.5_S3_1	213 .5	102 0	192 .6	933	259 .4	52. 8	242 .8	33. 91	162 .9	23. 3	43. 7	3.4 48	14. 26	1.5 9
Rafael_TWH 18.5_S3_2	220	107 1	198 .4	943	261 .8	54. 4	245 .9	34. 29	167 .2	23. 18	43. 6	3.4 3	14. 13	1.5 97
Rafael_TWH 18.5_S3_3	217 .2	109 4	203	958	261 .8	54. 5	248 .5	34. 57	165 .8	23. 86	45. 1	3.6 2	14. 53	1.6 37
Rafael_TWH 18.5_S4_1	402	185 9	299	126 3	322	66. 6	304 .1	43. 4	217 .4	32. 75	66	5.7 3	23. 55	2.7 1
Rafael_TWH 18.5_S4_2	439	191 0	305	132 6	348 .3	70. 5	329 .1	48. 3	242 .8	36. 9	74	6.5 7	27. 1	3.0 7
Rafael_TWH 18.5_S4_3	382	164 8	275 .6	120 2	317 .7	64	305 .2	43. 6	217 .8	32. 77	65. 3	5.6 3	23. 22	2.6 06
Rafael_TWH 18.5_S5_1	165 .9	891	164 .4	806	220 .1	41. 5	205 .5	28. 82	138 .6	19. 44	34. 7	2.5 59	9.9 6	1.1 58
Rafael_TWH 18.5_S5_2	163 .9	901	161 .6	773	212 .9	40. 1	204 .3	28. 1	135 .6	19	34. 13	2.5 31	9.7 1	1.1 34
Rafael_TWH 18.5_S5_3	162 .6	921	163 .4	781	207 .9	40. 58	199 .8	27. 66	133 .9	18. 48	33. 35	2.4 39	9.4 6	1.1 17
Rafael_TWH 18.5_S6_1	429	182 4	296 .1	129 3	336 .8	66. 3	322	46. 4	232 .6	34. 74	70. 3	6.1 6	25. 78	2.8 45
Rafael_TWH 18.5_S6_2	453	193 2	312	131 3	339 .5	68. 7	322 .1	46. 2	237	35. 73	72. 8	6.4	26. 8	3.0 06
Rafael_TWH 18.5_S6_3	406	179 9	284 .2	124 4	321 .8	64. 8	303 .7	44. 7	221 .4	33. 28	66. 7	5.8 4	24. 21	2.7 71
Rafael_TWH 18.5_S7_1	192 .9	922	199 .2	108 6	306 .9	55. 6	290	39. 61	187 .3	26. 04	48. 1	3.7 11	15. 09	1.7 83
Rafael_TWH 18.5_S7_2	173	105 0	211 .9	999	289 .2	53. 4	260 .7	35. 1	165 .2	23. 38	42. 1	3.2	12. 8	1.4 87
Rafael_TWH 18.5_S7_3	175 .5	960	200	101 6	298 .5	55. 2	273 .8	37. 38	176 .9	24. 26	44. 4	3.3 82	13. 35	1.5 45
Rafael_TWH 18.5_S8_1	269	129 6	199 .1	870	225 .5	46. 9	214 .4	30. 18	148	21. 26	41. 3	3.3 5	13. 56	1.5 2

Rafael_TWH 18.5_S8_2	308.1	1380	217.1	978	248.5	51.5	239.5	34.33	169.6	25.14	49.3	4.04	16.74	1.8 51
Rafael_TWH 18.5_S8_3	262.1	1211	194.7	864	218.6	46.5	215.9	30.49	148.8	21.55	41.5	3.29	13.18	1.5 06
Rafael_TWH 18.5_S9_1	408	1706	278.3	1185	312	63.9	296.7	43.4	219.6	33.1	68	5.9	24.4	2.7 04
Rafael_TWH 18.5_S9_2	327	1516	245.2	1051	274.8	57.5	268.8	37.62	189.2	27.75	54.5	4.55	18.99	2.0 87
Rafael_TWH 18.5_S9_3	309.5	1454	231.4	972	256.9	55.2	251.6	35.92	176.7	25.68	51	4.19	17.16	1.8 83
Rafael_TWH 18.5_S10_1	353.7	1569	265.6	1204	315.8	64.4	294.8	41.7	208.7	30.98	61.4	5.3	21.97	2.4 32
Rafael_TWH 18.5_S10_2	400.3	1641	283.4	1333	353.7	70.1	332.3	47.59	238.2	34.49	70.8	6.07	25.19	2.8 45
Rafael_TWH 18.5_10_3	370	1634	268.5	1246	328.7	68	306.7	44.2	218.5	32.87	67.8	6.15	28.3	3.4 3
Rafael_TWH 18.5_S10_1	240.2	1237	237.4	1085	301.6	59.9	290.2	40.28	191.4	26.92	49.9	3.96	15.62	1.7 77
Rafael_TWH 18.5_S11_2	215.3	1116	210.6	1025	290	56.4	267.8	37.1	175.6	24.63	45.9	3.58	14.48	1.6 38
Rafael_TWH 18.5_S11_3	210.2	1075	210.1	1016	287.1	57.6	264.2	37.3	176.4	24.7	45.6	3.48	13.75	1.5 99

Run 5														
Sample ID	La	Ce	Pr	Nd	Sm	Eu	Gd	Tb	Dy	Ho	Er	Tm	Yb	Lu
Rafael_TWH 16.5_S1_1	568	1965	274.1	1218	296.7	67.5	296.3	47	248.3	40.6	88.4	8.39	36.9	3.9 4
Rafael_TWH 16.5_S1_2	600	2041	285.6	1232	291.3	67.2	318.6	47.2	250.6	41.6	90.7	8.65	36.5	3.9 8
Rafael_TWH 16.5_S1_3	553	2037	285.8	1211	279.2	67.4	316.4	46.5	245.9	41.3	90.8	8.55	37.3	3.9 9
Rafael_TWH 16.5_S2_1	362.3	1393	202.1	889	210.7	50.9	238.5	32.57	163.6	25.2	49.3	4.24	16.88	1.8 9
Rafael_TWH 16.5_S2_2	393.1	1456	212.6	933	221.8	51.5	254.4	34.41	176.1	27.57	55.8	4.91	19.76	2.1 8
Rafael_TWH 16.5_S2_3	392.2	1472	218.8	935	223.9	53.7	251.3	35.2	182.5	28.67	58.1	5.18	20.4	2.3 3
Rafael_TWH 16.5_S3_1	448.6	1396	219.3	1016	254.2	57.4	284.8	41.9	221.3	35.6	74.6	6.94	28.3	3.1 5
Rafael_TWH 16.5_S3_2	423	1570	223.4	1001	234.4	53.2	268.9	37.6	201	32.2	67.3	6.21	25.64	2.8 11
Rafael_TWH 16.5_S3_3	402	1610	221.3	972	227.9	52	253.4	35.67	189.7	29.85	62.4	5.74	23.96	2.5 83
Rafael_TWH 16.5_S4_1	441	1692	228.4	923	220.3	48.6	240.1	35.3	189.3	30.5	65.8	6.24	26.2	2.8 4
Rafael_TWH 16.5_S4_2	549	1941	253.5	1037	241.8	57.5	268	40.7	227.5	38.7	86.8	8.74	37.8	4.1 1
Rafael_TWH 16.5_S4_3	540	1908	252.1	984	226.2	55.3	259	38.6	215.8	36.9	82	8.12	34.9	3.7 5

Rafael_TWH 16.5_S5_1	493	1633	246.9	1094	254.2	58.9	299.8	42.75	226.7	36.4	77.4	7.38	31	3.38
Rafael_TWH 16.5_S5_2	517	1823	264	1132	267.7	59.8	290.6	43.9	236.7	37.9	81.6	7.68	31.8	3.49
Rafael_TWH 16.5_S5_3	522	1839	263.3	1151	270.8	61.1	298.4	44	235	38.8	83.7	7.86	33.1	3.6
Rafael_TWH 16.5_S6_1	609	2192	341.1	1426	340.5	73.3	360	53.2	278.9	45.2	100	9.65	41.7	4.53
Rafael_TWH 16.5_S6_2	624	2385	354	1528	358	78.1	370	54.5	286.4	46.9	102.3	9.99	43.2	4.72
Rafael_TWH 16.5_S6_3	590	2266	341	1393	326.5	70.3	345	50.5	268.3	43.2	93.6	9.03	38.6	4.19
Rafael_TWH 16.5_S7_1	478.8	1600	274.5	1283	313.1	71.5	342.4	45.39	233.8	35.9	74.7	6.84	28.86	3.227
Rafael_TWH 16.5_S7_2	481	1558	271.3	1293	330.3	75.4	353.8	47	239.3	37.1	77.4	7.07	30.22	3.329
Rafael_TWH 16.5_S7_3	456	1878	288.6	1213	283.1	67.5	292	40.2	198.9	30.62	64.7	5.83	24.51	2.679
Rafael_TWH 16.5_S8_1	471	1527	219.2	949	227.1	53.2	250.8	38	207.2	34.4	73.8	7.15	30.8	3.36
Rafael_TWH 16.5_S8_2	467	1655	224.5	971	229.7	54.2	250.8	38.41	211.9	34.8	75.6	7.4	32	3.46
Rafael_TWH 16.5_S8_3	492	1699	229.7	991	230.7	54.6	249.2	39.7	214.2	36.02	80.4	7.69	33.1	3.63
Rafael_TWH 16.5_S9_1	502	1846	261.9	1077	254.8	59.6	287.3	40.6	215.9	35.1	75.7	7.13	29.8	3.29
Rafael_TWH 16.5_S9_2	509	1811	262.6	1055	248.9	57.7	283.9	40.1	213.8	34.96	77.1	7.25	30.69	3.44
Rafael_TWH 16.5_S9_3	454.2	1465	226.3	1033	253.9	59.5	281.3	39.92	213.7	33.85	71.8	6.57	28.19	3.073
Rafael_TWH 16.5_S10_2	414.9	1233	217.2	1021	254.1	52.25	282.6	41.39	218.1	34.78	73.7	6.91	28.76	3.341
Rafael_TWH 16.5_S10_3	420.7	1435	227.9	989	242.5	51	271.7	39.33	209.5	33.85	72.2	6.82	28.53	3.268
Rafael_TWH 16.5_S11_1	476	1340	221	1040	270.9	58.3	288.9	44.8	240.9	37.8	79.2	7.35	30.9	3.37
Rafael_TWH 16.5_S11_2	452	1304	212.8	1025	257.6	58.9	288.7	42.18	227.9	36.21	76.4	7.03	29.91	3.255
Rafael_TWH 16.5_S11_3	459.5	1595	234.7	1036	249.6	57.6	276.9	40.2	215.1	35.31	76	7.13	29.5	3.24
Rafael_TWH 16.5_S12_1	488	1659	243.2	1043	254	59.2	267.7	40.41	218.5	34.75	76.2	7.2	30.69	3.36
Rafael_TWH 16.5_S12_2	539.6	1712	251.5	1115	265.7	64.6	313.6	44.48	242.3	40.08	88	8.49	36.33	4.019
Rafael_TWH 16.5_S12_3	559	1708	259.1	1176	283.3	66.4	332.1	48	263	43.3	94.9	9.15	39.3	4.37
Rafael_TWH 16.5_S13_1	492	1802	273	1235	288.3	65.2	303	41.8	220	33.8	71.6	6.4	27.27	3.01
Rafael_TWH 16.5_S13_2	482.3	1423	241	1143	282.7	66.1	315.7	43.75	228.9	36.74	78.4	7.3	30.82	3.415
Rafael_TWH 16.5_S13_3	497	1803	272.3	1183	286.1	63.1	305.9	42.8	223.4	35.8	76.4	7.19	31.2	3.47

Rafael_TWH 17.5_S1_1	153 .8	48 3	54. 8	214 .6	50. 1	11. 39	64. 2	8.4 3	48. 9	8.7 1	20. 61	2.2 03	10. 37	1.2 39
Rafael_TWH 17.5_S1_2	142 .2	48 6	53. 4	206 .5	47	10. 79	61. 6	7.8 2	45. 4	8.0 7	19. 17	2.0 31	9.7 1	1.1 42
Rafael_TWH 17.5_S1_3	128 .4	39 8	46. 8	183 .6	43. 2	10. 46	61. 2	7.3 4	42. 6	7.5 4	18. 07	1.9 39	9.5	1.1 16
Rafael_TWH 17.5_S2_1	170 .5	53 6	58. 9	228 .7	51. 7	11. 54	73. 1	8.4 1	49. 7	8.9	21. 46	2.3 49	11. 68	1.4 19
Rafael_TWH 17.5_S2_2	170 .4	59 3	63. 1	227 .8	52. 6	11. 42	76. 2	8.6 3	51. 5	9.0 7	22. 11	2.3 48	11. 13	1.3 15
Rafael_TWH 17.5_S2_3	155 .2	53 7	57	220 .7	49. 7	11. 04	67. 6	8.5 1	49. 1	8.9	21. 05	2.2 38	10. 53	1.2 66
Rafael_TWH 17.5_S3_1	148 .6	46 1	51. 5	208 .6	46. 5	10. 48	57. 3	8.0 2	47. 6	8.4 3	20. 82	2.2 84	11. 2	1.3 29
Rafael_TWH 17.5_S3_2	139 .6	45 4	49. 9	193 .4	44. 8	10. 22	55	7.5 4	44. 3	7.9	19. 29	2.0 91	10. 05	1.2
Rafael_TWH 17.5_S3_3	127 .6	44 9	47. 4	182 .8	41. 8	9.8 6	57. 1	7.2 1	42. 3	7.7	18. 77	2.0 03	9.8 1	1.1 51
Rafael_TWH 17.5_S4_1	191 .5	80 5	93. 8	362	87	15. 52	99. 1	12. 2	66. 5	11. 26	25. 82	2.5 32	10. 91	1.3 03
Rafael_TWH 17.5_S4_2	193 .9	80 2	96. 4	370	83	15. 36	99. 4	12. 41	67. 1	11. 31	25. 79	2.5 9	11. 41	1.3 31
Rafael_TWH 17.5_S4_3	202 .6	72 4	91. 6	385 .2	90. 7	17. 39	111 .3	13. 64	75. 5	12. 64	29. 48	2.9 6	13. 08	1.5 19
Rafael_TWH 17.5_S5_1	202 .1	67 0	73. 2	280	62. 6	14. 1	85. 8	10. 06	58. 3	10. 08	24. 2	2.5 2	11. 6	1.3 79
Rafael_TWH 17.5_S5_2	211	70 7	76. 9	281	63. 8	14. 54	86. 2	10. 3	59. 7	10. 48	24. 8	2.5 4	11. 75	1.3 93
Rafael_TWH 17.5_S5_3	214	67 9	74. 4	293	65. 4	14. 27	85. 5	10. 31	57. 2	9.8 5	23. 83	2.4 16	11. 13	1.3 39
Rafael_TWH 17.5_S6_1	153 .2	49 8	52. 8	194 .6	42. 4	10. 17	58. 5	7.4	42. 7	7.5 9	18. 73	1.9 75	9.2 8	1.1 04
Rafael_TWH 17.5_S6_2	145 .9	46 3	49. 6	186 .2	42. 6	10. 02	55. 2	7.3 3	43. 1	7.8 3	18. 9	2.0 69	10. 11	1.2 07
Rafael_TWH 17.5_S6_3	158 .8	48 1	51. 7	200 .4	45. 8	10. 53	60. 3	7.7 8	44. 9	8.0 3	20. 14	2.2 2	10. 86	1.2 86
Rafael_TWH17.5_ S6_4	157 .8	47 5	52. 8	199 .9	45. 9	10. 48	59. 6	7.8 9	45. 5	8.1 8	20. 19	2.1 91	11. 04	1.3 47
Rafael_TWH 17.5_S6_5	164 .4	48 6	53	207 .3	47	10. 91	61	7.8 7	47. 4	8.5 6	20. 66	2.2 16	10. 93	1.3 17

Run 6														
Sample ID	La	Ce	Pr	Nd	Sm	Eu	Gd	Tb	Dy	Ho	Er	Tm	Yb	Lu
Rafael_TWH 17.5_S7_1	189 .6	606	64. 6	250 .9	56. 4	12. 34	60. 1	9.2 1	54	9.7	22. 98	2.4 16	11. 68	1.3 83
Rafael_TWH 17.5_S7_2	193	655	68. 5	246 .9	53. 4	11. 96	56. 7	8.6 9	50. 7	8.9	21	2.2 18	10. 62	1.2 89
Rafael_TWH 17.5_S7_3	183 .1	601	62	232 .5	49. 8	10. 99	54. 5	8.3 1	48. 7	8.7 4	21. 01	2.1 62	10. 16	1.2 25
Rafael_TWH 17.5_S8_1	188	604	65. 6	248 .4	54	12. 36	59. 2	9.0 9	53. 2	9.5 8	22. 51	2.3 9	10. 96	1.3 72

Rafael_TWH 17.5_S8_2	180.5	558	61.8	230.6	51.9	11.46	57.1	9.04	52	9.42	22.82	2.406	11.27	1.378
Rafael_TWH 17.5_S8_3	179.1	556	61.3	229.5	50.9	11.44	55.4	8.7	50.7	9.35	22.49	2.378	11.4	1.41
Rafael_TWH 17.5_S9_1	177.4	577	61.7	230.5	50.6	11.36	55.1	8.53	49.8	9.25	22.15	2.399	11.35	1.377
Rafael_TWH 17.5_S9_2	180.7	570	60.7	229.3	49.8	11.44	55.1	8.44	49.5	9.04	21.64	2.343	11.42	1.373
Rafael_TWH 17.5_S9_3	179.9	563	59.1	226.6	51	11.26	55.2	8.44	51	9.27	22.43	2.451	11.92	1.437
Rafael_TWH 17.5_S10_1	147.8	472	53.4	208.9	47.7	11.48	51.2	8.17	48	8.63	20.81	2.218	10.74	1.307
Rafael_TWH 17.5_S10_2	139.4	460	50.9	198.7	46.1	10.66	49.3	7.79	45.2	8.08	19.77	2.063	9.9	1.17
Rafael_TWH 17.5_S10_3	143.7	384.4	49.7	208	49.2	11.18	53.8	8.51	50.15	8.91	21.33	2.28	10.86	1.335
Rafael_TWH 17.5_S11_2	173.6	510	56.6	219.3	48.1	10.43	51.4	8.09	47.2	8.58	20.08	2.167	10.83	1.311
Rafael_TWH 17.5_S11_3	179.4	521	57.6	229.7	49.3	10.68	54.2	8.43	49.7	8.98	21.32	2.32	11.27	1.363
Rafael_TWH 17.5_S12_1	122.7	400	46.8	187.9	45.1	10.65	46.7	7.29	43.3	7.68	18.05	1.899	9.48	1.075
Rafael_TWH 17.5_S12_2	124.4	382	46.4	189.6	46.1	11.01	48	7.53	43.8	7.73	18.42	1.944	9.56	1.114
Rafael_TWH 17.5_S12_3	147.5	335.3	47.71	215.9	54.6	11.86	59.2	9.47	56.1	10.17	24.4	2.668	13.72	1.577
Rafael_TWH 17.5_S13_1	258	709	87.1	334	72.6	14.54	73.3	11.23	63.2	11.12	26.3	2.69	12.36	1.499
Rafael_TWH 17.5_S13_2	225.8	677	83	318.7	70.6	14.36	72.8	11.08	61.9	10.71	25.1	2.65	12.55	1.489
Rafael_TWH 17.5_S13_3	176.2	562	64.9	245.3	57	11.9	61.8	9.42	54.8	9.65	23.15	2.48	11.61	1.443
Rafael_TWH 17.5_S14_2	185.3	551	65.8	258.9	57.5	12.66	63.4	9.64	56.3	10.02	23.84	2.499	12.29	1.449
Rafael_TWH 17.5_S14_3	182.1	553	65.1	250.1	58.7	12.59	62.4	9.7	56	10.05	24.21	2.544	12.08	1.433
Rafael_TWH 17.5_S15_1	184.6	584	64.1	247.2	54.6	11.44	58.4	9.21	53	9.54	22.92	2.46	11.53	1.41
Rafael_TWH 17.5_S15_2	182.2	584	63.5	245.7	54.8	11.65	58.4	9.26	54.8	9.81	23.82	2.555	11.89	1.418
Rafael_TWH 17.5_S15_3	197.3	594	65.8	267	59.7	12.05	61.7	10	57.2	10.4	25.5	2.67	12.65	1.542
Rafael_TWH 17.5_S16_1	196.5	580	66.3	251.7	55.8	11.82	58.6	9.15	53.5	9.77	24.1	2.58	12.68	1.513
Rafael_TWH 17.5_S16_3	166.4	503	57.2	224.5	51.3	11.57	54.4	8.62	50.4	8.93	21.55	2.284	10.91	1.28
Rafael_TWH 17.5_S17_2	141.3	441	50.5	196.1	45.9	10.33	49.1	7.59	44.9	8.21	19.93	2.242	11.38	1.418
Rafael_TWH 17.5_S17_3	150.5	462	54	209.1	48.6	11.3	53.8	8.31	50.2	9.05	22.17	2.524	12.66	1.567
Rafael_TWH 17.5_S18_1	122.9	372	42.3	166.8	39.5	9.69	44.5	7.14	43.1	7.87	18.94	2.037	10.16	1.239

Rafael_TWH 17.5_S18_2	121.6	368	41.7	166.4	39.2	9.74	45.5	7.14	42.7	7.81	18.6	2.067	9.91	1.168
Rafael_TWH 17.5_S18_3	121.9	377	42.5	166.7	38.8	9.57	44.1	7.03	43.3	7.95	18.84	2.04	10.4	1.175
Rafael_TWH 18_S1_1	202.5	762	125.2	582	148.1	30.3	148.2	22.08	116	17.29	33.3	2.73	11.29	1.263
Rafael_TWH 18_S1_2	244.1	956	148.8	646	155.2	32.71	159	24.41	127.8	19.65	38.7	3.327	13.6	1.559
Rafael_TWH 18_S1_3	277.9	870	151	720	182.2	37.76	201.6	31.74	170.7	27.2	56	4.98	19.94	2.274
Rafael_TWH 18_S2_1	261.7	1007	162.3	742	185.1	39.4	191.8	29.99	159	25.19	51.6	4.67	19.09	2.17
Rafael_TWH 18_S2_2	250.7	1093	166.8	724	182.9	38	183	28.17	150.8	23.78	48.3	4.33	17.43	1.941
Rafael_TWH 18_S2_3	254.3	1075	165.6	729	184.9	37.9	192.4	29.48	156.9	24.77	51.5	4.56	18.29	2.05
Rafael_TWH 18_S3_1	238.4	996	155.4	696	171.2	35.9	180.5	26.93	141.9	22.01	44.6	3.83	15.43	1.754
Rafael_TWH 18_S3_2	235.4	985	152.4	669	167.6	35.6	173.1	26.17	137.1	21.13	42.2	3.68	15.04	1.663
Rafael_TWH 18_S3_3	231.3	984	155.9	678	168.2	35.85	173	27.03	138.4	21.19	43	3.71	15.15	1.682
Rafael_TWH 18_S4_1	279.1	1081	170.3	770	189.9	39.6	206.5	32.1	174.4	27.7	57.1	5.11	20.6	2.27
Rafael_TWH 18_S4_2	269.6	1175	179.4	741	181.2	38.1	189	29.1	155.5	24.21	49.5	4.4	18.11	1.993
Rafael_TWH 18_S4_3	304.9	1269	186.9	765	187	38.5	197.9	30.55	165.6	26.3	55.6	5.16	21.14	2.358
Rafael_TWH 18_S5_3	236	880	142	660	164.5	35.5	160.9	24.97	128.9	20.5	41.1	3.48	14.57	1.62
Rafael_TWH 18_S6_1	245.8	1073	161.8	688	167.2	36.9	181.2	28.2	143.6	21.78	45.3	4.12	15.7	2.01
Rafael_TWH 18_S6_2	280.9	1146	170.6	704	175.1	35.32	184.2	28.33	151.3	24.16	50.8	4.59	18.81	2.134
Rafael_TWH 18_S7_1	263.8	1108	173.7	746	179.8	35	186.6	27.86	147.8	22.75	47.2	4.03	16.41	1.848
Rafael_TWH 18_S7_2	243	1064	166.1	725	182.6	33.97	183.1	27.43	143.9	22.01	45	3.99	16.24	1.93
Rafael_TWH 18_S7_3	229.1	1017	161.7	709	175.9	34.18	177.1	26.38	137.6	20.98	42.2	3.61	14.45	1.622
Rafael_TWH 18_S8_1	251.2	732	139.7	734	197.3	37.1	213.5	33.16	176.9	27.25	54.8	4.72	19.11	2.28
Rafael_TWH 18_S8_2	254.1	938	154.3	713	180	38.4	188.9	29.49	156.4	24.53	49.6	4.25	17.2	1.885
Rafael_TWH 18_S8_3	300.3	880	158.2	792	201.8	42.4	226.2	34.7	189.2	30.15	62.5	5.54	22.62	2.47
Rafael_TWH 18_S9_1	212.5	847	132	596	148	31.22	150.4	22.47	118.1	18	36.5	3.1	13.01	1.454
Rafael_TWH 18_S9_2	290.5	1109	162.9	696	166.4	35.6	180	27.09	146.1	23.07	48.2	4.39	18.43	2.11
Rafael_TWH 18_S9_3	290.7	1158	167.9	707	171.8	36.7	181.4	27.98	153.3	24.51	52.9	4.7	19.48	2.204

Rafael_TWH 18_S10_1	237 .1	991	149 .1	639	155 .8	32. 06	159 .4	23. 59	125 .9	19. 12	39. 3	3.4 5	14. 25	1.5 91
Rafael_TWH 18_S10_2	234 .9	916	149	650	157 .3	32. 11	167	24. 4	129 .2	20. 09	39. 8	3.5 32	14. 24	1.5 66
Rafael_TWH 18_S10_3	205 .3	771	130 .6	617	156 .9	31. 5	160 .7	23. 64	122 .8	18. 34	35. 6	2.9 5	11. 99	1.4 11
Rafael_TWH 18_S11_1	236 .8	979	149 .4	647	163 .1	34. 7	168 .3	25. 49	136 .8	20. 87	42. 4	3.6 6	14. 75	1.6 35
Rafael_TWH 18_S11_2	226 .3	975	144 .5	665	167 .7	35	167 .9	25. 59	133 .9	20. 71	41. 6	3.6 2	14. 96	1.5 89
Rafael_TWH 18_S11_3	221 .2	898	139 .8	637	157 .3	33	161 .9	24. 75	131 .2	20. 25	40. 6	3.5 3	14. 75	1.6 18
Rafael_TWH 18_S12_1	221 .2	930	142 .8	626	158	33. 71	163 .5	24. 49	128 .3	19. 64	38. 85	3.3 88	13. 84	1.5 09
Rafael_TWH 18_S12_2	237 .2	928	143 .1	628	156	33. 9	166 .7	24. 81	129 .8	19. 91	40. 57	3.4 64	13. 96	1.5 57
Rafael_TWH 18_S12_3	229 .9	916	145 .2	635	160 .4	33. 94	165 .9	24. 62	129 .1	19. 99	39. 6	3.4 2	13. 78	1.5 25
Rafael_TWH 18_S13_1	273 .8	103 3	158 .9	734	204	38. 1	192 .2	29. 1	148 .7	22. 85	47. 7	4.0 1	18	1.9 1
Rafael_TWH 18_S13_2	277 .5	115 1	176 .7	777	184 .9	37. 8	194	28. 82	151 .2	23. 78	48. 2	4.2 2	17. 26	1.9 42
Rafael_TWH 18_S13_3	279 .2	117 5	173	749	181 .5	38. 9	185	28. 35	149 .7	23. 2	48	4.2 5	17. 62	2.0 27
Rafael_TWH 18_S14_1	212 .5	939	145 .6	633	159 .2	33. 03	168	24. 74	129 .4	19. 62	39. 4	3.3 3	13. 32	1.4 81
Rafael_TWH 18_S14_2	206 .5	883	144 .3	640	157 .4	33. 73	163 .7	24. 51	126 .9	19. 26	38. 22	3.1 44	12. 66	1.3 82
Rafael_TWH 18_S14_3	120 0	284 0	309	108 3	200 .4	36	182 .9	24. 94	126 .4	19. 08	39. 09	3.2 04	12. 67	1.4 22
Rafael_TWH 18_S15_1	243 .5	998	161 .9	710	169 .1	32. 79	171 .7	25. 27	133 .2	20. 26	40. 8	3.5 5	14. 6	1.6 78
Rafael_TWH 18_S15_3	237	892	148 .3	686	172	32. 8	171 .7	25. 09	128 .1	19. 52	37. 9	3.2 5	13. 23	1.5
Rafael_TWH 18_S16_1	258 .3	103 7	160 .3	691	172 .5	34. 7	176 .3	26. 72	141 .9	22. 18	44. 6	3.9 8	16. 2	1.8 27
Rafael_TWH 18_S16_2	283 .5	112 3	173	740	183 .9	35. 12	192 .2	28. 27	151 .8	23. 5	48	4.2 3	17. 14	1.9 55
Rafael_TWH 18_S16_3	300 .4	112 2	170 .1	751	180 .7	36. 6	188 .3	28. 6	153 .1	23. 59	48. 4	4.4	18. 95	2.1 4
Rafael_TWH 18_S17_1	219 .4	844	143 .5	673	173 .2	36. 4	177 .9	26. 14	133 .6	19. 77	38. 4	3.2 2	13. 41	1.4 94
Rafael_TWH 18_S17_2	221 .9	885	144	658	168 .2	34. 79	168 .2	24. 77	127 .9	18. 97	37. 6	3.0 95	12. 81	1.3 87
Rafael_TWH 18_S17_3	229 .5	904	146 .6	664	171 .1	33. 8	167 .6	24. 49	125 .2	18. 74	37. 4	3.0 7	12. 58	1.4 07
Rafael_TWH 18_S18_1	235 .1	869	143 .6	692	175	35. 32	185	28. 05	149 .4	23. 4	46. 8	4.1 4	16. 54	1.8 17
Rafael_TWH 18_S18_2	245 .9	984	154 .8	712	176 .6	36. 37	184 .7	27. 87	149 .1	23. 07	46. 8	4.1 1	16. 7	1.8 68
Rafael_TWH 18_S18_3	243 .5	805	142 .7	712	190 .4	38. 31	206 .5	31. 2	166 .4	25. 81	51. 7	4.5	17. 85	1.9 97

Rafael_TWH 18_S19_1	285 .1	893	133 .7	605	151 .2	33. 28	173 .4	27. 14	153 .8	24. 79	51. 5	4.7 4	19. 35	2.1 76
Rafael_TWH 18_S19_2	311 .3	101 2	144 .9	632	153 .7	33. 6	174 .5	27. 29	153 .7	25. 33	53. 4	4.9 5	20. 19	2.3 43
Rafael_TWH 18_S19_3	295 .6	101 2	143 .2	637	157 .1	34. 6	175 .2	27. 5	154 .8	25. 1	53. 5	4.9 8	20. 8	2.2 9
Rafael_TWH 18_S20_1	259 .8	102 3	158 .6	733	184 .9	36. 9	195 .6	29. 49	160 .2	25. 23	52. 3	4.6	19. 02	2.1 11
Rafael_TWH 18_S20_2	270 .2	111 0	169 .9	749	191	37. 3	197 .2	29. 17	157 .7	24. 62	51. 3	4.6 1	19. 14	2.1 14
Rafael_TWH 18_S20_3	287 .9	112 4	169 .2	750	182 .8	37. 6	193 .8	29. 57	162 .8	25. 62	55	4.8 8	20. 43	2.2 62
Rafael_TWH 18_S21_1	263 .4	107 8	169 .8	738	189 .3	38. 7	198 .3	30. 4	159 .1	25. 2	51. 9	4.6 4	18. 52	2.0 6
Rafael_TWH 18_S21_2	287	112 9	169 .9	776	198	39. 3	206	31. 3	170 .1	27	57	5.0 6	20. 5	2.3 3
Rafael_TWH 18_S21_3	276 .5	112 7	175 .5	769	194	39. 8	201 .8	31. 1	168 .5	26. 4	53. 7	4.9 3	19. 8	2.1 7
Rafael_TWH 18_S21_4	282 .8	106 9	173 .1	805	201	41	209 .1	31. 7	168 .9	26. 9	53. 4	4.8 7	20. 1	2.2 5

Run 7														
Sample ID	La	Ce	Pr	Nd	Sm	Eu	Gd	Tb	Dy	Ho	Er	Tm	Yb	Lu
Rafael_TWH 16_S1_2	138 .5	264 .5	29. 97	113 .9	24. 01	5.5 9	31. 49	5.0 2	33. 16	6.8 8	17. 84	2.0 75	10. 45	1.2 93
Rafael_TWH 16_S2_1	121 .1	233 .9	26. 04	100 .8	22. 48	4.9 6	29. 1	4.6 8	30. 39	6.0 1	15. 83	1.7 56	8.4 6	1.0 32
Rafael_TWH 16_S2_2	122 .9	228 .5	26. 02	106 .2	23. 74	5.1 2	31. 88	5.1 2	33. 26	6.6 7	17. 37	1.9 73	9.3 1	1.1 66
Rafael_TWH 16_S2_3	122 .6	216 .4	26. 15	107 .3	24. 89	5.3 2	32. 04	5.0 6	33. 12	6.6 4	17. 17	1.8 2	8.5 9	1.0 7
Rafael_TWH 16_S3_1	139 .2	271 .2	27. 64	102 .7	21. 85	5.9 9	30	4.7 9	32. 4	6.8 5	18. 84	2.2 1	11. 82	1.4 16
Rafael_TWH 16_S3_2	145 .9	279	30. 1	111 .9	24. 43	6.4 5	31. 3	5.1 8	36	7.4 9	20. 62	2.5	13. 11	1.6 1
Rafael_TWH 16_S3_3	138 .2	253 .2	28. 05	104	22. 19	6.1 6	31. 88	5.1 2	35. 48	7.5 2	20. 81	2.4 99	12. 61	1.5 73
Rafael_TWH 16_S4_1	124 .7	218	26. 03	102 .3	20. 67	5.1 1	28. 09	4.4 2	29. 97	6.1 6	16. 5	1.8 73	9.5 6	1.1 91
Rafael_TWH 16_S4_2	137 .7	197 .4	26. 03	110 .4	25. 07	5.4 6	31. 82	5.2 3	34. 83	7.2	19. 34	2.2 9	11. 42	1.4 83
Rafael_TWH 16_S4_3	147 .5	190 .7	27. 13	125 .2	28. 36	6.1 1	38	6.2 9	42. 2	8.8 5	23. 39	2.7 34	13. 86	1.7 82
Rafael_TWH 16_S5_1	96. 4	205 .9	23. 63	92. 5	21. 15	4.0 2	24. 42	3.9 3	25. 05	4.7 8	12. 03	1.2 54	5.5 4	0.6 91
Rafael_TWH 16_S5_2	99	210 .8	23. 74	94. 9	20. 61	4.3 3	25. 6	3.9 2	25. 82	5.0 3	12. 74	1.3 73	6.3 9	0.7 92
Rafael_TWH 16_S5_3	99	224 .3	24. 61	90. 9	20. 82	4.6 9	25. 4	4.1	25. 65	5.1 8	13. 32	1.5 13	7.1 8	0.8 89
Rafael_TWH 16_S6_1	127 .2	273	28. 3	101 .8	21. 89	5.1 4	28	4.4 8	29. 6	6.0 5	15. 4	1.7 1	7.9 6	1.0 09

Rafael_TWH 16_S6_2	134 .3	249 .2	27. 01	105 .1	21. 96	5.3 8	29. 53	4.8 1	32. 3	6.6 2	17. 73	2.0 49	10. 31	1.2 42
Rafael_TWH 16_S6_3	139	257	27. 69	102 .7	21. 88	5.6 6	29	4.6 9	31. 2	6.4 1	17. 28	2.0 8	10. 61	1.3 14
Rafael_TWH 16_S7_1	195 .4	308	41. 04	171	37. 73	10. 41	51. 76	8.5 5	55. 86	10. 9	27. 31	2.8 96	13. 51	1.6 06
Rafael_TWH 16_S7_2	165	373	41. 1	149 .1	29. 8	9.0 1	39. 6	6.3 7	41. 6	8.0 8	20. 3	2.2 1	10. 19	1.1 78
Rafael_TWH 16_S7_3	187	425	45. 6	165 .5	33. 8	9.8 6	43. 4	6.9 6	44. 7	8.8 5	22. 3	2.3 6	11. 2	1.3 5
Rafael_TWH 16_S8_1	126 .7	276	28. 7	102 .8	22. 3	4.7 3	28. 5	4.4	28. 8	5.4 5	14	1.4 18	6.3 2	0.7 6
Rafael_TWH 16_S8_3	127 .1	262 .3	28. 09	106 .4	22. 24	4.6 8	30. 19	4.6 3	30. 26	5.9 6	14. 76	1.4 8	6.3 3	0.7 72
Rafael_TWH 16_S9_1	202 .9	423	48. 3	179 .3	37. 6	11. 02	48. 9	8	51. 7	10. 18	25. 6	2.9 4	13. 95	1.6 4
Rafael_TWH 16_S9_2	205 .1	459	51	190 .5	38. 7	10. 6	47. 9	7.7	49. 4	9.3 9	23. 3	2.5 6	12. 23	1.4 45
Rafael_TWH 16_S9_3	197 .4	310 .3	43. 03	181 .8	41. 24	11. 37	57. 2	9.2 5	61	11. 88	30. 08	3.3 5	15. 82	1.9 22
Rafael_TWH 16_S10_1	111 .4	240 .5	27. 9	105 .9	22. 94	6.1 3	29. 95	4.9 1	31. 99	6.3 2	15. 64	1.6 27	7.3	0.8 29
Rafael_TWH 16_S10_2	126 .6	257	29. 56	116 .1	25. 81	6.5 5	34. 62	5.5 6	36. 5	7.0 5	17. 61	1.8 04	8.1 5	0.9 7
Rafael_TWH 16_S10_3	127	265 .2	30. 43	118	25. 73	6.3 4	34. 89	5.6 5	37. 17	7.2 9	18. 41	1.9 61	8.7 5	1.0 66
Rafael_TWH 16_S11_1	82. 5	133 .1	17. 69	77. 6	17. 88	4.1 5	24. 65	3.9 5	25. 06	4.8 8	11. 9	1.2 24	5.4	0.6 63
Rafael_TWH 16_S11_2	66. 4	139 .2	16. 71	66. 8	15. 4	3.6 9	19. 5	3.0 97	19. 16	3.6 69	9.1 2	0.9 26	4.0 9	0.4 87
Rafael_TWH 16_S11_3	71. 3	139 .1	16. 72	69. 5	15. 96	3.7 64	21. 13	3.3 96	21. 89	4.1 45	9.9 5	0.9 88	4.1 5	0.4 95
Rafael_TWH 16_S12_1	112 .3	231 .9	26. 83	102 .2	22. 15	5.2 1	27. 43	4.4 7	29. 58	6.0 7	16. 31	1.8 82	9.3 9	1.2 01
Rafael_TWH 16_S12_2	123	229 .9	26. 11	102	22. 18	5.2 9	29. 03	4.6 7	32. 04	6.7 3	18. 44	2.1 02	10. 49	1.3 27
Rafael_TWH 16_S12_3	106 .4	204 .3	24. 14	97	21. 2	5.2 9	28. 27	4.5 61	31. 26	6.5 2	17. 57	2.0 77	10. 46	1.3 3
Rafael_TWH 16_S13_1	111 .3	210 .9	25. 45	103 .1	22. 97	5.2 1	30. 81	4.9 42	32. 26	6.3 7	16. 18	1.7 39	7.7 5	1.0 02
Rafael_TWH 16_S13_2	114 .1	214 .4	25. 25	101 .1	22. 02	5.0 4	30. 62	4.9 1	32. 3	6.3 8	16. 06	1.6 67	7.1 3	0.8 76
Rafael_TWH 16_S13_3	98. 9	195 .5	22. 76	87. 9	20. 81	4.6	26. 81	4.4 8	29. 48	5.7 8	14. 57	1.5 31	6.6 4	0.8 19
Rafael_TWH 16_S14_1	113 .5	189 .6	24. 42	101 .8	22. 71	4.6 3	30. 12	4.8	30. 5	5.8 6	15. 05	1.5 67	6.8 9	0.8 45
Rafael_TWH 16_S14_2	108 .9	203 .1	24. 64	97. 2	21. 61	4.2 4	28. 64	4.4 95	29. 31	5.6 3	13. 85	1.3 97	5.7 6	0.7 06
Rafael_TWH 16_S14_3	108 .3	199 .2	24. 26	95. 9	22. 31	4.0 62	28. 6	4.6 22	29. 66	5.7 41	13. 98	1.4 16	5.7 1	0.7 22
Rafael_TWH 16_S15_1	119 .7	286 .6	35. 73	141 .3	31. 01	7.0 2	33. 72	5.3 2	32. 23	6.1 2	15. 94	1.7 73	8.9 7	1.1 13

Rafael_TWH 16_S15_2	122 .9	284 .9	35. 07	139	30. 49	6.7 4	34. 18	5.4 4	33. 3	6.3	16. 2	1.8 28	9.3 1	1.1 16
Rafael_TWH 16_S15_3	125 .7	299 .7	36. 07	140 .5	31. 26	6.5 1	34. 95	5.4 4	33. 62	6.4 4	16. 45	1.8 38	9.1 2	1.1 52
Rafael_TWH 16_S16_1	170 .5	354 .9	38. 06	140	29. 21	7.9 6	39. 5	6.3 8	43. 06	8.7 2	22. 38	2.5 12	12. 3	1.4 76
Rafael_TWH 16_S16_2	168 .3	354 .9	37. 2	137 .1	27. 99	7.9	38. 01	6.1 6	42. 1	8.6 3	22. 65	2.5 82	12. 91	1.5 72
Rafael_TWH 16_S16_3	175 .8	334 .5	36. 69	138 .2	29. 77	8.0 4	41. 2	6.6 2	44. 84	9.2 6	24. 4	2.7 65	13. 58	1.6 74
Rafael_TWH 16_S17_1	141 .1	279 .8	29. 75	110 .6	23. 98	5.7 3	30. 6	4.9 5	33. 27	6.9 2	18. 4	2.1 57	10. 37	1.2 85
Rafael_TWH 16_S17_2	139 .8	271	29. 56	114 .7	24. 56	6.1 2	32. 2	5.1 8	34. 7	6.9 8	18. 87	2.1 96	10. 8	1.2 78
Rafael_TWH 16_S17_3	132 .1	269	27. 82	106	22. 65	5.8 6	28. 32	4.6 2	31. 5	6.3 9	17. 02	1.9 7	10. 06	1.1 84
Rafael_TWH 16_S18_1	150 .1	305	32. 3	115 .7	24. 63	6.4 2	34. 2	5.5 1	36. 8	7.4 7	19. 46	2.2 24	10. 79	1.3 62
Rafael_TWH 16_S18_2	150 .3	290 .5	30. 96	115 .8	24. 26	6.3 4	34. 4	5.6 2	38. 6	7.9 6	21. 42	2.4 61	11. 99	1.4 58
Rafael_TWH 16_S18_3	147 .5	288 .2	31. 3	114 .6	23. 53	6.3 3	32. 8	5.4 6	36. 8	7.6 2	19. 99	2.2 74	10. 94	1.3 35
Rafael_TWH 15.5_S1_1	398 .9	107 1	151 .8	706	183 .1	35. 85	209 .1	32. 28	184 .8	31. 4	70. 1	7.1 5	31. 75	3.8 6
Rafael_TWH 15.5_S1_2	397 .8	118 2	157	692	177 .5	33. 6	197 .2	30. 6	173	28. 9	64. 3	6.4 8	28. 5	3.4 7
Rafael_TWH 15.5_S1_3	378 .1	134 8	153 .9	638	154 .8	32. 3	164 .5	25. 69	143 .8	24. 49	55. 2	5.6 1	26. 13	3.0 57
Rafael_TWH 1.55_S2_1	343 .9	946	127	579	150	29. 43	175 .4	27. 95	163 .6	28. 12	63. 4	6.4 4	28. 33	3.4 48
Rafael_TWH 15.5_S2_2	277 .3	996	115 .9	461	116	25. 9	128 .9	20. 82	119 .5	20. 65	47. 8	4.9 7	22. 6	2.6 8
Rafael_TWH 15.5_S2_3	301 .8	103 4	125 .4	518	130 .4	26. 95	151 .2	23. 68	138 .5	23. 52	54. 3	5.4 6	24. 1	2.8 8
Rafael_TWH 15.5_S3_1	277	830	105	460 .5	120 .8	27. 24	137 .4	22. 22	129 .5	22. 51	51. 6	5.2 25	23. 98	2.7 87
Rafael_TWH 15.5_S3_2	287 .1	923	109 .4	449 .8	111 .5	26. 55	129 .4	20. 62	120 .2	21. 23	49. 2	5.1 2	24. 17	2.8 42
Rafael_TWH 15.5_S3_3	350 .8	849 .4	115 .7	549 .1	145 .7	31. 17	173 .8	27. 47	162 .8	28. 39	64. 9	6.8 1	31. 33	3.7 28
Rafael_TWH 15.5_S4_1	391 .5	121 4	151 .4	623	153 .7	33. 39	166 .8	26. 09	146 .7	24. 55	54	5.2 3	23. 32	2.7 5
Rafael_TWH 15.5_S4_3	377 .9	138 9	155 .8	612	150 .3	30. 99	162 .3	25. 33	143 .2	23. 85	52. 3	5.1 2	22. 28	2.6 43
Rafael_TWH 15.5_S5_1	358 .3	142 6	170 .9	682	164	28. 62	185	29. 15	162 .4	27	60. 2	5.9 8	25. 1	3.1 5
Rafael_TWH 15.5_S5_2	382 .4	140 5	170 .8	685	166 .4	30. 57	182 .4	28. 59	158 .6	26. 55	57. 8	5.7 5	24. 87	3
Rafael_TWH 15.5_S5_3	339 .7	124 5	157 .2	641	165	28. 72	187 .3	29. 52	168 .4	28. 15	61. 9	6.2 2	26. 64	3.3 4
Rafael_TWH 15.5_S6_1	353	120 4	143 .4	574	141 .2	30. 38	156 .3	24. 62	141 .5	24. 06	53	5.4 1	24. 4	2.8 8

Rafael_TWH 15.5_S6_2	363.2	1169	138.1	560	139.5	29.86	152.9	24.29	139.3	24.02	54.6	5.6	25.2	2.9
Rafael_TWH 15.5_S6_3	352.5	1025	126.3	539	134.8	28.96	152.4	23.98	138.8	23.97	55.4	5.55	25.71	2.99
Rafael_TWH 15.5_S7_1	288.1	966	110.8	451	114.1	27.45	120.6	19.08	108.8	18.56	42.6	4.34	20.7	2.36
Rafael_TWH 15.5_S7_2	292.1	1006	113.8	465	115.5	28.29	122.9	19.26	110.8	18.77	42.4	4.44	21.7	2.47
Rafael_TWH 15.5_S7_3	316.9	1018	118.4	491	119.4	28.46	126.7	20.36	118.5	20.53	48.1	5.13	24.7	2.85
Rafael_TWH 15.5_S8_1	354.9	1245	143.1	582	142.7	29.57	162.6	25.52	145.3	24.65	55.8	5.65	24.78	2.93
Rafael_TWH 15.5_S8_2	339.6	1169	139	562	141.3	28.78	160.8	25.64	148.6	25.04	56.7	5.7	25.13	3.067
Rafael_TWH 15.5_S8_3	359.2	1092	138.9	604	151.9	31.67	174.9	27.81	160.4	27.34	61.3	6.2	27.08	3.26
Rafael_TWH 15.5_S9_1	387	1121	136.8	564	136.6	30.77	150.9	23.43	134	22.47	50.9	5.2	24.17	2.68
Rafael_TWH 15.5_S9_2	440	1003	138.5	646	166.5	35.09	192.2	30.37	175.8	29.88	67.9	6.97	31.5	3.63
Rafael_TWH 15.5_S9_3	351.2	1102	132.6	545	134.5	31.22	152.1	23.7	132.5	22.5	49.8	4.93	22.14	2.509
Rafael_TWH 15.5_S10_1	329.1	1166	135.5	560	137	28.17	146.4	22.78	130.7	22.08	49.3	4.96	22.68	2.63
Rafael_TWH 15.5_S10_2	312	1103	131.7	535	130.1	27.3	143.2	22.11	126.1	21.3	47.5	4.81	21.5	2.53
Rafael_TWH 15.5_S10_3	300	1125	129.9	524	129	26.7	151.6	23.8	139.2	23.4	53.3	5.16	21.9	2.66
Rafael_TWH 15.5_S11_1	236.7	817	98.7	413.8	108.1	25.21	125.4	19.53	115.2	19.79	45	4.64	21.48	2.553
Rafael_TWH 15.5_S11_2	230.1	808	96.6	412.9	105.3	25.05	125	19.95	116.3	19.79	44.9	4.61	21.16	2.49
Rafael_TWH 15.5_S11_3	254.7	764	100	445.4	117.7	27.29	138.7	22.37	130.4	22.33	51	5.23	24.21	2.826
Rafael_TWH 15.5_S12_1	379.3	1093	140.5	590	145.2	31.73	166.8	25.75	147.5	25	56.6	5.68	26	3.09
Rafael_TWH 15.5_S12_2	361	1221	141	561	133.9	30.6	148.7	23	130.2	22.01	49.6	5	22.4	2.59
Rafael_TWH 15.5_S12_3	384.9	1140	143.2	594	147.1	32.18	161.7	25.45	144.2	24.07	53.8	5.43	24.5	2.88
Rafael_TWH 15.5_S13_1	303.2	1000	122	501	124.1	27.36	138.3	22.11	127.9	21.84	49.8	5.1	23.22	2.69
Rafael_TWH 15.5_S13_2	295.3	1043	120.8	475	118.9	26.89	133.6	21.53	124.7	21.31	49	4.99	22.55	2.64
Rafael_TWH 15.5_S13_3	314.2	865	113.9	507.7	131	28.9	156	25.03	145.9	24.96	57.2	5.9	26.89	3.195
Rafael_TWH 15.5_S14_1	353	1002	124.4	527	129.5	29.78	143.3	22.55	130.6	22.34	51	5.3	24.52	2.799
Rafael_TWH 15.5_S14_2	303.2	1033	122.4	493	121.1	27.72	139.3	21.3	121.8	20.43	46.3	4.62	20.77	2.376
Rafael_TWH 15.5_S14_3	310.6	1055	123.4	509	123.7	29.24	141.3	21.58	124.2	20.96	47.3	4.75	21.61	2.54

Rafael_TWH 15.5_S15_1	265.6	882	106.1	462	117.1	26.54	130	20.7	120.3	20.79	48.1	4.9	23.6	2.7
Rafael_TWH 15.5_S15_2	261	910	109.4	456.1	115.8	26.5	126.1	20.25	116.9	19.93	46	4.75	22.43	2.6 45
Rafael_TWH 15.5_S15_3	268.6	867	106.8	459.1	115.8	27.06	133.5	21.23	124.3	21.41	49	5.07	23.09	2.6 64
Rafael_TWH 15.5_S16_1	362.8	1297	147.9	558	131.8	31.3	153.5	23.4	138	23.2	50.8	4.87	20.8	2.4 1
Rafael_TWH 15.5_S16_2	389.6	1320	146.9	578	135.1	30.57	148.8	22.71	131.1	22.03	48.5	4.72	20.46	2.4 2
Rafael_TWH 15.5_S16_3	396.5	1302	146.9	576	134.9	30.32	147	22.64	129.3	21.53	48.1	4.83	21.5	2.6
Rafael_TWH 15.5_S17_1	347.5	1113	142.6	598	149.7	28.02	171.3	27.11	155.8	26.05	58.5	5.9	25.2	3.1 1
Rafael_TWH 15.5_S17_2	353.8	1121	142.4	614	155.1	28.8	178.7	27.93	161.3	27.31	59.8	6.06	25.83	3.1 2
Rafael_TWH 15.5_S17_3	349.7	1275	143.5	592	138.9	29.84	150.3	23.5	132.7	22.19	49.8	5.09	22.47	2.7 1
Rafael_TWH 15.5_S18_1	363.4	1205	134.7	561	134.7	30.93	143.6	22.13	127.2	21.37	49.1	5.02	23.8	2.7 26
Rafael_TWH 15.5_S18_2	366.7	1071	131.2	541	131.9	30.09	143.9	22.14	127.9	21.61	48.9	4.94	22.4	2.5 21
Rafael_TWH 15.5_S18_3	356.4	1094	131.1	550	134.1	31.5	145.6	23.24	134.3	22.44	50.9	5.23	24.4	2.8 7
Rafael_TWH 15.5_S19_1	417.3	1368	163.4	674	164.9	35.54	180.5	27.39	156.8	26.01	58.3	5.97	26.93	3.1 3
Rafael_TWH 15.5_S19_2	386.8	1259	153.5	629	155.3	35.2	167.1	26.12	144.8	24.39	55.4	5.59	25.56	2.9 6
Rafael_TWH 15.5_S19_3	446.1	1496	180.2	728	173.2	37.7	184.8	28.26	159.5	26.11	57.3	5.62	25.11	2.8 81
Rafael_TWH 15.5_S20_1	346.3	1135	133.7	544	136.5	29.34	150.3	24.24	135.9	23.15	52.6	5.22	24.1	2.7 9
Rafael_TWH 15.5_S20_2	374.7	1104	139.7	609	149.5	31.7	170.3	26.88	156.6	26.64	59.1	6.08	27.2	3.2 4
Rafael_TWH 15.5_S20_3	360	1286	141.7	556	132.3	29.46	143.3	22.39	128.6	21.44	48.3	4.93	22.22	2.6 03
Rafael_TWH 15.5_S21_1	277	874	107.4	456	115.5	26.6	127.8	19.65	113.3	18.66	42.4	4.34	20.35	2.4 07
Rafael_TWH 15.5_S21_2	253.3	908	110.7	460	115.7	26.83	123	19.57	112.6	18.66	41.21	4.28	19.78	2.2 92
Rafael_TWH 15.5_S21_3	260.4	905	115.6	509	131.8	28.43	145.6	23.12	130.6	21.85	48.1	4.87	21.86	2.5 8
Rafael_TWH 15_S1_1	452	1555	196.6	808	193.1	39.2	206.3	30.77	172	28.58	63.8	6.33	28.1	3.2 8
Rafael_TWH 15_S1_2	463	1523	205.4	846	201.9	40.2	223.7	33.3	185.8	30.8	67.6	6.56	29.1	3.4 2
Rafael_TWH 15_S1_3	494	1526	207.2	895	212.8	41	226.2	33.8	186.1	31.5	71.5	7.23	33.7	3.9
Rafael_TWH 15_S2_1	673	2270	275	1127	263	55	265	40.6	218	35.2	79.3	8.3	39.5	4.3 7
Rafael_TWH 15_S2_2	657	1982	267	1078	261.8	53.4	270	41.74	229.3	37.47	85.1	8.73	40.1	4.5 1

Rafael_TWH 15_S2_3	580	1949	253.3	1014	238.8	47.5	251	37.7	209	33.6	75.4	7.84	36.9	4.24
Rafael_TWH 15_S3_1	434.5	1291	180.3	763	189.2	38.1	207.7	31.36	176.9	29.31	66.1	6.65	30.04	3.431
Rafael_TWH 15_S3_2	426.4	1525	188.6	777	186	39.1	197.5	29.9	168.1	28.4	63.2	6.31	28.9	3.32
Rafael_TWH 15_S3_3	419	1502	194.9	787	192	39.9	209	31.8	178	30.3	67.8	6.76	30.3	3.38
Rafael_TWH 15_S4_1	478	1534	190.9	775	181.6	38.1	191.2	29.1	163.3	27.7	63.2	6.16	27.8	3.11
Rafael_TWH 15_S4_2	493	1531	193.3	767	177.6	38.1	192.1	28.96	164	27.5	62.2	6.24	28.4	3.175
Rafael_TWH 15_S4_3	496.5	1269	179.9	803	199.9	42.6	223.2	34.63	198.8	33.89	75.7	7.67	34.4	3.95
Rafael_TWH 15_S5_2	273.4	1074	138.8	562	139.9	30.8	151.2	23.25	129.7	21.7	48.3	4.84	21.96	2.537
Rafael_TWH 15_S6_1	410	1394	175	730	177	37.3	187.9	27.9	157.8	26	57.9	6.04	28.9	3.19
Rafael_TWH 15_S6_2	370	1404	184	752	180	38.5	194	30	167.4	27.47	61.8	6.35	28.51	3.214
Rafael_TWH 15_S6_3	393	1420	175.8	719	173.3	37.9	188.1	29.69	168.8	27.51	63.1	6.42	29.5	3.43
Rafael_TWH 15_S7_2	466	1442	192.8	806	187.1	37.94	203.5	31.47	173.8	28.49	63.2	6.09	27.07	3.19
Rafael_TWH 15_S8_1	571.7	1466	217.1	978	239.9	46.42	263.3	40.72	227.5	37.91	84.9	8.53	37.2	4.4
Rafael_TWH 15_S8_2	558.2	1427	214.3	981	238.6	46.61	263.8	40.4	228.4	38.19	85	8.51	38.01	4.41
Rafael_TWH 15_S8_3	542.6	1557	217.1	933	225.2	45.6	242.3	36.99	207.2	34.53	76.1	7.56	33.22	3.86
Rafael_TWH 15_S9_1	271.2	986	134.6	574	145	29.46	156.2	23.95	135.5	22.51	50.5	5.04	23.1	2.731
Rafael_TWH 15_S9_2	340.5	1213	169.3	710	175.9	36.18	190.1	29.52	167.7	27.83	61.5	6.18	27.38	3.242
Rafael_TWH 15_S8_3	334.3	1250	169.4	709	180.7	38.7	195.4	30.7	169.9	28.6	64.2	6.42	28	3.35
Rafael_TWH 15_S9_1	528	1390	207.3	958	237.3	46.5	259.3	40.1	226.1	36.5	80.9	7.99	35.6	4.18
Rafael_TWH 15_S9_2	551	1791	231.6	956	223.7	43.7	237.1	35.59	196.9	32.47	71.3	6.88	30.09	3.583
Rafael_TWH 15_S9_3	536	1861	236.3	930	213.5	43.9	224.6	33.78	187.9	30.64	66.8	6.55	28.1	3.33
Rafael_TWH_14.5_S1_1	523	1758	245.8	1034	247.3	50.7	266.5	40.8	231.2	38.1	85.1	8.35	36.4	4.18
Rafael_TWH_14.5_S1_2	525	1715	237.1	1003	244	49.7	259.1	39.6	224.9	36.5	82.5	8.26	37	4.21
Rafael_TWH_14.5_S1_3	458	1518	225.7	1022	252.8	46.5	267.2	41	223	36.2	78.7	7.75	34.5	4.1
Rafael_TWH_14.5_S2_1	398.1	1421	204.2	891	222.5	43.4	233.1	36.72	208	34.41	77.4	7.68	33.7	3.97
Rafael_TWH_14.5_S2_2	386.3	1386	193.4	806	206.9	42.3	217.9	33.5	191.1	32.1	72.2	7.4	33.9	3.85

Rafael_TWH_14.5_S2_3	352	1298	176	742	185.8	38.6	194.9	29.92	172.8	28.55	66.5	6.89	31.5	3.54
Rafael_TWH_14.5_S3_1	376.5	1263	178.3	770	191.4	37.82	190.7	30.02	168.4	27.95	63.2	6.3	28.72	3.333
Rafael_TWH_14.5_S3_2	288.9	950	133	589	152.3	33.37	167.8	25.8	149.4	25.19	57.2	5.82	27.06	3.15
Rafael_TWH_14.5_S4_1	443	1542	216.8	928	224.7	39.74	240.3	37.05	207.7	33.86	74.1	7.14	30.53	3.69
Rafael_TWH_14.5_S4_2	412.9	1565	210.6	887	217.2	39.8	228	34.63	195.4	32.21	70.3	6.98	30.03	3.58
Rafael_TWH_14.5_S4_3	470	1620	216.1	894	219.2	43.4	223.7	34.62	194.9	32	72.8	7.23	33.2	3.94
Rafael_TWH_14.5_S5_1	476	1422	216.9	1007	256	49.7	275.6	43	243.4	40.1	88.9	8.98	40.2	4.71
Rafael_TWH_14.5_S5_2	419.3	1494	216.8	955	246.1	45.8	261.4	40.5	227.6	37.6	84.4	8.36	36.4	4.33
Rafael_TWH_14.5_S5_3	517	1769	248.8	1075	261.1	45.4	252.6	38.64	213.4	34	74.2	7.31	33.2	3.87
Rafael_TWH_14.5_S6_1	441	1516	210.1	890	220.4	46.1	234.8	37.6	213.2	35.7	80.2	8.08	36.4	4.16
Rafael_TWH_14.5_S6_2	538.8	1370	218.7	1089	284.3	52.67	310.2	49.68	280.2	47.2	105.3	10.69	47.9	5.48
Rafael_TWH_14.5_S6_3	434	1726	228.3	978	236.4	47	237.4	36.5	201.4	32.3	70.3	7.22	31.1	3.68
Rafael_TWH_14.5_S7_1	531	1720	240.2	1026	245.1	45.5	257.5	38.6	210.5	34.3	74.9	7.23	31.4	3.61
Rafael_TWH_14.5_S7_2	504	1639	228.6	990	235.8	43.4	253.9	39.3	213.6	35.2	76.5	7.58	32.2	3.83
Rafael_TWH_14.5_S8_1	383.6	1340	181.5	742	182.8	40.6	199	32.79	188.6	31.28	70.7	7.15	32.1	3.77
Rafael_TWH_14.5_S8_2	333.6	1241	176.9	734	189.2	39.7	206.4	32.54	184.9	30.5	70.1	6.95	31	3.7
Rafael_TWH_14.5_S8_3	333.7	1240	164.4	700	176.6	37.3	193.1	30.32	171.5	28.6	64.1	6.35	28.66	3.39
Rafael_TWH_14.5_S9_1	145	308	37.7	142	31.8	6.24	24	3.75	22.3	4.25	11.1	1.58	10.5	1.47
Rafael_TWH_14.5_S9_2	508	1705	226.1	935	216.2	44.5	224.3	33.3	181.2	29.18	62.5	5.87	25.63	2.95
Rafael_TWH_14.5_S9_3	500	1669	221.1	936	222.3	47.1	222.7	33.16	181.9	29.44	64.2	6.42	29.5	3.38
Rafael_TWH_14.5_S10_1	532	1774	235.4	1005	239.8	50.3	249.9	36.99	203.9	33.24	70.7	6.69	29.8	3.42
Rafael_TWH_14.5_S10_3	527	1714	231.6	952	234.4	49.2	238.9	36.15	205.9	34.3	78	8.02	37.6	4.42
Rafael_TWH_14.5_S11_1	382	1539	221.6	948	236.7	47.1	253.2	39.19	217.9	35.69	79.4	7.81	33.3	3.94
Rafael_TWH_14.5_S11_2	377.1	1551	224.5	950	236.7	47.1	247.6	38.3	207.7	34.1	73.3	7.1	30.3	3.66
Rafael_TWH_14.5_S11_3	501	1799	252	1053	251.6	47	251.7	38.06	208.9	33.87	74.3	7.29	31.9	3.74
Rafael_TWH_14.5_S12_1	500.3	1796	251.3	1062	253	44.3	265.9	40.5	221	36.4	80	7.8	33	3.82

Rafael_TWH_14.5_S12_2	518.6	1770	248.1	1039	253.5	44.56	258.1	39.62	220.2	36.08	79.5	7.9	34.3	4.08
Rafael_TWH_14.5_S12_3	516	1929	261.4	1071	257	44.5	257.2	38.25	208.6	33.81	73.3	7.01	29.95	3.57
Rafael_TWH_14.5_S13_1	364.6	1031	149	633	151.3	33.42	165	25.58	144.4	24.38	54.4	5.26	23.94	2.749
Rafael_TWH_14.5_S13_2	335.3	1048	139.6	581	139.7	31.48	156.9	24.64	142	23.68	53.3	5.37	24.21	2.747
Rafael_TWH_14.5_S13_3	323.2	1027	138.8	579	142.6	31.49	156	24.42	140.8	23.71	52.1	5.18	24.01	2.724
Rafael_TWH_14.5_S14_2	575	1874	254.7	1030	239.5	48.5	245.7	36.6	200.9	32.59	71.1	6.87	29.57	3.36
Rafael_TWH_14.5_S14_3	526.3	1746	234.9	983	231.1	48.23	231.4	34.89	190.6	31.05	67.6	6.56	29.8	3.35
Rafael_TWH_14.5_S15_1	326.1	945	125	513	121.6	26.46	135.2	21.43	122.7	21.22	48.1	4.94	22.66	2.6
Rafael_TWH_14.5_S15_2	356.9	986	130.4	522	119.3	26.68	136.6	21.5	124.6	21.27	49	5	22.91	2.671
Rafael_TWH_14.5_S15_3	385.2	976	139.1	585	137.4	29.9	143.1	21.91	125.2	21.25	47.8	4.89	23.79	2.71
Rafael_TWH_14.5_S16_2	385.6	1439	199.6	862	219.2	46	230.7	37.34	212.2	35.3	80.2	8.02	36.1	4.2
Rafael_TWH_14.5_S16_3	393.8	1384	200	867	221.1	44.35	233.5	36.92	210.9	34.86	78.6	7.88	35	4.04
Rafael_TWH_14.5_S17_1	376.5	1388	195.6	838	209.4	40.4	212.8	32.91	183.9	30.1	66.8	6.67	30.1	3.45
Rafael_TWH_14.5_S17_2	370.5	1306	185.4	794	198.5	40.7	205.6	31.97	180.6	29.6	65.5	6.67	29.8	3.41
Rafael_TWH_14.5_S17_3	391.2	1395	191	812	199.2	39.77	204.7	32	179.6	29.59	65.4	6.62	29.69	3.395
Rafael_TWH_14.5_S18_2	531	1903	251.7	1064	254.7	49.7	249	39.1	212.8	34.9	76.1	7.48	33.2	3.72
Rafael_TWH_14.5_S19_1	476.5	1482	197.9	815	193.8	41.2	203.8	31.49	176.8	29	64.2	6.27	28	3.21
Rafael_TWH_14.5_S19_2	453.7	1396	188.5	795	191.1	42.2	204.5	31.53	178.8	29.59	66.6	6.53	28.5	3.25
Rafael_TWH_14.5_S19_3	450.4	1389	187.3	770	185.2	40.15	203.9	31.52	176	29.19	65.2	6.48	27.93	3.22
Rafael_TWH_14.5_S20_1	423	1582	203.1	839	200.1	43.82	205.9	31.86	176	28.14	61.1	5.89	25.45	2.85
Rafael_TWH_14.5_S20_2	433.2	1487	208.6	858	209.5	44.3	228.5	34.94	194	31.5	68.8	6.6	28	3.17
Rafael_TWH_14.5_S20_3	440	1470	205.7	871	217.2	45	234.7	36.1	196.6	32.1	70	6.73	29	3.4
Rafael_TWH 14_S1_1	217.6	458.8	56.1	243.8	59.3	13.52	74.4	11.97	74.2	13.61	32.32	3.4	15.22	1.823
Rafael_TWH 14_S1_2	207.5	460.8	55.8	234.5	57.4	13.1	69.4	11.29	69.6	12.61	30.36	3.177	14.02	1.733
Rafael_TWH 14_S1_3	212	564	62.9	242.5	56.1	13.04	67.3	10.68	65.5	11.7	27.8	2.8	12.78	1.482
Rafael_TWH 14_S2_1	203.3	527	62.1	255.1	60.8	13.83	69.7	11.48	67.7	12.4	30.2	3.26	15.1	1.8

Rafael_TWH 14_S2_2	202	520	63. 2	258 .6	60. 9	13. 85	72	11. 66	70. 8	12. 51	29. 7	3.1 3	14. 01	1.6 46
Rafael_TWH 14_S2_3	192 .5	494	59. 8	244 .7	59. 6	13. 7	69	10. 84	63. 6	11. 11	26. 8	2.8 5	13. 48	1.5 07
Rafael_TWH 14_S3_1	192 .8	480	53. 4	214 .5	50. 5	10. 64	60	9.4 8	57. 8	10. 46	25. 3	2.6 9	12. 14	1.4 47
Rafael_TWH 14_S3_2	188 .5	451	50. 9	208 .3	49. 2	10. 93	60. 8	10. 12	61. 7	11. 23	26. 72	2.7 51	12. 07	1.4 86
Rafael_TWH 14_S3_3	198 .3	396 .9	49. 46	214 .6	51. 4	11	63. 5	10. 54	64. 3	11. 82	27. 92	2.9 46	12. 84	1.5 62
Rafael_TWH 14_S4_1	201 .9	525	56. 8	225 .7	53. 8	11. 97	62. 7	10. 07	61. 9	11. 12	26. 54	2.8	12. 77	1.5 08
Rafael_TWH 14_S4_2	229 .3	505	59. 8	252 .6	59. 3	12. 71	69. 5	11. 07	66. 9	12. 33	29. 1	3.1 1	14. 3	1.7 38
Rafael_TWH 14_S4_3	196 .7	501	54. 3	216 .3	50. 8	11. 53	60. 5	9.7 1	59. 4	10. 83	25. 58	2.6 94	12. 74	1.4 92
Rafael_TWH_14_ S5_1	209 .2	545	59. 5	228 .6	55. 4	12. 74	64. 8	10. 59	63. 4	11. 39	26. 94	2.8 38	12. 51	1.5 08
Rafael_TWH_14_ S5_2	227 .5	478	59. 3	255 .6	61. 2	13. 46	74. 3	11. 9	71. 7	12. 93	30. 41	3.1 6	13. 9	1.6 62
Rafael_TWH_14_ S5_3	212 .2	533	59	229 .8	55. 5	12. 6	68. 2	11. 25	66. 9	12. 13	28. 51	2.9 39	12. 84	1.5 81
Rafael_TWH_14_ S6_3	234 .1	509	60. 4	248 .4	58. 6	13. 06	69. 7	11. 32	67. 6	12. 2	29. 33	3.0 9	13. 82	1.6 88
Rafael_TWH_14_ S7_1	212 .8	512	58. 7	238 .9	56. 6	12. 3	67. 9	10. 93	65. 6	11. 83	27. 95	2.9 98	13. 52	1.6 22
Rafael_TWH_14_ S7_2	195 .3	465	53. 5	217 .5	50. 9	11. 16	60. 5	9.6 9	58. 4	10. 33	24. 63	2.6 63	12. 29	1.4 5
Rafael_TWH_14_ S7_3	182 .6	476	53. 2	214 .4	49. 4	11. 57	59. 8	9.3 9	57. 3	10. 46	24. 9	2.5 9	12. 51	1.4 67
Rafael_TWH_14_ S8_1	208 .5	368 .2	52. 29	245	63	13. 37	81. 1	12. 94	78. 8	14. 21	33. 91	3.5 94	16. 45	2.0 18
Rafael_TWH_14_ S8_3	190 .9	423 .3	53. 4	222 .5	56. 6	11. 95	65	10. 5	63. 7	11. 43	26. 83	2.8 27	12. 81	1.5 25
Rafael_TWH_14_ S9_2	202 .4	441 .2	54. 61	233 .4	56. 8	12. 9	68. 4	10. 9	65. 6	11. 82	28. 04	2.9 41	13. 23	1.5 81
Rafael_TWH_14_ S10_1	172 .3	440 .7	51. 6	206 .9	50. 9	10. 73	61. 7	9.9 3	60. 1	10. 81	25. 26	2.6 6	11. 83	1.4 31
Rafael_TWH_14_ S10_2	181 .2	492	55. 4	217 .7	52	11. 26	60. 6	9.8 9	58. 9	10. 54	25. 3	2.6 4	12. 62	1.4 63
Rafael_TWH_14_ S11_1	188 .3	482	52. 8	206 .3	49. 3	11. 23	58	9.2 6	56. 4	10. 17	24. 07	2.4 81	11. 15	1.3 46
Rafael_TWH_14_ S11_2	181 .4	449 .8	51. 49	206 .3	48. 6	11. 17	59. 1	9.4 1	56. 7	10. 42	24. 42	2.5 23	11. 54	1.3 59
Rafael_TWH_14_ S11_3	185 .3	448	50. 8	203 .5	47. 5	11. 08	56. 9	9.0 4	55. 4	10. 18	24. 21	2.5 67	11. 83	1.3 97
Rafael_TWH_14_ S12_1	176 .2	492	55. 6	226	54. 8	11. 93	65. 8	10. 48	63. 1	11. 15	26	2.6 1	11. 48	1.3 58
Rafael_TWH_14_ S12_2	171 .3	473	54. 2	215 .5	52. 1	11. 98	61. 4	9.6 8	57. 6	10. 23	23. 59	2.4 87	11. 18	1.3 45
Rafael_TWH_14_ S12_3	181 .5	473	54. 7	222	52. 6	12. 18	60. 6	9.7 4	57. 7	10. 23	24. 36	2.4 77	11. 2	1.3 48

Rafael_TWH_14_S13_1	206.5	543	60.8	252.2	58.9	12.96	67.6	10.75	64.1	11.46	27.1	2.85	13.57	1.698
Rafael_TWH_14_S13_2	209.1	525	61.1	257.4	59.8	12.76	68.4	10.83	64.6	11.52	27.2	2.8	12.73	1.56
Rafael_TWH_14_S13_3	208.5	537.9	60.7	245.7	57.1	12.45	66	10.4	62.1	11.02	26.5	2.734	12.43	1.518
Rafael_TWH_14_S14_1	186.8	467	52.5	203.2	48.2	10.84	54	8.34	50.1	8.82	20.79	2.17	10.04	1.185
Rafael_TWH_14_S14_2	180.9	420.2	50.15	207.7	50.3	10.87	59.7	9.62	58.6	10.4	24.64	2.498	10.85	1.334
Rafael_TWH_14_S14_3	160.1	422.9	47.18	184.8	44.7	9.83	52.4	8.43	51.1	9.1	21.37	2.187	9.49	1.148
Rafael_TWH_14_S15_1	196	550	73.6	328	81.9	16.93	85.1	12.9	72.9	12.07	27.5	2.8	13.3	1.548
Rafael_TWH_14_S15_3	172.7	489	53.4	207	50.2	11.19	57.4	9.08	54.4	9.52	22.77	2.433	11.37	1.327
Rafael_TWH_14_S16_1	241.9	798	101.9	403	96.9	18.4	99.3	15.53	89.7	15.28	34.6	3.59	16.22	1.95
Rafael_TWH_14_S16_3	232.8	761	94.1	389	94.2	17.99	98.5	15.4	89	15.3	35.7	3.47	15.36	1.835
Rafael_TWH_14_S17_1	174	428	48.5	196.8	45.6	10.44	54.4	8.64	51.6	9.21	21.88	2.247	10.09	1.205
Rafael_TWH_14_S17_2	179.8	415	49.7	204.8	47.3	10.61	57.7	9.11	54.5	9.7	23.55	2.426	11.06	1.328
Rafael_TWH_14_S17_3	163.9	396.8	46.59	193.5	47.7	10.76	59	9.9	62.3	11.93	31.6	3.96	23.7	3.43
Rafael_TWH_14_S18_1	186.8	479	56.6	231.9	54.8	12.69	65.5	10.62	64.5	11.53	26.94	2.858	13.19	1.563
Rafael_TWH_14_S18_2	185.4	412.2	54.2	229.8	56.4	12.79	68	11.08	67.7	12.03	28.68	2.984	13.54	1.62
Rafael_TWH_14_S19_1	181.2	560	66.7	262.3	64.2	13.7	70	10.86	62.2	10.84	25.1	2.58	12.04	1.461
Rafael_TWH_14_S19_3	208.5	670	77.4	309	71	14.83	77.4	12.09	69.3	11.94	27.1	2.74	12.34	1.448
Rafael_TWH 13.5_S1_1	298.3	1113	141	556	130.6	27.34	132.9	20.67	117.6	19.2	41.9	4.2	19.19	2.23
Rafael_TWH 13.5_S1_2	313.2	1077	137	550	130.8	27.81	137.7	21.8	123.5	20.83	45.8	4.52	19.88	2.304
Rafael_TWH 13.5_S1_3	330.4	1173	154.7	609	144	28.66	145.9	22.72	127.5	21.3	47.8	4.77	21.1	2.433
Rafael_TWH 13.5_S2_1	298.2	1000	126.7	503	117.2	25.81	131.6	20.52	118.7	19.92	44.9	4.51	19.85	2.29
Rafael_TWH 13.5_S2_2	312.8	880	122.1	523.3	128.1	28.08	144.1	22.94	134	22.98	51.7	5.17	22.62	2.693
Rafael_TWH 13.5_S2_3	303.6	953	123.6	510	122.8	27.74	142.8	22.23	127.9	21.81	49.1	4.93	21.21	2.425
Rafael_TWH 13.5_S3_1	233.4	811	99.8	415	99.3	22.76	104.8	16.84	96.2	16.32	37.2	3.86	17.52	1.982
Rafael_TWH 13.5_S3_2	225.1	752	95.6	398	96.6	21.76	106.8	17.26	100.9	17.68	40.7	4.14	18.41	2.141
Rafael_TWH 13.5_S3_3	222.3	686	90.1	384.2	94.2	21.93	104	17.11	100.4	17.47	40.57	4.21	19.63	2.317

Rafael_TWH 13.5_S4_1	257.7	781	101.7	427	104.3	21.76	112.3	17.98	106.5	18.16	41.9	4.33	19.92	2.29
Rafael_TWH 13.5_S4_2	272.4	771	100.4	414.5	98.4	21.9	104.9	16.45	96.6	16.71	38	4.03	20.12	2.412
Rafael_TWH 13.5_S4_3	276.9	884	109.6	449	105.6	22.41	114.1	18.33	106.8	18.27	42.3	4.5	20.86	2.47
Rafael_TWH 13.5_S5_1	219.1	593	63	241.6	52.3	13.35	68.7	10.84	67.9	12.2	29.8	3.06	13.58	1.592
Rafael_TWH 13.5_S5_2	201	529	55.7	220.1	47.8	12.43	60.8	9.7	61.1	11.17	26.3	2.78	12.18	1.433
Rafael_TWH 13.5_S5_3	215	463.5	53.85	229.1	52.7	13.4	69.3	11.25	72.1	13.35	31.73	3.323	14.69	1.695
Rafael_TWH 13.5_S6_2	303.8	1064	135.4	566	131.5	26.14	139.9	22.22	128.6	21.76	49.1	4.89	21.52	2.52
Rafael_TWH 13.5_S6_3	260.2	886	119.9	492	119.8	24.53	129.3	20.65	118	20.07	45.6	4.48	20.27	2.33
Rafael_TWH 13.5_S7_1	307	1081	132.3	523	118.6	26.24	125.3	19.53	111.2	18.67	41.5	4.14	18.4	2.06
Rafael_TWH 13.5_S7_3	300.2	1083	132.7	517	119.3	25.86	127	19.88	113.8	19.31	43	4.31	18.49	2.16
Rafael_TWH 13.5_S8_1	255.7	801	97.2	381.4	88.6	20.12	100.2	15.73	92.7	15.9	36.6	3.72	16.52	1.907
Rafael_TWH 13.5_S8_2	260.9	814	98.2	386.6	90.2	20.49	102.3	16.28	96.6	16.65	38.2	3.86	16.99	1.949
Rafael_TWH 13.5_S8_3	258	821	97.1	390	88.2	20.09	99.9	15.91	95.1	16.82	38.8	4.03	17.7	2.09
Rafael_TWH 13.5_S9_1	222.5	737	89	355.2	82.9	18.65	97.1	15.46	93	16.5	39.06	4.04	18.75	2.208
Rafael_TWH 13.5_S9_2	226.5	652	83.9	353.6	84.9	19.7	97.8	16.33	99.6	17.71	41.4	4.41	20.87	2.432
Rafael_TWH 13.5_S9_3	219.4	592	80.6	359.7	89.8	19.95	104.8	17.1	104.6	18.31	42.6	4.53	21.29	2.544
Rafael_TWH 13.5_10_1	249.3	748	97	407.9	98.5	20.53	111.3	17.75	106.7	18.5	42.6	4.46	20.42	2.414
Rafael_TWH 13.5_S10_2	234	792	100	402.3	97.8	19.39	114.6	18.28	108.3	18.84	43.4	4.52	19.88	2.41
Rafael_TWH 13.5_S10_3	216.9	733	91	371.1	88.5	18.37	103.4	16.54	98.8	17.46	40.3	4.07	18.24	2.226
Rafael_TWH 13.5_S11_1	186.2	571	65.8	264.5	63.3	15.52	77.2	12.81	77.8	14.02	32.32	3.315	15.47	1.797
Rafael_TWH 13.5_S11_2	187.6	577	66.8	275.3	64.6	15.49	77.9	12.61	77.5	13.89	32.54	3.379	15.54	1.799
Rafael_TWH 13.5_S11_3	197.5	577	69.1	278.3	66.7	15.97	79.6	13.08	79.7	14.17	32.85	3.407	15.9	1.838
Rafael_TWH 13.5_S12_1	250.8	823	94.5	385	88.1	19.94	95	14.71	86.2	14.83	33.6	3.54	17.5	1.962
Rafael_TWH 13.5_S12_2	286.6	765	101.9	429.1	100.4	21.44	107.5	17.1	97.7	17.28	40	4.22	20.42	2.357
Rafael_TWH 13.5_S12_3	285.8	785	103	430	103.5	22.02	109.2	17.15	98.8	17.14	39.8	4.07	19.8	2.28
Rafael_TWH 13.5_S13_1	205.9	571	63.5	266	61.4	15.85	72.1	11.68	70.4	12.6	29.2	3.02	14.78	1.73

Rafael_TWH 13.5_S13_2	213.5	566	64.3	253.4	59.2	15	69.5	11.01	67.7	11.93	28.6	2.9	13.5	1.541
Rafael_TWH 13.5_S13_3	187.5	509	58.7	242.2	56.8	14.69	70.6	11.23	69.9	12.63	29.5	3.13	14.36	1.667
Rafael_TWH 13.5_S14_1	290	948	121	476	112.4	24.56	119.8	19.65	112.4	19.13	43.4	4.33	19.5	2.32
Rafael_TWH 13.5_S14_2	266.4	912	109.9	443	104.6	23.25	116	18.08	104.8	18.13	39.6	3.99	17.55	2.035
Rafael_TWH 13.5_S14_3	276.9	915	114.2	465.4	108.5	23.66	115.4	18.45	107.2	17.98	40.4	4.01	17.88	2.099
Rafael_TWH 13.5_S15_1	250.1	824	100.5	391.8	93.6	20.68	103.3	16.69	96.9	16.8	38.3	3.85	17.2	2.008
Rafael_TWH 13.5_S15_2	246.4	814	100.1	394.1	94.3	20.01	106.6	16.84	100.2	17.23	39.1	3.94	17.43	2.057
Rafael_TWH 13.5_S15_3	254.3	852	105.7	415.9	98.8	20.45	111.4	17.87	104.4	18.07	41	4.09	17.89	2.122
Rafael_TWH 13.5_S16_1	209.2	640	87	367.2	89.7	19.24	102.4	16.63	97.9	17.34	40.2	4.06	18.34	2.224
Rafael_TWH 13.5_S16_2	204.6	705	86.9	358.8	87.8	17.66	100.6	16	94.7	16.25	37.53	3.86	17.47	2.129
Rafael_TWH 13.5_S16_3	203.4	686	85.7	350.5	83.8	17.85	95.8	15.4	91.8	15.99	36.91	3.81	17.39	2.082
Rafael_TWH 13.5_S17_1	195.8	426.5	51.48	221.1	53.4	13.56	67.7	11.12	69.6	13.09	31.99	3.458	16.43	1.918
Rafael_TWH 13.5_S17_2	194.4	481	55.6	221	51	13.36	65.1	10.36	62.1	11.3	27.7	2.92	14.13	1.6
Rafael_TWH 13.5_S17_3	196.3	480	55.1	224.2	51.5	13.5	61.6	10.18	64	11.92	29.4	3.15	15.71	1.772
Rafael_TWH 13.5_S18_1	258.2	839	102.1	414	96.8	20.39	105.6	16.67	97.5	16.64	38	3.91	17.92	2.067
Rafael_TWH 13.5_S18_2	271	823	102.2	418	99.7	21.07	103.3	16.97	100.4	16.88	39.6	4	18.17	2.07
Rafael_TWH 13.5_S18_3	240.6	740	93.7	380.6	92.3	20.4	100.2	16.21	95	16.3	38	3.9	18.18	2.076
Rafael_TWH 13.5_S19_1	191.6	599	71.2	294	71.1	16.62	83.1	13.38	80.9	14.08	32.9	3.28	14.98	1.72
Rafael_TWH 13.5_S19_2	217.7	515.5	73.2	327.6	83.2	18.88	99.4	16.69	100.1	17.83	40.79	4.22	19.36	2.21
Rafael_TWH 13.5_S19_3	230.4	540	73.3	332	83.9	19.17	105.9	17.34	106.5	18.9	44.3	4.67	21.51	2.505
Rafael_TWH 13.5_S20_1	259.2	830	102.6	408	96.1	20.64	102.1	16.63	95.2	16.19	37.6	3.82	17.63	2.05
Rafael_TWH 13.5_S20_2	260.8	837	100.2	400.1	95	20.46	102.9	16.36	95.7	16.61	38.3	3.97	17.77	2.091
Rafael_TWH 13.5_S20_3	259.8	770	99.7	409.6	100.2	21.16	111.3	17.76	104.3	17.8	40.7	4.1	18.46	2.174
Rafael_TWH 13.5_S21_2	311.5	922	118.3	493	118.2	25.37	126.2	20.33	118.5	20.21	46.42	4.71	22.02	2.535
Rafael_TWH 13.5_S21_3	284.4	931	113.6	451.3	104.9	23.94	115.5	18.4	106.2	18.41	42.8	4.27	19.13	2.253
Rafael_TWH 13.5_S22_1	219.9	682	82.3	321.2	77.7	17.96	86.4	13.96	84.7	15.06	35.5	3.71	17.01	1.973

Rafael_TWH 13.5_S22_2	216 .6	684	82. 9	329 .9	77. 9	17. 96	87. 8	14. 02	84. 7	14. 85	34. 9	3.6 8	17. 02	2.0 59
Rafael_TWH 13.5_S22_3	222 .3	712	84	339	79. 2	18. 74	89	14. 46	86. 6	15. 31	35. 53	3.6 9	16. 8	1.9 32
Rafael_TWH_13_ S1_1	330 .8	119 0	172 .9	726	178 .4	33. 43	179 .9	27. 86	155 .2	25. 35	56. 4	5.5 7	24. 9	2.8 8
Rafael_TWH_13_ S1_2	323 .2	119 8	172 .2	707	173 .4	32. 96	179 .7	27. 46	153 .7	25. 2	56. 5	5.6 2	25. 01	2.8 4
Rafael_TWH_13_ S1_3	345 .2	123 7	175 .6	765	182 .8	34. 29	181 .1	28. 37	155 .5	25. 79	56. 4	5.6 4	25. 34	2.9 7
Rafael_TWH_13_ S2_2	331 .6	105 8	153 .4	639	153 .9	29. 75	159 .6	24. 8	140 .4	23. 41	51. 1	5.0 5	22. 1	2.5 15
Rafael_TWH_13_ S2_3	364 .7	100 7	155 .8	685	166 .1	31. 95	173 .9	27. 03	152 .3	25. 37	56. 8	5.6 5	25. 17	2.8 81
Rafael_TWH_13_ S3_1	323 .7	106 8	152 .1	637	147 .6	29. 94	161 .5	24. 59	138 .5	23. 3	51. 7	5.0 4	22. 4	2.5 3
Rafael_TWH_13_ S3_2	439 .5	886	157 .7	799	202 .5	34. 56	231 .8	36. 88	214 .2	36. 4	81. 9	8.3 6	35. 9	4.4
Rafael_TWH_13_ S3_3	335 .7	103 8	151 .7	645	152	30. 31	157 .2	24. 56	138 .6	22. 72	49. 9	4.9	22. 08	2.5 5
Rafael_TWH_13_ S4_1	359 .7	116 8	167 .8	723	167 .6	31. 93	174 .6	26. 71	150 .4	25. 36	56. 7	5.5 5	25. 3	2.8 8
Rafael_TWH_13_ S4_2	431	134 5	183 .8	765	169 .5	32. 4	170 .1	26. 1	146 .7	24. 3	54. 6	5.3 9	23. 9	2.6 9
Rafael_TWH_13_ S4_3	354 .3	990	159 .5	728	176 .4	32. 74	187 .7	29. 32	167 .2	27. 8	61. 5	5.9 9	26. 7	3.0 7
Rafael_TWH_13_ S5_1	352 .4	122 6	179 .7	735	179 .7	34. 85	179	28. 06	157 .1	25. 82	58. 2	5.5 8	24. 46	2.8 1
Rafael_TWH_13_ S5_2	361 .4	122 8	177 .7	762	188 .2	37. 6	191 .7	29. 85	167 .7	27. 6	61. 7	5.9 6	27	3.0 2
Rafael_TWH_13_ S5_3	363 .6	115 6	173 .8	762	186 .8	37. 3	190 .4	30. 3	169 .4	27. 7	61. 8	6.2 7	28	3.1 3
Rafael_TWH_13_ S6_1	380 .1	124 6	177 .9	758	178 .8	34. 42	179 .2	27. 5	152 .4	25. 37	55. 8	5.6	24. 69	2.8 86
Rafael_TWH_13_ S6_2	394 .5	128 3	182 .5	753	177 .4	33. 63	177 .4	28. 06	151 .2	25	55. 8	5.5 5	24. 6	2.7 5
Rafael_TWH_13_ S6_3	372	118 9	174 .7	733	175 .2	33. 35	178 .6	27. 84	156 .1	25. 86	56. 9	5.6 6	24. 96	2.8 35
Rafael_TWH_13_ S7_1	298 .1	976	134 .4	536	125	25. 5	121 .8	19. 1	108 .9	18. 44	41. 7	4.3 1	20. 6	2.2 9
Rafael_TWH_13_ S7_2	290 .4	945	133 .6	549	131 .8	25. 73	141 .9	22. 07	125	20. 97	47	4.7 4	21. 2	2.5
Rafael_TWH_13_ S7_3	274 .5	944	132	541	126 .5	25. 12	135 .8	21. 3	121 .7	20. 75	45. 7	4.6 3	20. 14	2.3 58
Rafael_TWH_13_ S8_1	360 .1	124 8	178 .9	744	178 .7	32. 41	174 .6	27. 35	152 .9	25. 32	56. 9	5.5 8	24. 8	2.8 8
Rafael_TWH_13_ S8_2	378 .2	125 9	184 .6	753	177 .6	34. 51	184 .3	28. 46	160 .4	26. 54	59. 1	5.8	25. 2	2.8 6
Rafael_TWH_13_ S8_3	363 .5	125 7	176 .3	742	174 .4	33. 78	173 .8	26. 78	149 .3	24. 46	54. 6	5.4 3	24. 26	2.7 9
Rafael_TWH_13_ S9_1	315 .9	114 2	146 .1	595	133 .1	27. 98	133 .8	20. 23	112 .2	19. 01	42. 7	4.2 4	20. 28	2.2 55

Rafael_TWH_13_S9_2	355.8	1183	167.8	716	167.2	32.28	170.7	26.04	145.6	24.24	54.1	5.38	24.51	2.84
Rafael_TWH_13_S9_3	343.8	1144	161.5	676	162.2	30.9	167.8	25.89	144.2	24.39	54	5.36	24.5	2.82
Rafael_TWH_13_S10_1	366.5	1253	189.8	805	195.4	35.22	202.3	30.86	170.8	27.98	61.6	5.97	26	3.01
Rafael_TWH_13_S10_3	387.1	1343	194.9	812	193.2	37.43	196.1	30.12	165.9	26.74	59.5	5.86	26.63	3.13
Rafael_TWH_13_S11_1	258.5	809	114.9	490	119.3	24.37	125.2	20.28	116.7	19.5	43.9	4.38	19.81	2.25
Rafael_TWH_13_S11_2	260.9	801	112.9	470.1	116.2	23.69	122.7	19.17	110.6	18.99	43.2	4.41	20.26	2.3 47
Rafael_TWH_13_S11_3	249.1	789	110.4	469	111.6	24.03	112.5	17.45	101.6	16.94	38.1	3.94	19.2	2.25
Rafael_TWH_13_S12_2	239.6	773	109	451.7	107.1	20.45	118.6	18.55	107.9	18.58	42.6	4.3	19.14	2.27
Rafael_TWH_13_S12_3	253.4	835	116.7	483	112.9	20.42	122.8	19.44	113.1	19.22	44.1	4.42	18.93	2.28
Rafael_TWH_13_S13_1	375	1096	158.9	667	158.2	31.02	164.2	25.89	145.7	24.48	54.6	5.42	24.34	2.79
Rafael_TWH_13_S13_2	314.8	972	139.5	596	142.3	29.55	152.8	24.37	138.7	23.59	52.7	5.26	24.23	2.7 91
Rafael_TWH_13_S13_3	312.6	967	139.3	606	148.6	29.22	157.6	24.44	138.6	23.43	53.3	5.37	24.36	2.7 86
Rafael_TWH_13_S14_1	345.2	1174	176.3	755	180.6	30.89	186.1	29.53	165.1	27.01	60.1	5.99	25.6	2.99
Rafael_TWH_13_S14_2	362	1149	174.1	745	181.4	31.41	187.7	29.18	164.8	27.4	61	5.96	25.96	3.0 84
Rafael_TWH_13_S15_1	295.6	881	127.6	527.6	127	25.27	132.6	21.22	120.2	20.33	45.8	4.57	20.28	2.3 59
Rafael_TWH_13_S15_2	331.8	973	141.5	589	135.8	26.89	141.3	22.17	126.9	21.46	49.2	5.03	23.49	2.81
Rafael_TWH_13_S15_3	314.8	931	134.3	575	135.5	26.54	141.3	22.08	126.2	21.38	48.6	4.87	22.8	2.7
Rafael_TWH_11_S1_1	77.1	171.8	20.99	87.1	20.88	4.51	23.63	3.5 08	20.92	3.8 83	9.49	1.0 02	4.67	0.5 92
Rafael_TWH_11_S1_3	69.9	148	19.13	82.8	20.88	4.55	23.55	3.5 96	21.39	3.88	9.35	1.01	4.7	0.5 84
Rafael_TWH_11_S2_1	104.3	226	25.9	105.7	23	4.4	23.9	3.85	22.5	4.24	10.66	1.1 14	5.85	0.7 31
Rafael_TWH_11_S2_2	91.6	197.3	23.05	93.7	21.36	4.51	24.52	3.6	21.59	4.07	10.02	1.0 86	5.17	0.6 32
Rafael_TWH_11_S3_1	88.8	186.6	21.71	86.2	19.78	4.46	21.94	3.3 39	20.12	3.82	9.69	1.0 85	5.06	0.6 47
Rafael_TWH_11_S3_2	78.4	164.1	19.78	79.7	18.27	4.21	21.39	3.2 45	19.64	3.7 35	9.54	1.05	5	0.6 19
Rafael_TWH_10_S1_1	162.3	377	47.4	199.3	46	9.37	49.2	7.34	45.1	8.36	20.82	2.3 56	12.1	1.5
Rafael_TWH_10_S1_2	128.5	271.7	35.4	148.9	33.83	6.81	38.5	5.88	34.85	6.38	15.49	1.61	7.34	0.8 99
Rafael_TWH_10_S1_3	151	378	45.1	179.1	40.6	8.13	44.6	6.92	40.9	7.52	17.94	1.8 64	8.73	1.0 64

Rafael_TWH_10_S2_1	163.4	368.6	50.4	221.2	51.1	10.42	55.7	8.3	47.5	8.28	20.02	2.106	10.35	1.315
Rafael_TWH_10_S2_2	185.8	539	70.3	288.8	65.8	12.56	68.1	10.12	57.4	9.76	22.37	2.17	9.98	1.175
Rafael_TWH_10_S2_3	237	521.7	74.3	347.8	85.1	15.75	94.9	14.26	82	14.39	33.81	3.593	16.91	2.169
Rafael_TWH_10_S3_1	217.2	599	81	335.4	74.4	12.75	75.1	10.53	59	10.09	23.15	2.203	9.57	1.126
Rafael_TWH_10_S3_2	204.6	618	78.4	312.9	68.5	11.99	67.8	9.6	53.5	9.13	20.73	2.019	8.81	1.058
Rafael_TWH_10_S3_3	203.7	583	76.6	313.6	68.6	12.6	68.3	9.67	54.1	9.2	20.95	2.058	8.92	1.039
Rafael_TWH_10_S4_1	186.4	340.3	46.3	197.3	46.4	8.87	48.3	7.38	45.9	8.87	23.2	2.69	14.5	1.85
Rafael_TWH_10_S4_2	142.8	341.4	41.78	165.1	37.6	7.56	42.7	6.45	39.8	7.32	17.64	1.846	8.25	1.01
Rafael_TWH_10_S4_3	147.4	357.7	44.3	177.1	40.2	7.71	43.6	6.68	40.4	7.5	18.31	1.873	8.88	1.025
Rafael_TWH_10_S5_1	154.4	335	44.2	181	42.9	8.52	48.2	7.13	44.8	8.09	19.6	2.2	10.85	1.33
Rafael_TWH_10_S5_2	176	401	47.4	193.6	44.8	8.82	45.9	6.88	40.9	7.53	18.52	1.992	9.52	1.15
Rafael_TWH_10_S5_3	148.1	358.7	44.5	175.9	41.2	8.08	44.8	6.58	40.4	7.52	18.4	1.929	9.09	1.04
Rafael_TWH_10_S6_1	203.8	585	78.7	324.4	73.7	11.61	74.3	10.81	60.6	10.4	23.25	2.269	9.73	1.223
Rafael_TWH_10_S6_2	119.9	341.9	47.3	197.9	46.8	9.36	48.8	7.4	42.1	7.2	16.5	1.574	7.15	0.818
Rafael_TWH_10_S6_3	150.3	438	57.4	237.2	54.6	10.7	56.1	8.3	46.5	8.11	18.15	1.774	7.69	0.919
Rafael_TWH_10_S7_1	111.6	262	35.29	147.6	35.92	7.62	38.1	5.74	34.05	6.29	14.92	1.495	7.08	0.807
Rafael_TWH_10_S7_2	108.4	271	34.64	142.5	33.35	7.47	37.4	5.72	35.42	6.48	15.68	1.668	7.95	0.906
Rafael_TWH_10_S7_3	113.1	275.9	34.84	144.3	34.86	7.65	38.7	6.04	36.3	6.55	16.04	1.652	7.76	0.923
Rafael_TWH_9.5_S1_1	172.1	477	55.9	225.4	53.7	14.54	60.4	9.44	57.7	10.73	26.3	2.84	13.93	1.617
Rafael_TWH_9.5_S1_2	153.4	425	51.3	202.9	48.7	12.9	55.4	8.96	54.4	10.03	23.89	2.595	12.48	1.464
Rafael_TWH_9.5_S1_3	155.4	444	50.6	208.2	48.7	13.27	55.5	9.18	55	10.18	25.05	2.72	13.11	1.517
Rafael_TWH_9.5_S2_1	214.2	742	97.9	408	96.8	17.07	104.7	15.84	87	14.45	31.13	2.973	12.86	1.628
Rafael_TWH_9.5_S2_3	189.8	688	90.9	378.5	85.6	16.99	93.5	13.8	77	12.66	27.38	2.496	10.71	1.3
Rafael_TWH_9.5_S3_1	127.5	326.7	42.9	190.3	48.1	11.25	61	9.63	56.4	10.09	22.4	2.26	9.96	1.226
Rafael_TWH_9.5_S3_2	145.4	412	49	207.4	52.5	12.4	64.4	10.14	59.28	10.48	23.81	2.402	10.91	1.361
Rafael_TWH_9.5_S3_3	118.6	357.6	43.5	178.5	44	10.98	55	8.54	50.9	8.69	19.6	1.895	8.38	1.003

Rafael_TWH_9.5_S4_1	172	479	56.7	226	52.9	13.43	59.5	9.49	57.6	10.45	24.69	2.62	12.39	1.494
Rafael_TWH_9.5_S4_2	170.8	455	57.6	234.3	55.4	14.32	64.1	9.82	60.1	10.73	25.49	2.7	13.1	1.563
Rafael_TWH_9.5_S4_3	173	463	56.4	227.6	54	13.48	62.9	9.88	59.1	10.72	25.17	2.617	12.25	1.456
Rafael_TWH_9.5_S5_1	120.1	404.1	50.2	211.5	50.5	11.21	51.7	7.87	45.78	7.85	17.63	1.761	7.81	0.881
Rafael_TWH_9.5_S5_2	126	409	52.8	217.5	52.2	11.55	54.3	8.3	48	8.37	19.28	1.959	9.33	1.164
Rafael_TWH_9.5_S5_3	117.9	368.1	47.5	198.6	47.38	10.26	48.6	7.56	42.61	7.3	16.72	1.652	7.47	0.864
Rafael_TWH_9.5_S6_1	151.4	311	34.2	135.9	30.4	7.27	34.2	5.23	32.9	6.36	16.58	1.9	9.96	1.177
Rafael_TWH_9.5_S6_2	140.7	283.4	32	127.4	28.93	10.71	83	5.37	34.77	6.8	17.29	1.988	9.53	1.13
Rafael_TWH_9.5_S6_3	143.8	276.1	30.88	122.6	27.72	6.86	34.82	5.33	33.94	6.72	17.37	1.991	9.12	1.1
Rafael_TWH_9.5_S7_1	132.1	293.4	31.47	122.7	28.34	8.62	81.1	5.29	33.47	6.38	16.05	1.734	7.6	0.916
Rafael_TWH_9.5_S7_2	137	316.6	32.03	121.7	27.38	6.27	35.4	5.13	31.8	6.09	14.87	1.633	7.05	0.802
Rafael_TWH_9.5_S7_3	137.1	293.4	31.9	125.6	28.7	6.82	42.8	5.47	33.17	6.25	15.61	1.697	7.61	0.851
Rafael_TWH_9.5_S8_1	116	240.5	27	104.9	23.8	6.25	29.71	4.64	30.07	5.85	14.98	1.627	7.69	0.897
Rafael_TWH_9.5_S8_2	110.6	228.5	25.33	99.4	22.53	5.91	28.47	4.37	28.11	5.46	13.87	1.515	7.16	0.843
Rafael_TWH_9.5_S8_3	121.7	252.3	27.64	107.2	23.71	6.12	29.54	4.58	29.5	5.65	14.64	1.606	7.59	0.867
Rafael_TWH_9.5_S9_1	123.9	369.6	50.8	207.4	48	9.13	50.5	7.92	45.09	7.65	17.47	1.7	7.59	0.942
Rafael_TWH_9.5_S9_2	132.6	420	56	226.5	51	9.17	53	8.17	46.9	8.01	18.03	1.701	7.06	0.863
Rafael_TWH_9.5_S9_3	148.4	462	60.1	239.7	55.2	9.86	59.4	8.93	51.8	9	19.96	1.921	7.75	0.956

Vita

Rafael was raised in Fairfax Station, Virginia. He attended Clemson University where he graduated in August, 2016 with a Bachelor of Science degree in Geology with a concentration in Hydrogeology. Upon receiving his bachelor's degree, Rafael was employed in the Economic Geology sector where he was involved in development and production operations of gold deposits of the Carolina Slate Belt in Kershaw, South Carolina and the copper porphyry deposits of Morenci, Arizona. An interest in carbonates and geochemistry led to a pairing with Dr. Herrmann as his advisor.